Water adaptation strategy in anuran amphibians by aquaporins

THESIS

Water Adaptation Strategy in Anuran Amphibians by Aquaporins

Yuji Ogushi

Graduate School of

Science and Technology Educational Division

Department of Bioscience

Shizuoka University

December 2009

Contents of Thesis

Chapter 1

General introduction

Water is the major constituent of almost all life forms, accounting for approximately 50-95% of the body weight of all living organisms. It is essential for the continued survival of all organisms. Water has unique physical and chemical properties that have earned it the name of "universal solvent" due to its ability to act as a solvent for many substances. Organisms depend upon this property, and water maintains life by stabilizing biomolecular structures, contributing to intra- and extracellular biochemical reactions and functioning as a transport medium of biomolecules. Organisms originated in a primitive marine environment approximately 4 billion years ago and subsequently evolved gradually to life in fresh water or on dry land. As such, the evolution of organisms is intricately linked with water, and this inorganic molecule is of great importance for all living processes.

Anuran amphibians, the most numerous order of the Amphibia, are widely distributed throughout the world and have adapted to various water environments, ranging from freshwater and seawater to forests and arid desert (Pough, 2007; Frost, 2008). Most anurans go through an aquatic stage – the tadpole stage – before they metamorphose into their adult form, which is able to adapt to life on land. Adult anurans, with the exception of some aquatic species, are terrestrial and exposed to evaporative water loss through their thin skin when on dry land (Lillywhite, 2006). It is important to understand the adaptive processes to enable anurans to inhabit a wide range of ecological environments, in terms of water homeostasis. To adapt to their habitats, anurans have developed various complicated systems for maintaining water balance. For example, in general, most adult anuran amphibians do not drink water through their mouth, rather they absorb water through the ventral pelvic skin (also referred to as the

pelvic patch) and reabsorb water from urine in the urinary bladder (Bently & Main, 1972; Bently & Yorio, 1979).

The plasma membrane, formed by a phospholipid bilayer, functions as an exquisitely selective barrier against the entry of ions, small neutral solutes, and water into cells. It is slightly permeable to water by simple diffusion. However, some types of cells and tissues, such as the red blood cell, mammalian kidney, and anuran skin and urinary bladder, exhibit high water permeability, giving rise to the hypothesis that specialized water transport molecules (water channels) may exist in these cells and tissues. Freeze-fracture electron microscopic studies have suggested that intramembrane particles in the amphibian urinary bladder and skin may be water channel proteins because they translocate from the cytoplasmic pools to the plasma membrane following stimulation by vasopressin (Chevalier *et al.*, 1974; Kachadorian *et al.*, 1975; Brown *et al.*, 1983).

Aquaporin family

In 1992, a water channel was identified in the plasma membrane of red blood cells, which was subsequently named aquaporin (AQP) (Agre *et al.*, 1995). Aquaporins are a class of integral membrane proteins that form a selective water pore in the plasma membrane of various cells of animals, plants, and microorganisms (Zardoya, 2005). There are at least 13 different members of the AQP protein family (AQP0-AQP12) that mediate bidirectional water transport across the plasma membrane in response to osmotic gradients and differences in hydrostatic pressure. A common characteristic of the AQP protein family members is that they contain a conserved sequence of asparagine, proline, and alanine, called the NPA motif. Aquaporin proteins can be categorized into two subfamilies, orthodox AQPs and aquaglyceroporins, based on their transport function. Orthodox AQPs, such as AQP0, AQP1, AQP2, AQP4, and AQP5,

conduct only water, whereas aquaglyceroporin, including AQP3, AQP7, AQP9, and AQP10, transport not only water but also small neutral solutes, such as glycerol and urea (Ishibashi *et al.*, 2000; Takata *et al.*, 2004). AQP6, AQP8, AQP11, and AQP12 have recently been grouped as unorthodox AQPs because their functions are not yet fully defined (Ishibashi, 2006; Rojek *et al.*, 2008).

AQP of anuran amphibians

In general, the anuran species adapted to the terrestrial environment, such as *Bufo* (terrestrial) and *Hyla* (arboreal), have a ventral pelvic skin that is highly permeable to water and a bladder that has a high capacity to store urine. In contrast, aquatic anuran species, such as *Xenopus laevis*, have a ventral pelvic skin with a low permeability to water and a urinary bladder with a low storage capacity (Bentley & Main, 1972; Bentley, 2002).

Recently, Dr. Tanaka's group has identified three distinct types of arginine vasotocin (AVT)-dependent AQPs in the tree frog: AQP-h2 and AQP-h3 in the ventral skin (Tanii *et al.*, 2002; Hasegawa *et al.*, 2003), AQP-h2 in the urinary bladder, and AQP-h2K in the kidney (Ogushi *et al.*, 2007). Transepithelial water transport seems to be accomplished by these AQPs in concert with AQP-h3BL (Akabane *et al.*, 2007). AQP-h2 and AQP-h3 are specifically expressed in the ventral pelvic skin of tree frogs, where water absorption occurs (Tanii *et al.*, 2002; Hasegawa *et al.*, 2003). In response to stimulation by AVT, these AQP proteins are translocated to the apical plasma membrane for the purpose of absorbing water through the membrane, whereas the water exits from the cytoplasm through the AQP-h3BL protein, moves into the connective tissues, and then enters capillaries through AQP1 for rehydration of the body (Suzuki & Tanaka, 2009). In contrast to AQP-h2 and AQP-h3, the localization of AQP-h3BL does not change following AVT stimulation (Akabane *et al.*, 2007). In addition to localizing

AQP-h3BL protein in the basolateral membrane, it was also demonstrated that both AQP-h2 and AQP-h3 proteins are located at the basolateral plasma membrane of the first-reacting granular cells in the non-stimulated ventral pelvic skin of tree frogs (Hasegawa *et al.*, 2003).

Although *Hyla* AQP-h2 is translocated from the cytoplasm to the apical plasma membrane of granular cells of the *Hyla* urinary bladder in response to AVT stimulation (Hasegawa *et al.*, 2005), AQP-h2 immunoreactivity in the *Xenopus* bladder remains in the cytoplasm, with little movement to the apical membrane after AVT stimulation (Mochida *et al.*, 2008). This finding indicates that the response of *Xenopus* to AVT is considerably weaker than that of semi-aquatic, terrestrial, and arboreal anurans (Ewer, 1952; Bentley, 2002; Hasegawa *et al.*, 2003, 2005). Thus, it would appear that anuran species possess different osmoregulatory systems through AVT-dependent AQPs, which are dependent upon ecological niches.

Anuran amphibian kidney

In adult anurans, AVT exerts antidiuretic effects on the kidney, as well as the urinary bladder, to aid water economy (Bentley, 2002). The renal effect of AVT is considered to be weak in the aquatic species, such as *X. laevis* (Kloas & Hanke, 1992), while the kidney of most adult anurans shows significant antidiuretic responses to AVT in two modes: a decreased glomerular filtration rate and an increased water reabsorption across the renal tubule (Pang, 1983; Bentley, 2002). The adult kidney is a mesonephros, and the nephrons comprise a glomerulus in the Bowman's capsule and a renal tubule that is divided into the following morphologically distinguishable segments: a neck segment, proximal tubule, thin intermediate segment, early distal tubule, late distal tubule, and connecting tubule linked to the collecting duct (Romer and Parsons, 1986; Uchiyama & Yoshizawa, 2002; Hillyard, *et al.*, 2009) (Fig. 1). The anuran renal tubule

does not have an extended U-shaped medullary portion like Henle's loop in the avian and mammalian kidneys, so that hyperosmotic urine cannot be produced in the anuran kidney (Bentley, 1998).

Proteolytic processing of pro-arginine-vasotocin

Hydrin is an intermediate peptide derived from a pro-vasotocin-neurophysin precursor. It plays a pivotal role in the water absorption/reabsorption process in the skin and bladder but is devoid of antidiuretic activity in the kidney (Michel *et al.*, 1993; Rouille *et al.*, 1989). Hydrin 2 (vasotocinyl-Gly) is present in an amount equal to that of AVT in the neurohypophysis of Ranidae and Bufonidae. In contrast, the aquatic frog *X. laevis* synthesizes hydrin 1 (vasotocinyl-Gly-Lys-Arg) as well as AVT. Both peptides are generated from a down-regulation in the processing, *i.e.*, hydrin 1 by a decrease in carboxypeptidase E activity and hydrin 2 by a reduction in the activity of the α-amidating enzymatic system. These hydrins are found in anuran amphibians, but not in other vertebrates, raising the question of whether hydrin has a stimulatory potency in the translocation of frog AQPs to the apical membrane in the principal cells of the pelvic skin.

The aim of this thesis

The aim of this thesis is to elucidate the adaptation mechanisms of anuran amphibians to various water environments of anuran amphibians in term of the water channel, AQP. In Chapter 2, I identified the anuran orthologue of mammalian AQP2, AQP-h2K, from the kidney of the tree frog, *H. japonica*, and analyzed its functions. Furthermore, phylogenetical relationships were analyzed by comparing the primary structures of various AQP molecules, elucidating that the AQP family is composed of at least AQP0-AQP5, AQP7-AQP10, and the two anuran-specific type, designated as

AQPa1 and AQPa2. Chapter 3 reports the regulatory system of water permeability in the ventral pelvic skin in the tree frog. I examined the water permeability in the pelvic skin utilizing AVT, hydrins (intermediate peptides of pro-AVT), and β-adrenergic effectors, because both AVT and β-adrenergic neuron regulate the water permeability of the frog ventral skin. The effects of antidiuretic hormone on osmotic water transfer across anuran pelvic skin had been extensively investigated in vitro (Warburg, 2000; Bentley, 2002). Interestingly, the response to antidiuretic hormone tends to be greater in anuran species normally occupying drier habitats than those from wet habitats (Bentley, 1974, 2002). In Chapter 4, to examine the involvement of AQPs in this difference, immunoblot analysis has been performed for the tissues of five Japanese anurans. According to their habitats, they can be divided into four groups. *Xenopus laevis* is aquatic, and *Rana catesbeiana* and *R. nigromaculata* are classified into a semi-aquatic group. *B. japonicus* and *H. japonica*, which expand their habitats to the drier land, are classified as a terrestrial species and tree-adapted species, respectively. Because the antibody against *Hyla* AQP-h2 was raised and utilized in the previous experiments (Hasegawa *et al.*, 2003), this antibody was applied to Western blot analysis for other anurans. AQP-h2 and AQP-h2-like protein were detected in the urinary bladder of all the species examined. The AQP-h2 homologue was detected in the pelvic skin of the terrestrial anuran, as in the tree-adapted anuran, but not in the other species. On the other hand, the cDNA encoding AQP-h3-homolog was identified in the ventral pelvic skin of all the anurans examined, by molecular cloning (Table 1-1). Based on these results, I postulated that the AQP-h2 is the urinary bladder-type AQP, while AQP-h3 is the ventral pelvic skin-type AQP. In contrast, the skin of the aquatic clawed frog, *X. laevis*, has a much lower water permeability that reduces excessive entry of water into the body and is not stimulated by AVT (Bentely & Mains, 1972; Bentely, 1966). I found that the pelvic skin-type AQP (AQP-x3) has lost the ability of efficient protein

production, and elucidated that the extra C-terminal tail in AQP-x3 and/or 33 nucleotides encoding this tail appear to participate in the posttranscriptional regulation of AQP-x3 gene expression by attenuating protein expression. The last chapter provides a summary and discussion of the results described in this dissertation.

Table 1. Phylogenetic distribution of AQP-h2-like protein and cDNA encording AQP-h3-like protein in ventral pelvic skin and urinary bladder

Species	Habitat	AQP-h2-like protein		cDNA for AQP-h3-like protein
		Pelvic skin	Urinary bladder	Pelvic skin
Hyla japonica	arboreal	+	+	+
Bufo japonicus	terrestrial	+	+	+
Rana catesbeiana	semiaquatic	-	+	+
Rana nigromaculata	semiaquatic	-	+	+
Xenopus laevis	aquatic	-	+	+

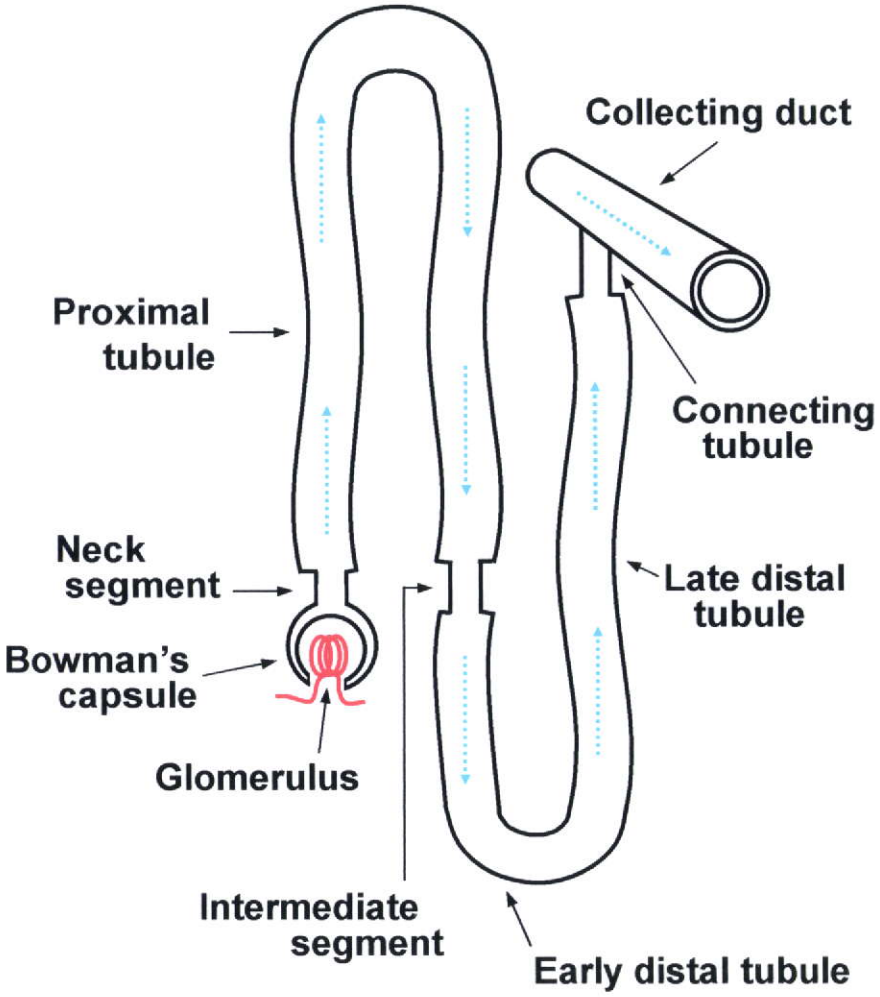

Fig. 1-1. Schematic illustration of an anuran nephron connected to a collecting duct. The anuran nephron is composed of a glomerulus, Bowman's capsule, a neck segment, proximal tubule, thin intermediate segment, early distal tubule, late distal tubule, and connecting tubule connected to the collecting duct. Blue dotted arrows depict the tubular fluid flow.

References

Agre P, Brown D, Nielsen S. (1995) Aquaporin water channels: unanswered questions and unresolved controversies. *Curr Opin Cell Biol* 7:472–483

Akabane G, Ogushi Y, Hasegawa T, Suzuki M, Tanaka S. (2007) Gene cloning and expression of an aquaporin (AQP-h3BL) in the basolateral membrane of water-permeable epithelial cells in osmoregulatory organs of the tree frog. *Am J Physiol Regul Integr Comp Physiol* 292:R2340–R2351

Bentley PJ. (1966) Adaptations of amphibia to arid environments. *Science* 152:619–623

Bentley PJ, MainAR. (1972) Zonal differences in permeability of the skin of some anuran Amphibia. *Am J Physiol* 223:361–363

Bentley PJ. (1974) Actions of neurohypophysial peptide in amphibians, replies, and birds. In: Geiger, S.R. (Ed.), Handbook of Physiology. Endocrinology IV, part 1. *Am. Physiol. Soc., Washington, pp.* 545–563

Bentley PJ, Yorio T. (1979) Do frogs drink? *J Exp Biol* 79:41–46

Bentley PJ. (1998) Hormones and osmoregulation, In: Bentley, P.J. (Ed.), Comparative Vertebrate Endocrinology, 3rd ed. Cambridge Univ., *Cambridge, pp.* 337–378

Bentley PJ. (2002) Endocrines and osmoregulation: a comparative account in

vertebrates. *Berlin: Springer, pp.* 155–186

Brown D, Grosso A, DeSousa RC. (1983) Correlation between water flow and intramembrane particle aggregates in toad epidermis. *Am J Physiol* 245: C334-342

Chevalier J, Bourguet J & Hugon J S. (1974) Membrane associated particles: distribution in frog urinary bladder epitherium at rest and after oxytocin treatment. *Cell Tissue Res* 152: 129-140

Ewer RF. (1952) The effects of posterior pituitary extracts on water balance with some general consideration of anuran water economy. *J Exp Biol* 29: 429-439

Frost DR. (2008) Amphybian species of the world: an Online Reference. Ver. 5.2 (15July,2008). Electronic Database accessible at http://research.amnh.org/herpetology/amphibia/index.php. Am Mus Nat Hist, New York

Hasegawa T, Tanii H, Suzuki M, Tanaka S. (2003) Regulation of water absorption in the frog skins by 2 vasotocin-dependent water-channel aquaporins, AQP-h2 and AQP-h3. *Endocrinology* 144:4087–4096

Hasegawa T, Suzuki M, Tanaka S. (2005) Immunocytochemical studies on translocation of phosphorylated AQP-h2 protein in granular cells of the frog urinary bladder before and after stimulation with vasotocin. *Cell Tissue Res* 322:407–415

Hillyard SD, Mobjerg N, Tanaka S, Larsen EH. (2009) Osmotic and ion regulation

in amphibians. In: Evans, D.H. (Ed.), Osmotic and Ionic Regulation: Cell and Animals. *CRC Press, Boca Raton, pp.* 367–441

Ishibashi K, KuwaharaM,Sasaki S. (2000) Molecular biology of aquaporins. *Rev Physiol Biochem Pharmacol* 141:1–32

Ishibashi K. (2006) Aquaporin superfamily with unusual npa boxes: S-aquaporins (superfamily, sip-like and subcellular-aquaporins). *Cell Mol Biol.* 52:20-7

Kachadorian WA, Wade JB, DiScala VA. (1975) Vasopressin: induced structural change in toad bladder luminal membrane. *Science* 190: 67-69

Kloas W, Hanke W. (1992) Localization and quantification of nonapeptide binding sitesin the kidney of *Xenopus laevis*: evidence for the existence of two different nonapeptide receptors. *Gen Comp Endocrinol* 85: 71–78

Lillywhite HB. (2006) Water relations of tetrapod integument. *J Exp Biol* 209: 202-226

Michel G, Ouedraogo Y, Chauvet J, Katz U, Acher R. (1993) Differential processing of provasotocin: relative increase of hydrin 2 (vasotocinyl-Gly) in amphibians able to adapt to an arid environment. *Neuropeptides* 25: 139-143

Mochida H, Nakakura T, Suzuki M, Hayashi H, Kikuyama S, Tanaka S. (2008) Immunolocalization of a mammalian aquaporin 3 homolog in water-transporting epithelial cells in several organs of the clawed toad *Xenopus laevis*. *Cell Tissue Res* 333:297–309

Ogushi Y, Mochida H, Nakakura T, Suzuki M, Tanaka S. (2007) Immunocytochemical and Phylogenetic Analyses of an Arginine Vasotocin-Dependent Aquaporin, AQP-h2K, Specifically Expressed in the Kidney of the Tree Frog, *Hyla japonica*. *Endocrinology* 148: 5891-5901

Pang PKT. (1983) Evolution of control of epithelial transport in vertebrates. *J Exp Biol* 106: 283–299

Pough FH. (2007) Amphibian biology and husbandry. *ILAR J* 48: 203-213

Rojek A, Praetorius J, Frøkiaer J, Nielsen S, Fenton RA. (2008) A current view of the mammalian aquaglyceroporins. *Annu Rev Physiol* 70: 301-327

Romer AS, Parsons TS. (1986) Urinary organs, In: Romer, A.S., Parsons, T.S. (Eds.), The vertebrate body, 6th ed. *CBS Coll. Publishing, New York, pp.* 396–417

Rouille Y, Michel G, Chauvet MT, Chauvet J. (1989) Hydrins, hydroosmotic neurohypophysial peptides: osmoregulatory adaptation in amphibians through vasotocin precursor processing. *Proc Natl Acad Sci USA* 86: 5272-5275

Suzuki T, Tanaka S. (2009) Molecular and cellular regulation of water homeostasis in anuran amphibians by aquaporins. *Comp Biochem Physiol A Mol Integr Physiol* 153:231-241

Takata K, Matsuzaki T, Tajika Y. (2004) Aquaporins: water channel proteins of the

cell membrane. *Prog Histochem Cytochem* 39:1–83

Tanii H, Hasegawa T, Hirakawa N, Suzuki M, Tanaka S. (2002) Molecular and cellular characterization of a water channel protein, AQP-h3, specifically expressed in the frog ventral skin. *J Membrane Biol* 188:43–53

Uchiyama M, Yoshizawa H. (2002) Nephron structure and immunohistochemical localization of ion pumps and aquaporins in the kidney of frogs inhabiting different environments. In: Hazon N, Flik G, eds. Osmoregulation and drinking in vertebrates. Oxford, UK: BIOS *Scientific Publishers, pp.* 109–128

Warburg MR, Rosenberg M, Roberts JR, Heatwole H. (2000) Cutaneous glands in the Australian hylid Litoria caerulea (Amphibia, Hylidae). Anat. *Embryol.* 201: 341–348

Zardoya R. (2005) Phylogeny and evolution of the major intrinsic protein family. *Biol Cell* 97:397–414

Chaptor 2

Immunocytochemical and Phylogenetic Analyses of an Arginine Vasotocin-Dependent Aquaporin, AQP-h2K, Specifically Expressed in the Kidney of the Tree Frog, *Hyla japonica*

Abstract

Water movement occurs across the plasma membrane of various cells of animals, plants, and microorganisms through specialized water-channel proteins called aquaporins (AQPs).We have identified a new member of the amphibian AQP family, AQP-h2K, from the kidneys of *Hyla japonica.* This protein consists of 280 amino acid residues with two NPA (Asn-Pro-Ala) sequence motifs and a mercury-sensitive cysteine residue just upstream from the second NPA motif. There are two putative N-linked glycosylation sites at Asn-120 and Asn-128 and one protein kinase A phosphorylation site at Ser-262. The AQP-h2K protein was specifically expressed in the apical membrane and/or cytoplasm of principal cells in the kidney collecting ducts. After stimulation with arginine vasotocin, it was translocated from the cytoplasmic pool to the apical membrane. Phylogenetic analysis of AQP proteins from anurans and mammals identified six clusters of anuran AQPs: types 1, 2, 3, and 5 and two anuran-specific types, designated a1 and a2. The cluster AQPa2 contains *Hyla* AQP-h2 and AQP-h3, which are expressed in the anuran urinary bladder and ventral pelvic skin. AQP-h2K belongs to the type 2, together with mammalian (human and mouse) AQP2, suggesting that AQP-h2K is an anuran ortholog of the neurohypophysial hormone-regulated mammalianAQP2 and that theAQP2 molecule is already present in the anuran mesonephros. (*Endocrinology* 148: 5891–5901, 2007)

Introduction

ANURAN AMPHIBIANS (frogs and toads), the most numerous order of the Amphibia, are widely distributed throughout the world and have adapted to a wide range of water environments. Adult anurans, with the exception of some totally aquatic species, are constantly exposed to the risk of water evaporation through their thin skin when on dry land. To adapt to their habitats, they have developed various complicated osmoregulatory systems for maintaining their water balance. Most adult anurans do not drink through their mouth; rather they absorb it through the ventral pelvic skin which, compared with that of other tetrapods, is highly permeable to water, respiratory gases, and some solutes (Bentley *et al.*, 1972; Bentley *et al.*, 1979). Water is also reabsorbed from the urine in the adult anuran urinary bladder in response to arginine vasotocin (AVT; the nonmammalian vertebrate counterpart of vasopressin). The amphibian kidney consists of eight morphologically distinguishable parts: a glomerulus, neck segment, proximal tubule, thin intermediate segment, early distal tubule, late distal tubule, connecting tubule, and collecting duct (Uchiyama *et al.*, 2002). Whereas some of the water filtrated through the glomerulus is considered to be reabsorbed from the nephron in the kidney, to date no amphibian kidney has been observed to produce hyperosmotic urine, possibly because the Henle's loop, a U-shaped medullary portion of the nephron, is not developed to the same extent as in birds and mammals (Bentley, 2002). However, there have been reports of significant amounts of water being reabsorbed from the renal tubule of the amphibian kidney in response to AVT (Sawyer, 1957) or noradrenaline (Gallardo *et al.*, 1980, Pang *et al.*, 1982). These results have been supported by the study by Uchiyama (Uchiyama, 1994) showing the possible presence of V2-type AVT receptors in the microdissected connecting tubule of the nephron of bullfrogs based on increases in cAMP levels in response to AVT. However, it has remained an open question whether an appreciable amount of water is reabsorbed

from the kidney during rehydration because the water taken up and discharged from the kidney accumulates in and is reabsorbed from the urinary bladder (Steen, 1929). Aquaporin (AQP) proteins are a class of integral membrane proteins that form selective water channels (pores) in the plasma membranes of various cells of animals, plants, and microorganisms. There is, however, a subfamily of AQPs, termed aquaglyceroporins, which form membrane pores that are permeated by certain small solutes, such as glycerol and urea. To date, 13 isoforms of AQPs (AQP0-AQP12) have been identified in mammals and characterized by cloning and sequencing of their cDNA (Ishibashi *et al.*, 2000, Takata *et al.*, 2004). We previously cloned cDNAs encoding three distinct AQPs (AQP-h1, AQP-h2, and AQP-h3) from the ventral pelvic skins of *Hyla japonica* (Tanii *et al.*, 2002; Hasegawa *et al.*, 2003). AQP-h1 was found to be homologous to mammalian AQP1 and showed a ubiquitous tissue distribution, AQP-h2 protein was expressed in the ventral pelvic skin and urinary bladder but not in the kidney, whereas AQP-h3 displayed a specific distribution that was restricted to the ventral pelvic skins. As for *H. japonica*, therefore, water is absorbed from the apical membrane of granular cells in the ventral pelvic skins and from the urinary bladder through the mediation of AQP-h2 together with AQP-h3 or by AQP-h2 alone, respectively. In the granular cells, these proteins are translocated to the apical membrane from the cytoplasmic pools in response to stimulation by AVT (Hasegawa *et al.*, 2003; Hasegawa *et al.*, 2005). In addition, AQP-h3BL, which was found to be homologous to mammalian AQP3, is expressed in the basolateral plasma membrane of these cells, thereby potentially forming the exit channel-proteins for the passage of water (Akabane *et al.*, 2007). Taken together, these findings provide solid evidence for both AQP-h2 and AQP-h3 dependence on AVT stimulation. However, immunofluorescence and Western blot staining did not reveal the presence of AQP-h2 or AQP-h3 proteins in the kidney (Tanii *et al.*, 2002, Hasegawa *et al.*, 2003). We report here the identification of a new member

of the amphibian AQP family, AQP-h2K, which has been isolated from the kidneys of *H. japonica*. This protein is predominantly expressed in apical plasma membrane or cytoplasm of the collecting duct cells. We also examined phylogenetic relationships among the three AVT-dependent AQPs in the tree frog, AQP-h2, AQP-h3, and AQP-h2K. Bayesian and neighbor-joining analyses revealed that AQP-h2K belongs to the same cluster as mammalian AQP2, whereas AQP-h2 and AQP-h3 belong to an anuran-specific AQPa2 cluster.

Materials and Methods

Animals

Adult tree frogs (*H. japonica*) were captured in a field near our university (Shizuoka University, Shizuoka, Japan), kept under laboratory conditions, and fed crickets. The animals were 2–2.5 cm long (body length) and weighed 1.0 –1.3 g; sex was not considered to be a relevant factor in our experiments. The kidneys were removed from anesthetized animals (MS 222; Nacalai tesque, Kyoto, Japan) for processing and subsequent use in cDNA cloning experiments. The animals were then killed, and various tissues, the kidney, urinary bladder, ventral pelvic skin, dorsal skin, heart, muscle, liver, lung, brain, testis, and ovary, were removed for analysis by RT-PCR and immunocytochemistry. All animal experiments were carried out in compliance with the Guide for Care and Use of Laboratory Animals of Shizuoka University.

Oligonucleotide design

The sense primer and antisense primer used for cloning *Hyla* AQPh2K are given in Table 1.

Cloning of the partial-length cDNA

The kidneys were used for total RNA preparation. The dissected kidneys were immediately frozen in liquid nitrogen, and total RNA was extracted with TRIZOL RNA extraction reagent (Invitrogen, Tokyo, Japan). RT-PCR was performed using Moloney-murine leukemia virus (M-MLV) reverse transcriptase (RT; Invitrogen) according to the manufacturer's instructions. PCR was performed using primers 1 and 2, as described previously (Akabane *et al.*, 2007). The PCR products were purified after gel electrophoresis and sequenced using an Aloka DNA sequencer [Model Lic-4200L(S); Aloka Co., Ltd., Tokyo, Japan]. *3' and 5' rapid amplication of cDNA ends (RACE)* The RACE technique was used to obtain the full-length *Hyla* AQPh2K mRNA sequence. For 3'-RACE, poly(A)$^+$ RNA was isolated from the total RNA using oligo-dT-coated latex beads (Oligotex-dT30 super; Takara, Kyoto, Japan) according to the manufacturer's instructions. Isolated RNA was primed with oligo-dT19 adaptor primer and reverse transcribed using M-MLV RT. A 1-μl aliquot of the RT product was then PCR amplified with primer 1 and the adaptor primer; subsequent amplification was performed using the 3' primer and the adaptor primer. After denaturation at 95 C for 5 min, PCR amplification program consisted of five cycles of 60 sec at 94 C, 60 sec at 60 C, and 90 sec at 72 C; five cycles of 60 sec at 94 C, 60 sec at 58 C, and 90 sec at 72 C; five cycles of 60 sec at 94 C, 60 sec at 56 C, and 90 sec at 72 C; and 15 cycles of 60 sec at 94 C, 60 sec at 55 C, and 90 sec at 72 C. The obtained clone was sequenced as described above. For 5'-RACE, poly(A)$^+$ RNA was primed with primer 2 and reverse transcribed using the M-MLV-RT. This first-strand cDNA was purified with a QIA Quick PCR purification kit (QIAGEN, Hilden, Germany), and a poly(A) tail was synthesized at the 3' terminus of the cDNA with 1 mm dATP and 0.8 U/20 μl of terminal deoxynucleotidyl transferase (Toyobo, Osaka, Japan). After the resultant cDNA was purified once again using the same kit, the second cDNA was synthesized

with Ex Taq polymerase (1.25 U/50 μl) and oligo-dT19 adaptor primer sequentially for 5 min at 93 C, 90 sec at 42 C, and 3 min at 72 C. A 1-μl aliquot of second-strand cDNA was then amplified by PCR with the 5' primer and the adaptor primer. This product was then amplified by PCR with the 5' nested primer and adaptor primer. These PCR amplifications were carried out under conditions identical with those described for the 3' RACE-PCR. The obtained clone was sequenced as described above. *Phylogenetic analysis* The amino acid sequences of human, mouse, and anuran AQPs were aligned using ClustalW(http://bioweb.pasteur.fr/seqanal/interfaces/ clustalw.html) (Thompson *et al.*, 1994), and alignment parameters were set according to an instruction manual by Hall (Hall, 2004), *e.g.* Gonnet 250 for protein weight matrix, 35 for the gap opening penalty, and 0.75 for the gap extension penalty in the pairwise alignment, and Gonnet series for protein weight matrix, 15 for the gap opening penalty and 0.3 for the gap extension penalty in the multiple alignment. An unrooted tree was generated by the Bayesian method (Mau *et al.*, 1999), using the MrBayes program version 3.1.2 (http://www.mrbayes.csit.fsu.edu/index.php) (Ronquist *et al.*, 2003). Metropolis-coupled Markov Chain Monte Carlo sampling was conducted for 2 million generations (four simultaneous Metropolis-coupled chains; sample frequency 100 generations; chain temperature 0.2) under the JTT (Jones *et al.*, 1992) +Γmodel. Among the sampled 20,000 trees, the first 5,000 trees were discarded as burnin, and the subsequent trees were used to construct a 50% majority-rule consensus tree. The credibility of clades was evaluated using Bayesian posterior probabilities. Another unrooted tree was inferred by the neighbor-joining (NJ) method (Saitou *et al.*, 1987) in the PAUP program version 4.0 β-10 (Sinauer Associates, Inc., Sunderland, MA). The mean character difference was used to estimate the evolutionary distance. Confidence in the NJ tree was assessed with 10,000 bootstrap replications (Felsenstein, 1985) and used to construct a 50% majority-rule consensus tree.

Antibodies

An oligopeptide corresponding to the C-terminal amino acids 269–280 (ST-202: QTIPRSGMTEKV) of the *Hyla* AQP-h2K, with an aminoterminal cysteine residue, was synthesized on a model 433A synthesizer (PE Applied Biosystems, Foster City, CA.). The crude peptide was purified by reverse-phase HPLC with a 0–60% linear gradient of CH_3CN in 0.1% trifluoroacetic acid. Purification of the peptide was confirmed by measuring its molecular mass by mass spectrometry. The antibody was raised in a rabbit or guinea pig immunized with the ST-202 peptide coupled to keyhole limpet hemocyanin (Pierce, Rockford, IL), as described previously (Tanaka *et al.*, 1992). Similarly, an antibody against *Hyla* AQP-h1 (Tanii *et al.*, 2002) was raised in rabbits using the C-terminal amino acids 256–269 [ST-153: (C)EYELDGEDARMEMK] as antigen. The rabbit anti-*Hyla* AQP-h3BL (15Akabane *et al.*, 2007) and bullfrog vacuole proton ATPase E-subunit (V-ATPase) (Yajima *et al.*, 2007) sera had been generated and characterized previously. *RT-PCR of Hyla tissue* The tissue expression of AQP-h2K mRNA was analyzed by RT-PCR. TRIZOL reagent was used to prepare total RNA from various *Hyla* tissues. Total RNA (20 μg) was first treated with DNase I (4 U; Takara), after which a 10-μg aliquot of the total RNA product was reverse transcribed at 37 C for 1 h and then at 52 C for 30 min in 20 μl of reaction buffer containing 1 mm of each deoxynucleotide triphosphate, 9.9 U M-M-LV RT (Takara), 20 U RNase inhibitor (Toyobo), and 7.5 mm oligo-dT19 primer (Operon, Tokyo, Japan). RT-PCR was performed basically by the same method described above, using primers 1 and 2. The RT-PCR products were analyzed on a 2% agarose gel containing ethidium bromide (0.5 μg/ml). Marker 6 (λ/Sty1 digest; Wako Pure Chemicals, Osaka, Japan) was used as the molecular-weight marker. *Osmotic water permeability of oocytes* The full-length *Hyla* AQP-h2K cDNAwas produced by

RT-PCR using the Kozak sequence with *Hyla* AQP-h2K-specific primer (GCCACCATGATGATGTCAGAC) and *Hyla* AQP-h2K-specific primer with poly$(A)_{25}$ [$(T)_{25}$GGTGTATTTACCAGATACC]. The product of the PCR amplification was cloned into the pGEM-5Z vector (Promega, Madison, WI). cRNAs were prepared from linearizedpGEM-5Zvectors containing the entire open reading frame of AQP-h2K by digestion with *Apa*I (Takara), followed by transcription and capping with SP6 RNA polymerase (mCAP RNA capping kit; Stratagene, La Jolla, CA). Stage V and VI *Xenopus* oocytes were defolliculated by collagenase (1 mg/ml; Roche Molecular Biochemicals, Meylan, France), microinjected with either cRNAs (50 ng) or water, and incubated for 3 d inBarth's buffer at 18 C, after which they were transferred from 200 mOsm to 70 mOsm Barth's buffer. The osmotically elicited increase in volume was monitored at 24 C under a BX50 microscope (Olympus, Tokyo, Japan) with a ·4 magnifying objective lens and a chargecoupled device camera connected to a computer. The coefficient of osmotic water permeability (Pf) was calculated from the initial slope of oocyte swelling according to accepted methodology (Fushimi *et al.*, 1993, Zhang *et al.*, 1990). In some experiments, AQP cRNA-injected oocytes were incubated with 0.3mM $HgCl_2$ for 10 min. To confirm whether AQP-h2K protein was expressed in *Xenopus* oocytes after the injection of AQP-h2K cRNA, we evaluated AQP-h2K cRNA injected or water-injected oocytes by Western blot analysis and immunostaining as described below.

Western blot analysis

The AQP-h2K cRNA-injected oocytes were homogenized in cell lysis buffer [50 mM Tris-HCl (pH 8.0), 0.15 m NaCl, 1% Triton X-100, 0.1 mg/ml phenylmethylsulfonyl fluoride, 1 μg/ml aprotinin] and centrifuged at 12,000 rpm in a microcentrifuge for 10 min to remove insoluble materials. The protein (10 μg) was

denatured at 70 C for 10 min in denaturation buffer comprising 3% sodium dodecyl sulfate, 70 mM Tris-HCl (pH 6.8), 11.2% glycerol, 5% 2-mercaptoethanol, and 0.01% bromophenol blue; subjected to electrophoresis on a 12% polyacrylamide gel; and then transferred to an Immobilon-P membrane (Millipore, Tokyo, Japan). The proteins on the membrane were reacted sequentially with rabbit anti-AQP-h2K (ST-202) serum diluted at 1:5000, biotinylated goat antirabbit IgG (Dako Japan, Kyoto, Japan), and streptavidin-conjugated horseradish peroxidase (Dako Japan). The reaction products on the membrane were visualized using an ECL Western blot detection kit (Amersham Pharmacia Biotech, Buckinghamshire, UK). To check the specificity of the immunoreaction, we performed an absorption test by preincubating anti-AQP-h2K (ST-202) with the antigen peptide (10 μg/ml). To determine whether the immunoreactive proteins were glycosylated, we treated the extracts from the cRNA-injected oocytes at 37 C with peptide-*N*-glycosidase F (Daiichi Pure Chemicals, Tokyo, Japan) before SDS-PAGE and Western blot in accordance with the manufacturer's instructions.

Immunofluorescence

The kidney, urinary bladder, and testis were fixed overnight at 4 C in periodate-lysine-paraformaldehyde fixative, dehydrated, and embedded in Paraplast. Thin (4 μm) sections were cut and mounted on gelatincoated slides, deparaffinized, and rinsed with distilled water and PBS. For single labeling of AQP-h2K or AQP-h1 protein, immunofluorescence staining was performed essentially as described previously (Tanaka *et al.*, 1997). The sections were sequentially incubated with 1% BSA-PBS, rabbit anti-AQP-h2K serum (1:2000), or rabbit anti-AQP-h1 serum (1:5000), and indocarbocyanine (Cy3)-labeled affinity-purified donkey antirabbit IgG (1:400; Jackson ImmunoResearch, West Grove, PA). For nuclear counterstaining, 4',

6-diamidino-2-phenylindole (DAPI) was included in the secondary antibody solution. The sections were finally washed with PBS and then mounted in PermaFluor (Immunon, Pittsburgh, PA). The specificity of the immunostaining was checked using an absorption test by preincubating the anti-AQP-h2K or anti-AQP-h1 antiserum with the corresponding antigen peptide (10 μg/ml). For double-immunofluorescence staining for AQP-h2K and AQP-h3BL, sections were first incubated with a mixture of guinea pig anti-AQP-h2K (1:2000) and rabbit anti-AQP-h3BL (ST-184: 1:2000) (Akabane *et al.*, 2007) and then reacted with a mixture of Alexa488-labeled goat anti-guinea pig IgG (1:200) and Cy3-labeled donkey antirabbit IgG (1:400; Jackson), and DAPI. Tree frogs, which had been immersed in a container filled with water for 30 min, were used in the stimulation experiments with AVT. The frogs were injected with 50 μl saline or 10^{-6} M [Arg $^{(8)}$]-AVT dissolved with saline (Peptide Institute, Osaka, Japan), and 15 min after the injection, the kidneys were fixed with the same fixative solution for examination by immunofluorescence microscopy. Some sections were double stained for both AQP-h2K and bullfrog V-ATPase (Yajima *et al.*, 2007) to identify the parts of a nephron. Specimens were examined with an Olympus BX61 microscope equipped with a BX-epifluorescence attachment (Olympus Optical, Tokyo, Japan).

Statistical analysis

Student's *t* test or the Cochran-Cox test for nonhomogeneous data were used for analyzing the results.

Results

cDNA cloning of Hyla AQP-h2K

Figure 2-1A shows the full-length cDNA sequence of *Hyla* AQP-h2K and deduced amino acids. The cDNA consisted of a 45-bp 5'-untranslated region and a

encoded a protein of 280 amino acids with a relative molecular mass calculated to be 30,531 Da. Hydropathy analysis predicted six transmembrane regions with an N terminus and a C terminus located in the cytoplasm, which is similar to other major intrinsic proteins family members (Fig. 2-1B). There were two putative N-linked glycosylation sites at Asn-120 and Asn-128, one protein kinase C phosphorylation at Ser-236, and one protein kinase A phosphorylation site at Ser-262 in the predicted amino acid sequence of AQP-h2K. The amino acid sequence also contained the conserved Asn-Pro-Ala (NPA) motif found in all major intrinsic protein family members as well as a cysteine just upstream from the second NPA motif. This full-length cDNA sequence has been deposited in DDBJ/ EMBL/GenBank (accession no. AB295642).

Phylogenetic analysis of amphibian

AQPs Hyla AQP-h2K showed the highest degree of amino acid sequence similarity to AQP2 (HC-2) of *H. chrysoscelis* (97%) (Zimmerman *et al.*, 2007), followed by a high degree of similarity to mammalian AQP2 (69%), including that of mouse, rat, and human. In addition, *Hyla* AQP-h2K showed sequence similarity to *Xenopus* AQP (61%; AAN75455), *Bufo marinus* AQP-t2 (60%; AAC6994), *Hyla* AQP-h2 (58%) (Hasegawa *et al.*, 2003), AQP-h3 (57%) (Tanii *et al.*, 2002), and *B. marinus* AQP-t3 (57%; AAC69695). Bayesian phylogenetic analysis of 25 mammalian AQPs and 19 anuan AQPs suggests that anuran AQPs are divided into six clusters, *i.e.* types 1, 2, 3, and 5 and two anuran-specific types, designated as a1 and a2 (the letter a represents anuran) (Fig. 2-2). The cluster AQPa1 comprises AQPxlo from *Xenopus laevis* oocytes (Virkki *et al.*, 2002) and another *X. laevis* AQP (BC090201). The cluster AQPa2 is composed of AQP-h2 (Hasegawa *et al.*, 2003) and AQP-h3 (Tanii *et al.*, 2002) from the tree frog, *H. japonica*, and AQP-t2 (AF020621) and AQP-t3

(AF020622) from the toad, *B. marinus*. Interestingly, the cluster AQP2 contains not only mammalian AQP2 but also AQP-h2K from *H. japonica* and AQP HC-2 from *H. chrysoscelis* (Zimmerman *et al.*, 2007). Anuran AQP1 molecules cloned from several frogs, including *Hyla* (AQP-h1; AB073315) and *Rana* (FACHIP) (Abrami *et al.*, 1994), belong to the cladeAQP1together with mammalian AQP1. The clade AQP3 consists of *Hyla* AQP-h3BL (Akabane *et al.*, 2007), *Xenopus* AQP3(AJ131847), and *Hyla* HC-3 (Felsenstein, 1985) as well asmammalian AQP3. The clade AQP5 comprises AQPs from *Xenopus* (AQPx5) (Kubota *et al.*, 2006) and *Bufo* (AQP-t4; AF020623) in addition to mammalian AQP5. NJ analysis corroborates the classification of anuran AQPs into six types (Fig. 2-3; data not shown for types 1, 3, or a1) and close relationships among AQP0, AQP2, AQP5, AQP6, and AQPa2 (Fig. 2-3).

Distribution of Hyla AQP-h2K mRNA expressed in various tissues

The distribution of *Hyla* AQP-h2K mRNA expression in various tissues was investigated by means of RT-PCR using total RNA from these tissues. AQP-h2K mRNA was observed in the kidney, urinary bladder, and testis but not the ventral pelvic skin (Fig. 2-4).

Expression of Hyla AQP-h2K in Xenopus oocytes

Transmembrane water flow through the *Hyla* AQP-h2K protein was evaluated by an expression analysis in *Xenopus* oocytes. After 3 d of incubation at 18 C, the oocytes were transferred from isotonic (200 mOsm) to hypoosmotic (70 mOsm) Barth's solution: swelling was monitored by means of a microscope with an attached charge-coupled device camera, and the Pf was calculated (Fig. 2-5A). The Pf of AQPh2K-injected oocytes was approximately 4-fold higher than that of water-injected oocytes. The stimulated water permeability was also significantly inhibited by 0.3mM

$HgCl_2$ (Fig. 2-5, A and B). When sections of the AQP-h2K cRNA-injected oocytes were immunostained with anti-*Hyla* AQP-h2K, an intense immunopositive reaction was observed in the plasma membrane (Fig. 2-5 C-1 and -2). The immunopositive sites were completely abolished by preabsorption of the antiserum with 10 μg/ml of the immunogen peptide (Fig. 2-5 C-3). In addition, no labels were observed in the water-injected oocytes (Fig. 2-5 C-4). To test the specificity of the antiserum toward the kidney, we conducted Western blot analysis of their membrane extracts. Because the ST-202 antiserum did not detect any bands in the kidney membrane extract (data not shown), we conducted a Western blot analysis using the extract of AQP-h2K cRNA-injected oocytes and found a major band at approximately 31 kDa and a weak smear band between 41 and 60 kDa (Fig. 2-5D, lane 1). The bands described above were not detected when anti-*Hyla* AQP-h2K was preabsorbed with the peptide used as the immunogen (Fig. 2-5D, lane 2). After digestion with peptide-*N*-glycosidase F, the smear band at 41–60 kDa became a band of 31 kDa, suggesting that the bands of apparent higher molecular mass represented glycosylated forms of the 31-kDa *Hyla* AQP-h2K protein (Fig. 2-5, lanes 3 and 4).

Localization of Hyla AQP-h2K in the kidneys

The anuran nephron is divided into eight parts, among which are the glomerulus, proximal tubule, late distal tubule, collecting duct, and neck segment (Uchiyama *et al.*, 2002). The collecting ducts consist of a monolayer of columnar epithelial cells, with the basal side surrounded by a thin connective tissue. When kidney sections were immunolabeled with anti-AQP-h2K, the labels were observed in the collecting ducts only (Fig. 2-6, A–C). The immunopositive labels were abolished at the background levels when the frog kidney sections were labeled with the preabsorbed antiserum with the antigen (10 μg/ml) (Fig. 2-6D). When sections of the kidneys from the tree frogs

kept in water were labeled with anti-*Hyla* AQP-h2K, the punctate labels were found throughout the cytoplasm (Fig. 2-7, A, C, and E). Conversely, after the stimulation of the tree frogs under the same conditions by AVT, the intense labels were found only in the apical plasma membrane of the collecting ducts (Fig. 2-7, B, D, and F). In addition, positive labels for AQP-h2K were not found in any of the cells of the urinary bladder (Fig. 2-8, A–C) and testes (Fig. 2-8, D–F). In the urinary bladder, all of the cells were found to react with the anti-serum (Fig. 2-8, A and B), but similar labels were seen in the sections of the preabsorbed test of antiserum (Fig. 2-8C). The labels were also visible in interstitial cells of the testicular stroma (Fig. 2-8, D and E), but the labels were not diminished in the cells of the testes (Fig. 2-8F) when anti-AQP-h2K is preabsorbed with the corresponding antigen peptide, indicating that these labels are nonspecific. *Hyla* AQP-h3BL, which is expressed specifically in the basolateral plasma membrane of water-permeable epithelial cells from *H. japonica* (Akabane *et al.*, 2007), was found to be expressed in a similar manner in the basolateral plasma membrane of the collecting duct principal cells in the presence and absence of AVT stimulation (Fig. 2-9, A and B). The cells showing V-ATPase were scattered throughout the epithelium of the collecting ducts and were unlabeled for AQP-h2K (Fig. 2-9, C and D). *Hyla* AQP-h1 was detected in the endothelial cells around the proximal tubules and the flattened cells of the parietal layer of Bowman's capsule but not in principal cells of the proximal tubules (Fig. 2-10, A, B, and D). The labels were abolished at the background levels when the antiserum was preincubated with the antigen peptide (Fig. 2-10C).

Discussion

We report here the full-length sequence of an mRNA encoding a novel AQP, AQP-h2K, that is specifically expressed in the principal cells of the collecting ducts of tree frogs. This AQP, denoted AQP-h2K, has been structurally characterized as having

two NPA motifs, two putative N-glycosylated sites, a cysteine at a mercurial sensitivity site just upstream of the second NPA motif, and six putative transmembrane domains. AQP-h2K also has a putative phosphorylation site by protein kinase A at Ser-262, which is identical with that of mammalian AQP2 (Brown *et al.*, 1998). The amino acid sequences of *Hyla* AQP-h2 and *Hyla* AQP-h3, both of which were cloned in previous studies, also contain a putative phosphorylation site recognized by protein kinase A (Tanii et al., 2002; Hasegawa et al., 2003). Phosphorylations are considered to play an important role in the trafficking of mammalian AQP2 and *Hyla* AQP-h2 to the apical plasma membrane (Hasegawa *et al.*, 2005; Denker *et al.*, 1988; Sabolic *et al.*, 1992). Accordingly, AQP-h2K, similar to *Hyla* AQP-h2 and AQP-h3, might be translocated from the cytoplasmic pools to the apical plasma membrane by AVT. The homology analysis revealed that the deduced amino acid sequence of AQP-h2K has a high degree of similarity to mammalian AQP2 and a moderate similarity to AQP-h2 and AQP-h3. The present Bayesian and NJ phylogenetic trees suggested evolutionary relationships between anuran AQPs and mammalian AQPs (Figs. 2-2 and 2-3). Previously we depicted an unrooted phylogenetic tree of these AQPs, which had been inferred by the NJ method (Suzuki *et al.*, 2007). These three phylogenetic trees show partially different topologies due to the difference in the analytical algorithm, amino acid substitution model, and/or parameter for sequence alignment. For instance, amino acid substitution models and parameters for sequence alignment are different between the previously reported NJ tree and the present NJ tree. The former tree was constructed with the default setting in the ClustalWprogram version 1.83 (http://clustalw.ddbj.nig.ac.jp/top-j.html) (Thompson *et al.*, 1994), *i.e.* Kimura's distance (Kimura, 1983) was adopted as amino acid substitution model in tree inference after the amino acid sequences of the AQPs were aligned with Blosum (Henikoff *et al.*, 1992) for protein weight matrix and 10 for the gap opening penalty and 0.1 for the gap

extension penalty in the pairwise alignment and with Blosum (Henikoff *et al.*, 1992) for protein weight matrix, 10 for the gap opening penalty, and 0.2 for the gap extension penalty in the multiple alignment (Suzuki *et al.*, 2007). On the other hand, the latter tree was inferred as described in *Materials and Methods*. The three phylogenetic trees are thus constructed under different conditions, but all the trees indicate that the hitherto reported anuran AQPs can be classified into six clusters: types 1, 2, 3, 5, a1, and a2 (Figs. 2-2 and 2-3) (Suzuki *et al.*, 2007). *Hyla* AQP-h2K is assigned to the type 2 together with mammalian AQP2, whereas both AQP-h2 and AQP-h3 belong to the type a2, suggesting that AQP-h2K is an anuran ortholog of mammalian AQP2, whereas AQP-h2 and AQP-h3 are paralogs of mammalian AQP2. *Xenopus* oocytes showed a significant increase in water permeability in the presence of AQP-h2K and an inhibition in water permeation in the presence of $HgCl_2$. Although this inhibitory action of $HgCl_2$ is inconsistent with the results reported on AQP2 (HC-2) of *H. chrysoscelis* by Zimmerman *et al.* (Zimmerman *et al.*, 2007), they would seem to be logical, given the fact that *Hyla* AQP-h2K protein contains a mercury-sensitive cysteine residue just upstream from the second NPA motif. Western blot analysis and digestion experiments with peptide-*N*-glycosidase F of AQP-h2K cRNA-injected oocytes showed one band at approximately 31 kDa and smear band at 41–60 kDa, indicating that the smear band is glycosylated forms. In contrast, Western blot analysis of the extract of *Hyla* kidneys did not produce a positive reaction, even when the membrane extracts of the kidneys, prepared with the ultracentrifuge or the Native membrane protein extract kit, were used (data not shown). This may be because the principal collecting duct cells expressing AQP-h2K protein occupy a very small area of the kidney. RT-PCR analyses on the expression of AQP-h2K mRNA in various *Hyla* tissues revealed that AQP-h2K was expressed in the kidney, urinary bladder, and testis. The immunofluorescence study demonstrated that AQP-h2K protein was localized in the apical plasma membrane or

cytoplasm of the principal cells of the kidneys *in situ* but that it was not present in the urinary bladder and testes, even though RT-PCR had detected AQP-h2K mRNA in the latter two organs. This finding suggests that AQP-h2K protein is not translated in the urinary bladder and testes. Because mammalian AQP1 is located in the principal cells of the kidney proximal tubules, which consequently reabsorb water constitutively (Denker *et al.*, 1988, Sabolic *et al.*, 1992, Nielen *et al.*, 1993, Maunsbach *et al.*, 1997), we investigated the localization of *Hyla* AQP-h1 in the anuran kidney by immunolocalization. *Hyla* AQP-h1 was not detectable in any of the cells of the proximal tubules. Anuran amphibian kidney is mesonephric, whereas the mammalian kidney is metanephric, and this difference may be derived from a shift from the mesonephros to metanephros during development. Two water transport pathways have been proposed for the salivary acinar cells of mammals: the paracellular and transcellular routes (Kawedia *et al.*, 2007). However, because water is considered not to be reabsorbed in the proximal tubules of anuran kidney and most of the reabsorbed water is stored in the urinary bladder (Steen, 1929), only AVT-dependent AQP, AQP-h2K, may be active in reabsorbing water in the kidney of anuran amphibians. Immunolocalization of *Hyla* AQP-h2K in the frog kidneys after AVT treatment resulted in enhanced signals for AQPh2K on the apical plasma membrane of the principal cells of the kidney collecting ducts. In mammals, AQP2 is involved in the reabsorption of water in the collecting duct of the kidney (Fushimi *et al.*, 1993; Klussmann et al., 2000) and is expressed in the apical plasma membrane and cytoplasm just beneath the apical membrane (Fushimi *et al.*, 1993; Nielsen *et al*, 1993). In response to antiduiric hormone (ADH), mammalian AQP2 is translocated from the cytoplasmic pool to the apical membrane, thereby enhancing the water permeability of the membrane (Nielsen *et al*, 1993, Nielsen *et al.*, 1995); conversely, in the nonstimulated condition, AQP2 is removed from the apical membrane by endocytosis, thereby decreasing water

permeability (Nielsen *et al.*, 1995). Thus, mammalian AQP2 is considered to be an ADH-regulated AQP. In the present study, we obtained data indicating that AQP-h2K resides in the vesicles distributed throughout the entire cytoplasm in the nonstimulated condition and that it is translocated to the apical plasma membrane in response to AVT. Based on these results, we propose that *Hyla* AQP-h2K is a water-channel molecule that is regulated in response to AVT. Several lines of evidence have shown that protein kinase A phosphorylation at the consensus Ser-256 is a necessary condition for the migration of mammalian AQP2 from the intracellular membrane vesicles to the apical plasma membrane (Kuwahara *et al.*, 1995; Fushimi *et al.*, 1997; Van Balkom *et al.*, 2002). Because there is a protein kinase A site at Ser-262 in AQP-h2K, phosphorylation at this site may be necessary for the translocation of AQP-h2K protein to the apical plasma membrane. We have previously shown that in the granular cells of the urinary bladder, *Hyla* AQP-h2 is phosphorylated in the vesicles within 2 min of AVT stimulation and subsequently translocated to the apical membrane of these same cells (Hasegawa *et al.*, 2005). Similar events may occur with *Hyla* AQP-h2K. Taken together, our present and previous data (Tanii *et al.*, 2002; Hasegawa *et al.*, 2003) demonstrated that an AVT-dependent AQP is expressed in the collecting ducts of the kidney of *H. japonica* and that there are three distinct types of AVT-dependent AQPs in this tree frog: AQP-h2, AQP-h3, and AQP-h2K. These AQPs show different tissue distribution and seem to play important roles in the hormone-dependent water transport in three anuran osmoregulatory organs: AQP-h2 and AQP-h3 in the ventral pelvic skin, AQP-h2 in the urinary bladder, and AQP-h2K in the kidney.

Acknowledgement

We are grateful to Dr. S. Hyodo (Ocean Research Institute, University of Tokyo) for his valuable advice on phylogenetic analysis.

Table 2-1
Primers used for cloning and PCR analysis of *Hyla* AQP-h2K sequence

Name	Primer sequence	
AQP-h2K		
primer 1	5'-CCTTACTGTTTCCATGATGATAGTC-3'	32 – 57 bp
primer 2	5'-TCTGTACTTCTTCTCTCTCAGAC-3'	882 – 905 bp
adaptor primer	5'-GACTCGAGTCGACATCGAT-3'	
3' RACE primer		
3' primer	5'-TCGGCTATATAAGTGGTGCC-3'	236 – 255 bp
5' RACE primer		
5' primer	5'-TGTCACTGACAGTCCAATGG-3'	538 – 559 bp
5' nested primer	5'-AAGGAAATCTGAGAGCCCAC-3'	288 – 308 bp
β-actin		
β-actin primer 1	5'-TACCTCATGAAGATCCTGACC-3'	562 – 582 bp
β-actin primer 2	5'-TGATCCACATCTGCTGGAAGG-3'	1052 – 1072 bp

A

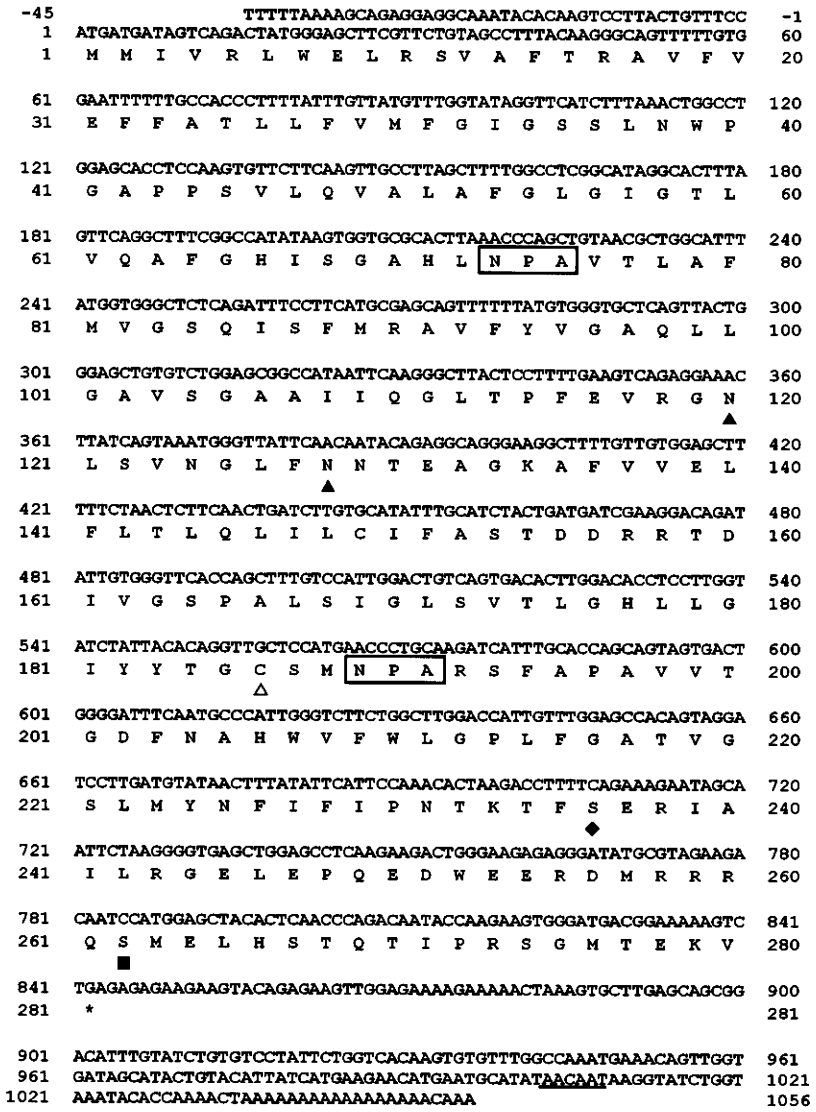

B

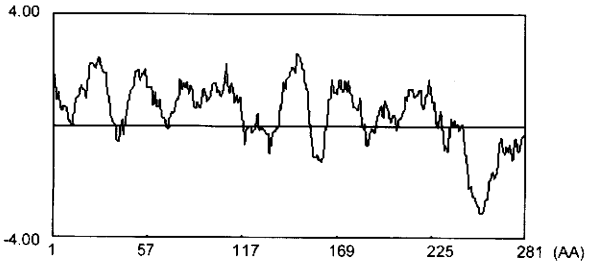

FIG. 2-1. A, Nucleotide and deduced amino acid sequence of aquaporin (*Hyla* AQP-h2K) cDNA. The predicted amino acid is shown below the nucleotide sequence (DDBJ/EMBL/GenBank accession no. AB295642). The *asterisk* indicates the terminal codon. NPA motifs are outlined. The *solid triangle* indicates a putative N-glycosylation site. The *diamond*, *square*, and *open triangle* indicate phosphorylation sites for protein kinase C and protein kinase A and the mercurial-inhibition site, respectively. **B**, Kyte-Doolittle hydropathy profile (window 11) of the deduced AQP-h2K amino acid sequence.

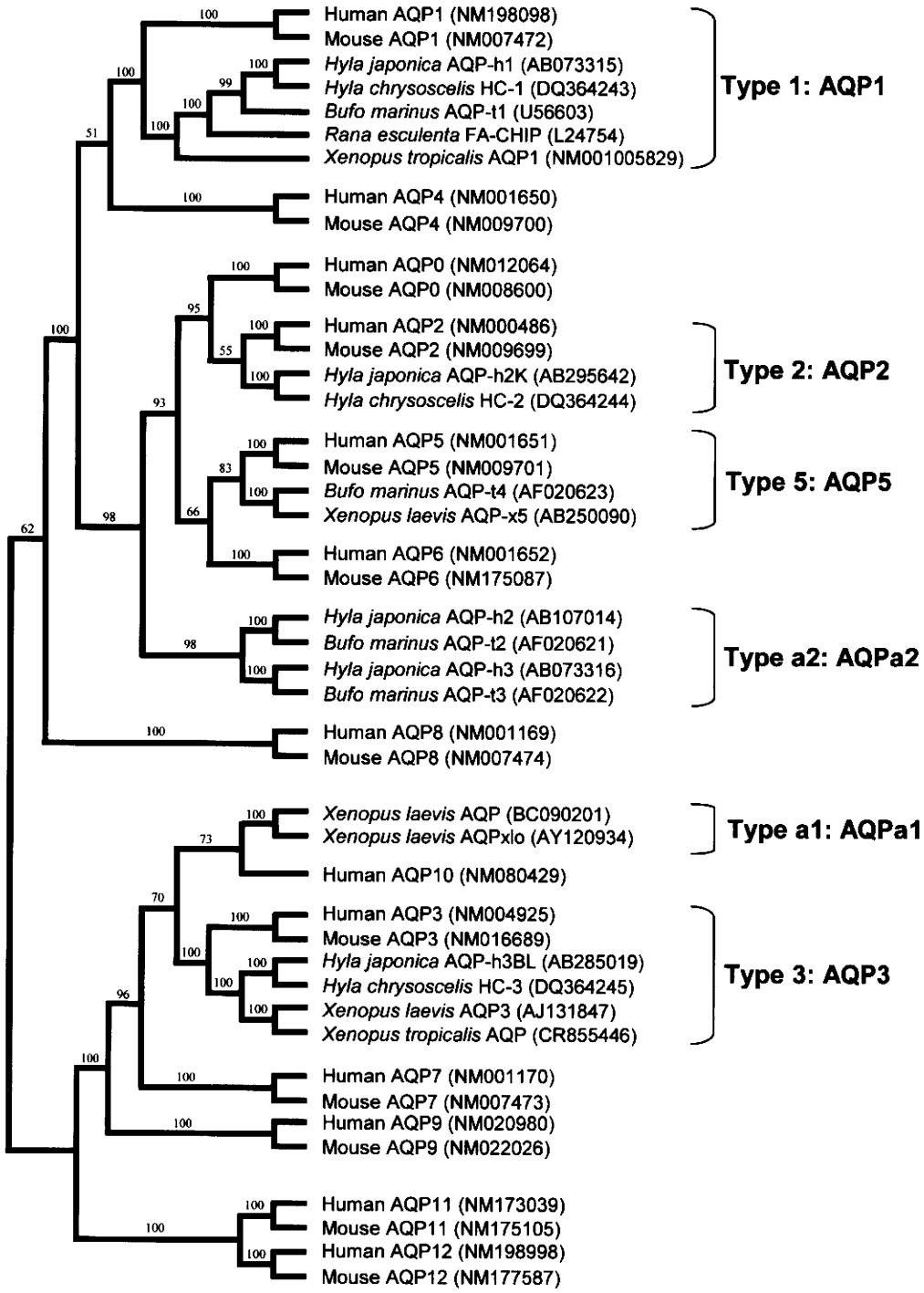

FIG. 2-2. Bayesian unrooted tree of AQP proteins from the human, mouse, and anurans. Anuran AQPs are assigned to six types, two of which (types a1 and a2) are unique to the anurans. *Hyla* AQP-h2K is classified in type 2 together with mammalian AQP2. The length of each branch is not proportional to evolutionary distance, and the numbers in the interior branches are Bayesian posterior probabilities (percent). The organism (genus), name, and accession number are indicated for each AQP.

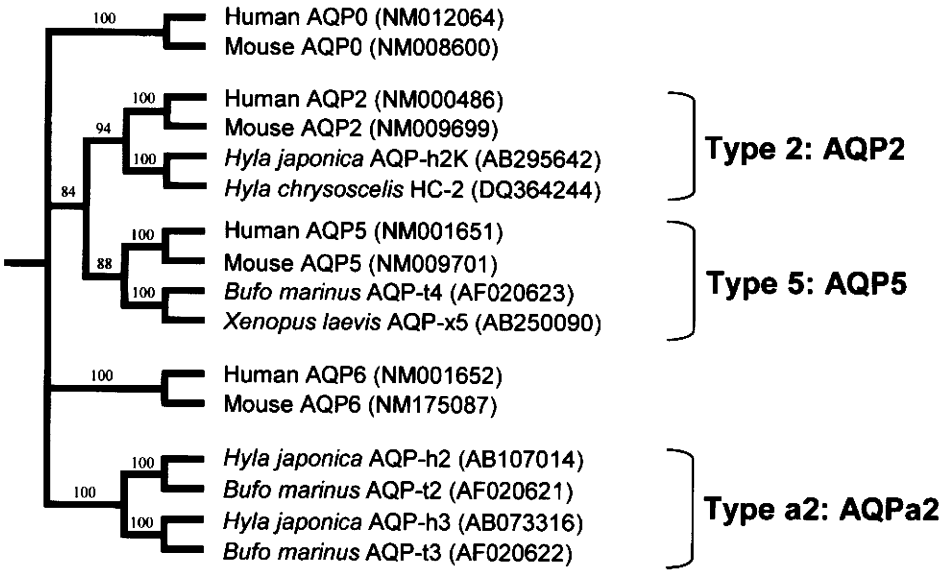

FIG. 2-3. Phylogenetic relationships among AQP0, AQP2, AQP5, AQP6, and AQPa2, seen in the NJ unrooted tree of AQP proteins from the human, mouse, and anurans. AQP-h2K, AQP-h2, and AQP-h3 from *H. japonica* are classified into two types: type 2 and type a2. *Hyla* AQP-h2K belongs to the type 2 together with mammalian AQP2. The length of each branch is not proportional to the estimated number of amino acid substitutions, and the numbers in the interior branches are bootstrap probabilities (percent; 10,000 replicates). The organism (genus), name, and accession number are indicated for each AQP.

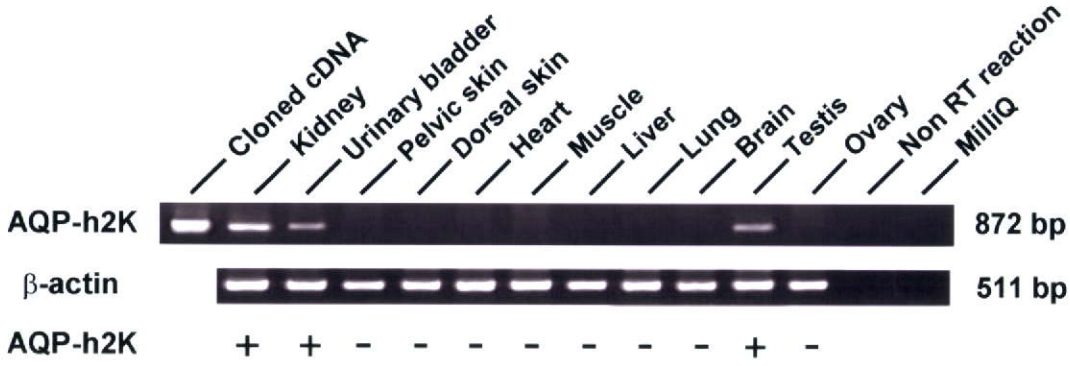

FIG. 2-4. Tissue expression of AQP-h2K mRNA by RT-PCR. RT-PCR products obtained using primers as described in *Materials and Methods* were separated on a 2% agarose gel and stained with ethidium bromide. RT and water represent the negative control using the kidney sample without a RT reaction and with water instead of cDNA, respectively. β-actin is used as positive control. +, Presence of the mRNA; -, absence of the mRNA.

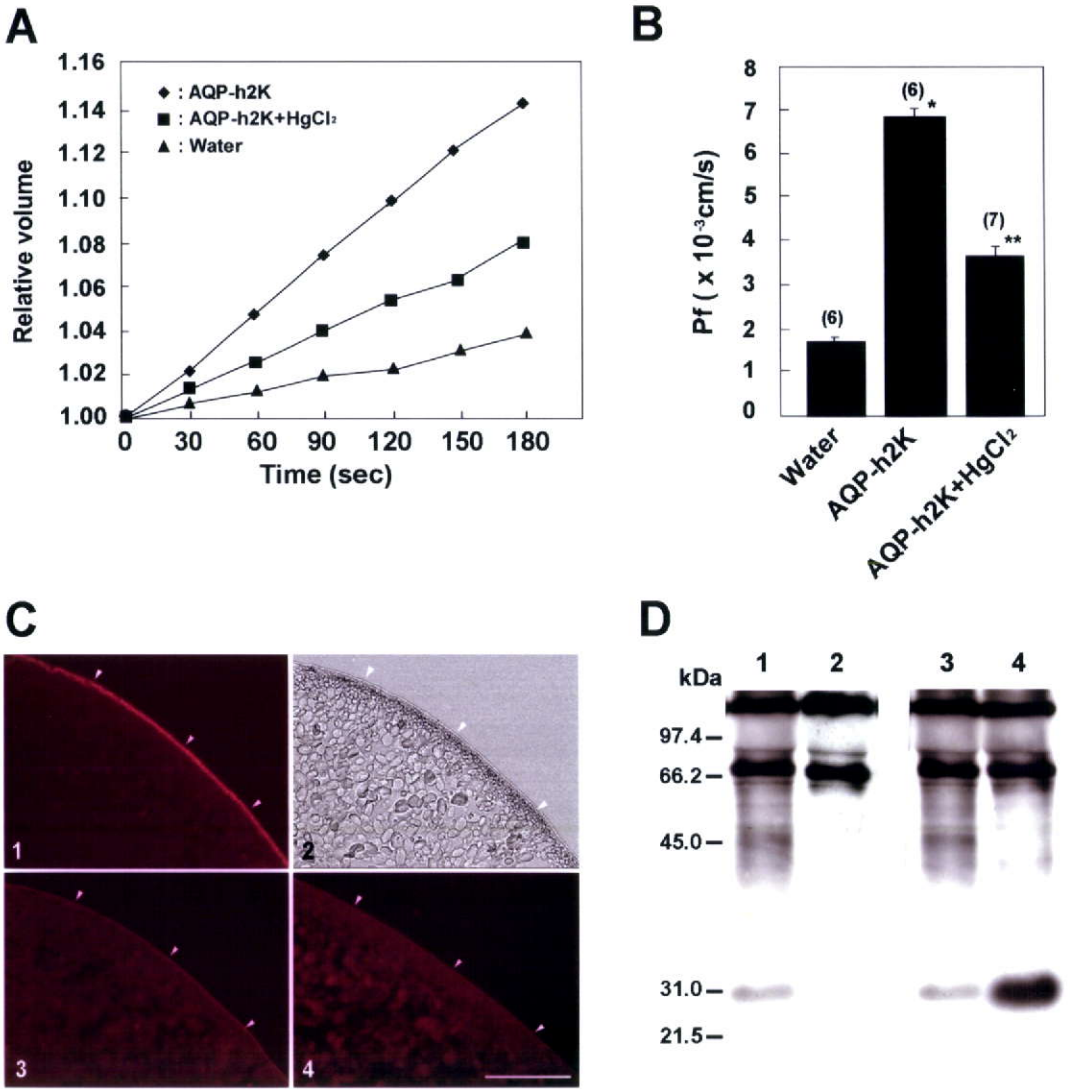

FIG. 2-5. Expression of AQP-h2K in *Xenopus* oocytes. **A,** Time course of the osmotic swelling. Oocytes were microinjected with water or cRNAs encoding AQP-h2K. Some of the AQP-h2K-injected oocytes were incubated with 0.3 mM $HgCl_2$. **B,** Pf was calculated from the initial rate of oocyte swelling. The representative data shown are given as the mean SE of measurements from five to six oocytes in each experimental group. *, *P* 0.01 *vs.* water; **, *P* 0.01 *vs.* AQP-h2K. **C,** Immunofluorescence images of the AQP-h2K protein in AQP-h2K-injected oocytes: after complete swelling of the oocytes, immunoreactive AQP-h2K substances are visible, predominately in the plasma membrane (1); the corresponding Nomarski differential interference image (2); in the absorption test, immunopositive substances obtained with anti-AQ-h2K are nearly abolished at background levels in the AQP-h2K-injected oocyte (3), and only background levels are observed in the water-injected oocyte with anti-AQP-h2K (4). *Arrowheads* indicate the plasma membrane. *Bar*, 50 μm. **D,** Western blot analysis of AQP-h2K-injected oocytes (lane 1) prepared after complete swelling. Immunoreactive bands are seen at 31 and 41–60 kDa in an extract of AQP-h2K cRNA-injected oocytes. The membrane was immunostained with the antiserum preabsorbed with the antigen peptide (10 g/ml; lane 2). Western blot analysis of extracts before and after digestion of the extracts by peptide-*N*-glycosidase F are shown. Specific bands with the extract of the cRNAinjected oocytes seen before and digestion (lane 3) are replaced by a signal band of 31 kDa, presumed to be the nonglycosylated form of *Hyla* AQP-h2K after digestion (lane 4).

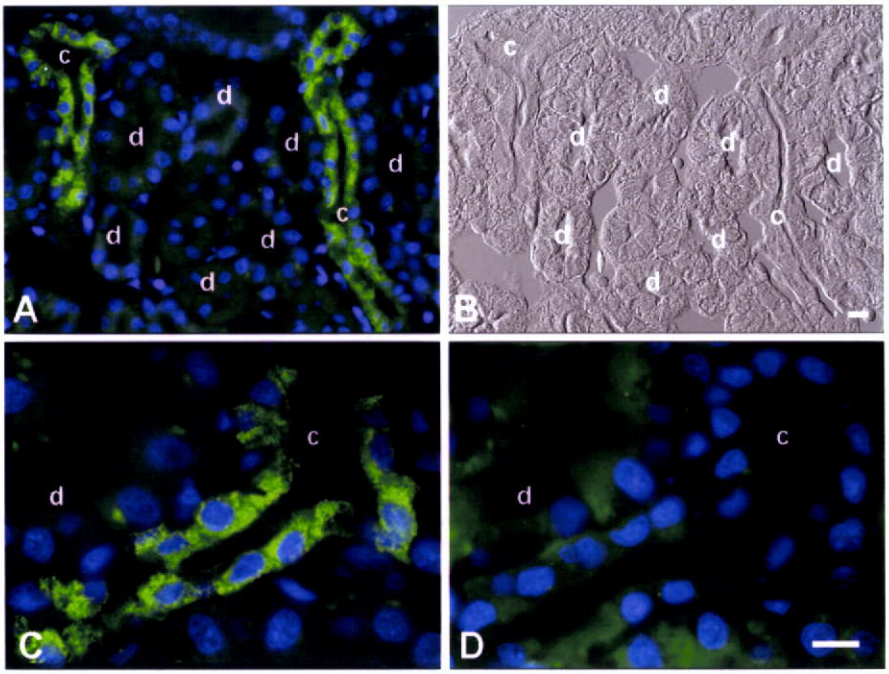

FIG. 2-6. Immunofluorescence localization of AQP-h2K in the collecting duct of kidney. Fluorescence images of AQPh2K (A, C, and D) and the corresponding Nomarski image (B) are shown. The labels (*green*) are clearly visible in the apical plasma membrane and subapical cytoplasm in principal cells of the collecting ducts (c). No labeling is seen in the other renal tubules, including the distal proximal tubules (d). C, Enlarged view of AQP-h2K-positive principal cells (*green*) in the collecting ducts. D, No labeling is visible in any of the kidney cells when anti-AQP-h2K is preabsorbed with the corresponding antigen peptide. Nuclei are counterstained with DAPI (*blue*). *Bar*, 50 μm (A and B); 10 μm (C and D).

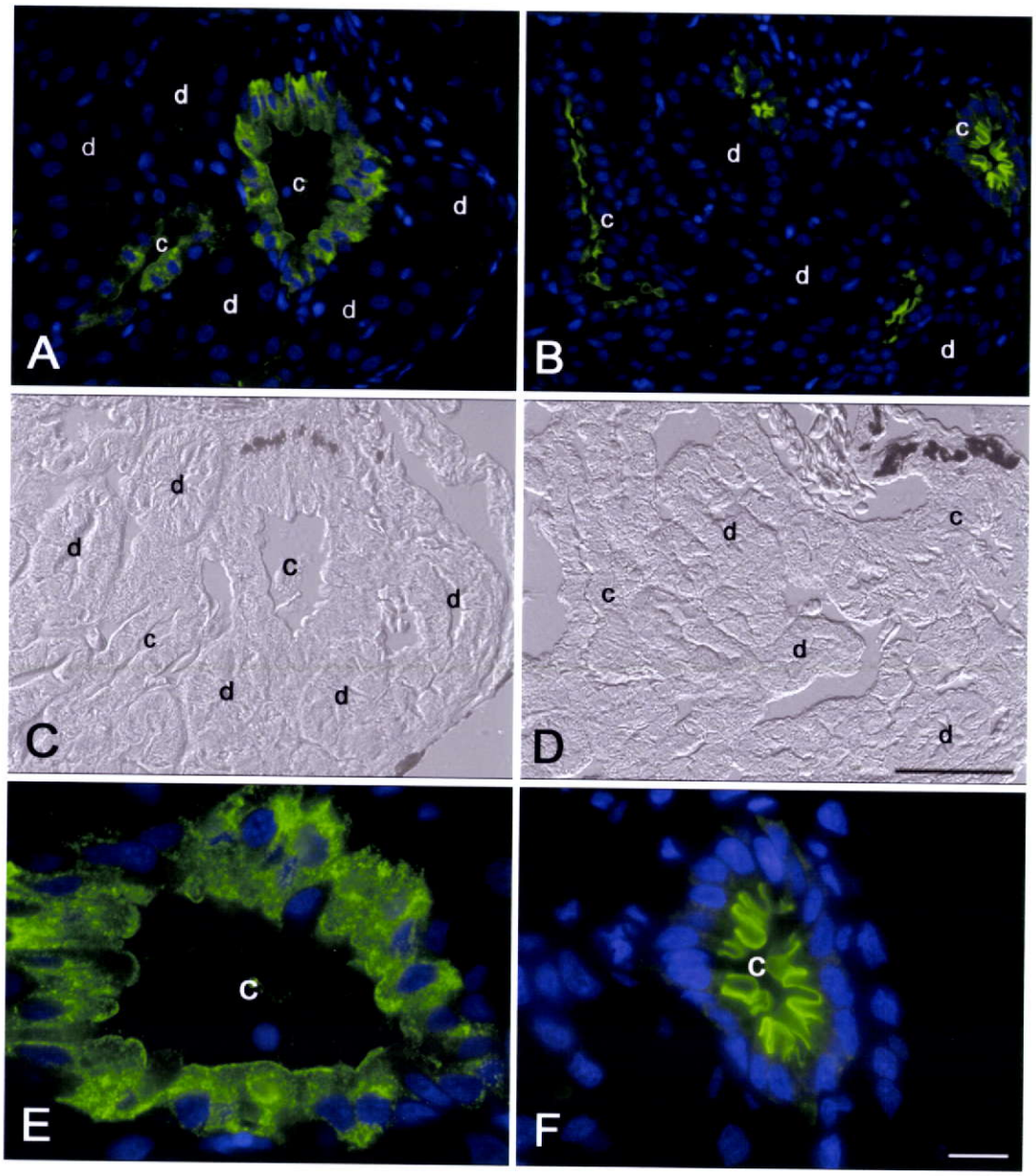

FIG. 2-7. Immunofluorescence micrographs showing the principal cells in the kidney collecting ducts labeled for AQP-h2K under nonstimulated and AVT-stimulated conditions, respectively. A and E, Immunolabeling results for AQP-h2K under the nonstimulated condition are shown (*green*). B and F, Immunolabeling results (*green*) for AQPh2K in response to AVT. Upon stimulation of AVT, the labeling for AQP-h2K (*green*) moved from the cytoplasm to the apical plasma membrane. C and D correspond to the Nomarski images to A and B, respectively. Nuclei are counterstained with DAPI (*blue*). c, Collecting duct; d, distal tubule. *Bar*, 50μm (A–D); 10μm (E and F).

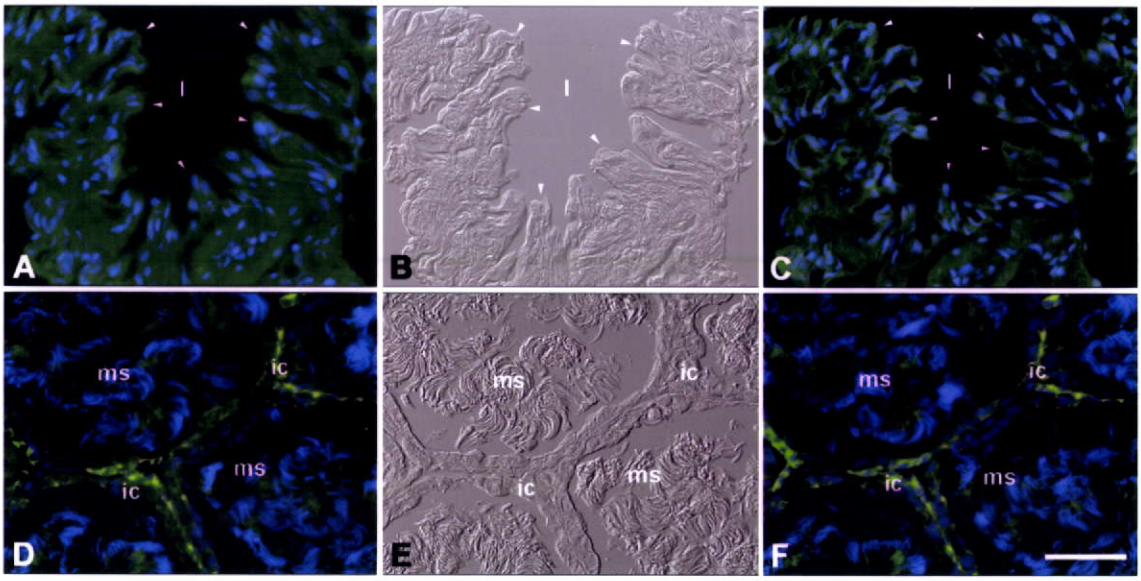

FIG. 2-8. Immunofluorescence images showing the urinary bladder and testis immunolabeled for AQP-h2K. Fluorescence images of AQP-h2K (A and D), the corresponding Nomarski images (B and E), and the preabsorption controls (C and F) are shown. No labeling is detected any of the cells of the urinary bladder (A–C). Nonspecific label is seen in most cells of the urinary bladder when anti-AQP-h2K is preabsorbed with the corresponding antigen peptide (C). The labels are visible in interstitial cells (ic) of the testicular stroma (D and E), but the labels are not diminished in the cells of the testes (F) when anti-AQP-h2K is preabsorbed with the antigen peptide. *Arrowheads* indicate epithelial cells of the urinary bladder. l, Lumen; ms, mature sperms; ic, interstitial cells. *Bar*, 10 μm.

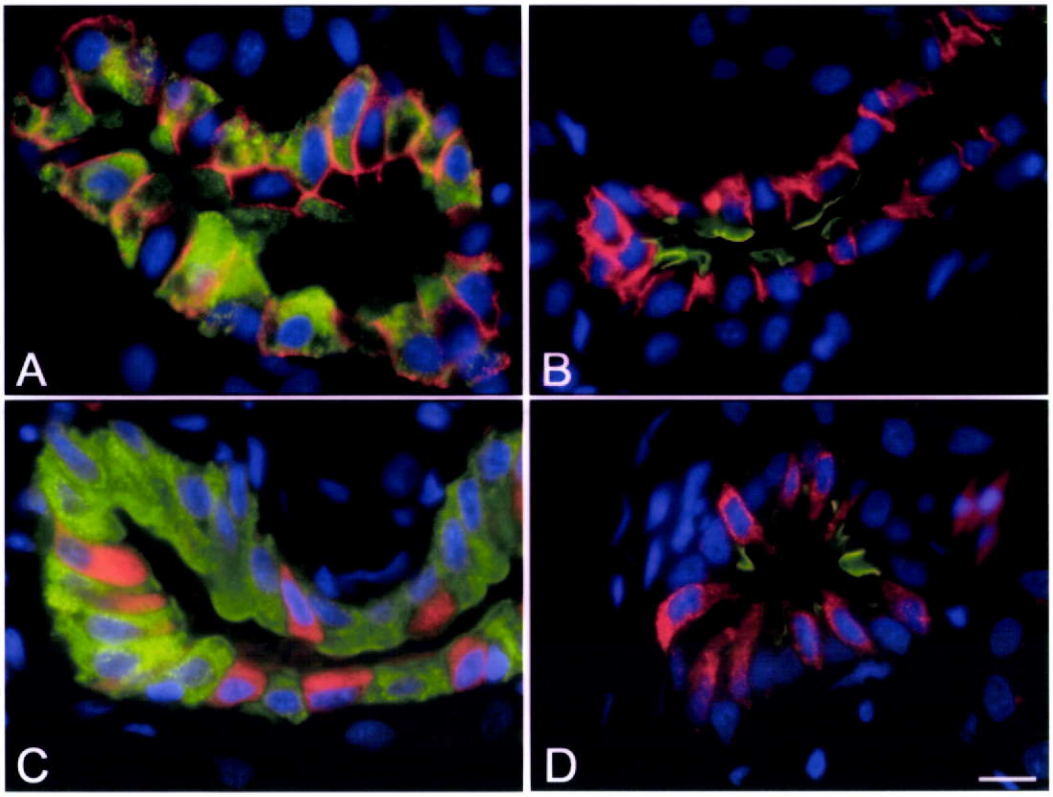

FIG. 2-9. Double-immunofluorescence images for AQP-h2K and AQPh3BL (A and B) and AQP-h2K and V-ATPase E-subunit in the kidney collecting ducts under nonstimulated (A and C) and vasotocin-stimulated (B and D) conditions are shown. The labeling sites for AQP-h2K (*green*) are different from those for the AQP-h3BL (*red*). Conversely, the labeling cells for AQP-h2K (*green*) are distinguished from those for the V-ATPase E-subunit (*red*). *Bar*, 10 m.

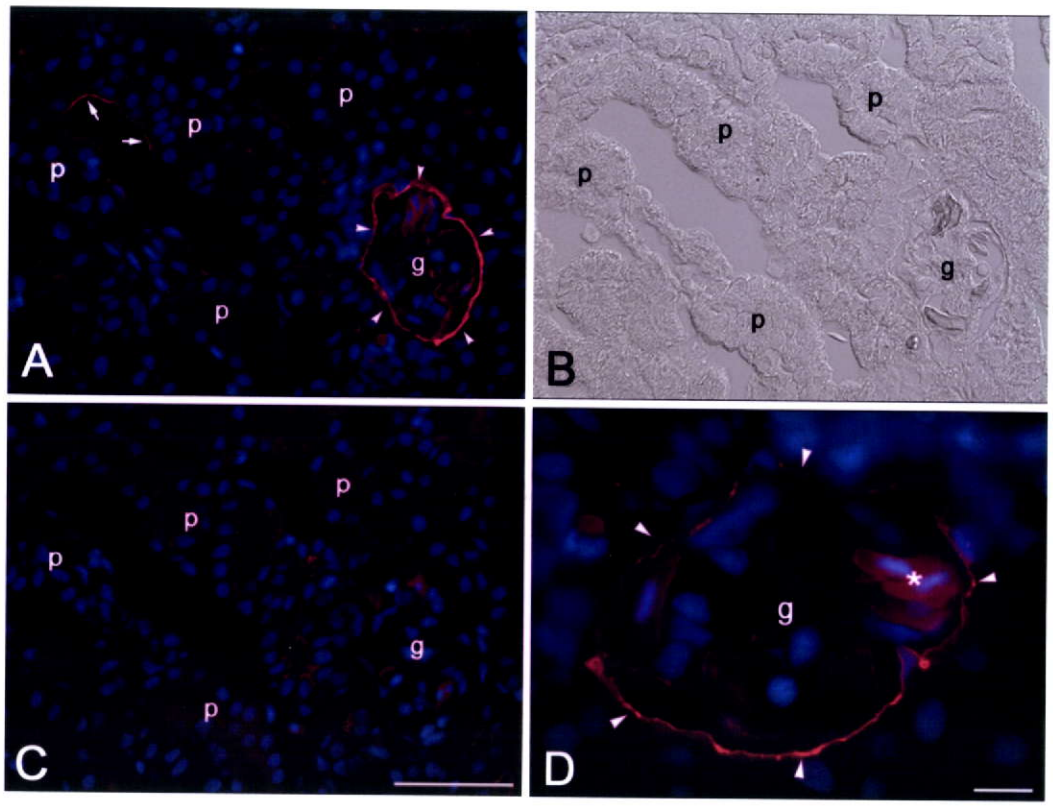

FIG. 2-10. Immunofluorescence localization of AQP-h1 in the kidney. A, C and D, Fluorescence images of AQP-h1. B, Corresponding Nomarski differential interference contrast image. A and D, Labels (*red*) are clearly visible in the endothelial cells (*arrows*) around the proximal tubules (p) and the flattened cells (*arrowheads*) of the parietal layer of the Bowman's capsule. C, No labeling is detected in any of the cells of the kidney when anti-AQP-h1 is preabsorbed with the corresponding antigen peptide. D, Enlarged view of AQP-h1-positive flattened cells of the pariental cells. G, Glomerulus; *asterisk*, red blood cells. *Bar*, 50 μm (A–C); 10 μm (D).

References

Abrami L, Simon M, Rousselet G, Berthonaud V, Buhler JM, Ripoche P. (1994) Sequence and functional expression of an amphibian water channel, FA-CHIP: a new member of the MIP family. *Biochim Biophys Acta* 1192:147–151

Akabane G, Ogushi Y, Hasegawa T, Suzuki M, Tanaka S. (2007) Gene cloning and expression of an aquaporin (AQP-h3BL) in the basolateral membrane of water-permeable epithelial cells in osmoregulatory organs of the tree frog. *Am J Physiol Regul Integr Comp Physiol* 292:R2340–R2351

Bentley PJ, Main AR. (1972) Zonal differences in permeability of the skin of some anuran Amphibia. *Am J Physiol* 223:361–363

Bentley PJ, Yorio T. (1979) Do frogs drink? *J Exp Biol* 79:41–46

Bentley PJ. (2002) Endocrines and osmoregulation: a comparative account in vertebrates. *Springer, Berlin, pp.* 155–186

Brown D, Katsura T, Gustafson CE. (1998) Cellular mechanisms of aquaporin trafficking. *Am J Physiol* 275:F328–F331

Denker BM, Smith BL, Kuhajda FP, Agre P. (1988) Identification, purification, and partial characterization of a novel Mr 28,000 integral membrane protein from erythrocytes and renal tubules. *J Biol Chem* 263:15634–15642

Felsenstein J. (1985) Confidence limits on phylogenies: an approach using the bootstrap. *Evolution* 39:783–791

Fushimi K, Uchida S, Hara Y, Hirata Y, Marumo F, Sasaki S. (1993) Cloning and expression of apical membrane water channel of rat kidney collecting tubule. *Nature* 361:549–552

Fushimi K, Sasaki S, Marumo F. (1997) Phosphorylation of serine 256 is required for cAMP-dependent regulatory exocytosis of the aquaporin-2 water channel. *J Biol Chem* 272:14800–14804

Gallardo R, Pang PK, Sawyer WH. (1980) Neural influences on bullfrog renal functions. *Proc Soc Exp Biol Med* 165:233–240

Hall BG. (2004) Phylogenetic trees made easy: a how-to manual. 2nd ed. Sunderland, MA: *Sinauer Associates*

Hasegawa T, Tanii H, Suzuki M, Tanaka S. (2003) Regulation of water absorption in the frog skins by 2 vasotocin-dependent water-channel aquaporins, AQP-h2 and AQP-h3. *Endocrinology* 144:4087–4096

Hasegawa T, Suzuki M, Tanaka S. (2005) Immunocytochemical studies on translocation of phosphorylated AQP-h2 protein in granular cells of the frog urinary bladder before and after stimulation with vasotocin. *Cell Tissue Res* 322:407–415

Henikoff S, Henikoff JG. (1992) Amino acid substitution matrices from protein blocks.

Proc Natl Acad Sci USA 89:10915–10919

Ishibashi K, Kuwahara M, Sasaki S. (2000) Molecular biology of aquaporins. *Rev Physiol Biochem Pharmacol* 141:1–32

Jones DT, Taylor WR, Thornton JM. (1992) The rapid generation of mutation data matrices from protein sequences. *Comp Appl Biosci* 8:275–282

Kawedia JD, Nieman ML, Boivin GP, Melvin JE, Kikuchi K, Hand AR, Lorenz JN, Menon AG. (2007) Interaction between transcellular and paracellular water transport pathways through Aquaporin 5 and the tight junction complex. *Proc Natl Acad Sci USA* 104:3621–3626

Kimura M. (1983) The neutral theory of molecular evolution. Cambridge, UK: *Cambridge University Press*

Klussmann E, Maric K, Rosenthal W. (2000) The mechanisms of aquaporin control in the renal collecting duct. *Rec Physiol Biochem Pharmocol* 141:33–95

Kubota M, Hasegawa T, Nakakura T, Tanii H, Suzuki M, Tanaka S. (2006) Molecular and cellular characterization of a new aquaporin, AQP-x5, specifically expressed in the small granular glands of *Xenopus* skin. *J Exp Biol* 209:3199–3208

Kuwahara M, Fushimi K, Terada Y, Bai L, Marumo F, Sasaki S. (1995) cAMPdependent phosphorylation stimulates water permeability of aquaporin-collecting duct water channel protein expressed in *Xenopus* oocytes. *J Biol Chem*

270:10384–10387

Mau B, Newton M, Larget B. (1999) Bayesian phylogenetic inference via Markov chain Monte Carlo. *Biometrics* 55:1–12

Maunsbach AB, Marples D, Chin E, Ning G, Bondy C, Agre P, Nielsen S. (1997) Aquaporin-1 water channel expression in human kidney. *J Am Soc Nephrol* 8:1–14

Nielsen S, Smith BL, Christensen EI, Knepper MA, Agre P. (1993) CHIP28 water channels are localized in constitutively water-permeable segments of the nephron. *J Cell Biol* 120:371–383

Nielsen S, DiGiovanni SR, Christensen EI, Knepper MA, Harris HW. (1993) Cellular and subcellular immunolocalization of vasopressin-regulated water channel in rat kidney. *Proc Natl Acad Sci USA* 90:11663–11667

Nielsen S, Chou CL, Marples D, Christensen EI, Kishore BK, Knepper MA. (1995) Vasopressin increases water permeability of kidney collecting duct by inducing translocation of aquaporin-CD water channels to plasma membrane. *Proc Natl Acad Sci USA* 92:1013–1017

Pang PK, Uchiyama M, Sawyer WH. (1982) Endocrine and neural control of amphibian renal functions. *Fed Proc* 41:2365–2370

Ronquist R, Huelsenbeck JP. (2003) MRBAYES 3: Bayesian phylogenetic inference under mixed models. *Bioinformatics* 19:1572–1574

Sabolic I, Valenti G, Verbavatz JM, Van Hoek AN, Verkman AS, Ausiello DA, Brown D. (1992) Localization of the CHIP28 water channel in rat kidney. *Am J Physiol* 263:C1225–C1233

Saitou N, Nei M. (1987) The neighbor-joining method: a new method for reconstructing phylogenetic trees. *Mol Biol Evol* 4:406–425

SawyerWH. (1957) Increased renal reabsorption of osmotically free water by the toad (*Bufo marinus*) in response to neurohypophysial hormones. *Am J Physiol* 189:564–568

Sluijs P, Deen PM. (2002) The role of putative phosphorylation sites in the targeting and shuttling of the Aquaporin-2 water channel. *J Biol Chem* 277:41473–41479

Steen WB. (1929) On the permeability of the frog's bladder to water. *Anat Rec* 43:215–220

Suzuki M, Hasegawa T, Ogushi Y, Tanaka S. (2007) Amphibian aquaporins and adaptation to terrestrial environments: a review. *CompBiochem PhysiolAMol Integr Physiol* 148:72–81

Takata K, Matsuzaki T, Tajika Y. (2004) Aquaporins: water channel proteins of the cell membrane. *Prog Histochem Cytochem* 39:1–83

Tanaka S, Kurosumi K. (1992) A certain step of proteolytic processing of proopiomelanocortin occurs during the transition between two distinct stages of

secretory granules maturation in rat anterior pituitary corticotrophs. *Endocrinology* 131:779–786

Tanaka S, Yora T, Nakayama K, Inoue K, Kurosumi K. (1997) Proteolytic processing of pro-opiomelanocortin occurs in acidifying secretory granules of AtT-20 Cells. *J Histochem Cytochem* 45:425–436

Tanii H, Hasegawa T, Hirakawa N, Suzuki M, Tanaka S. (2002) Molecular and cellular characterization of a water channel protein, AQP-h3, specifically expressed in the frog ventral skin. *J Membrane Biol* 188:43–53

Thompson JD, Higgins DG, Gibson TJ. (1994) CLUSTAL W: improving the sensitivity of progressive multiple sequence alignment through sequence weighting, position-specific gap penalties and weight matrix choice. *Nucleic Acids Res* 22:4673–4680

Uchiyama M. (1994) Sites of action of arginine vasotocin in the nephron of the bullfrog kidney. *Gen Comp Endocrinol* 94:366–373

Uchiyama M, Yoshizawa H. (2002) Nephron structure and immunohistochemical localization of ion pumps and aquaporins in the kidney of frogs inhabiting different environments. In: Hazon N, Flik G, eds. Osmoregulation and drinking in vertebrates. Oxford, UK: *BIOS Scientific Publishers*; 109–128

Van Balkom BW, Savelkoul PJ, Markovich D, Hofman E, Nielsen S, Van Der

Virkki LV, Franke C, Somieski P, Boron WF. (2002) Cloning and functional characterization of a novel aquaporin from *Xenopus laevis* oocytes. *J Biol Chem* 277:40610–40616

Yajima S, Kubota M, Nakakura T, Hasegawa T, Katagiri N, Tomura H, Sasayama Y, Suzuki, Tanaka S. (2007) Cloning and expression of the vacuolar proton-pumping ATPase subunits in the follicular epithelium of bullfrog endolymphatic sac. *Zool Sci* 24:147–157

Zhang RB, Logee KA, Verkman AS. (1990) Expression of mRNA coding for kidney and red cell water channels in *Xenopus* oocytes. *J Biol Chem* 265:15375– 15378

Zimmerman SL, Frisbie J, Goldstein DL, West J, Rivera K, Krane CM. (2006) Excretion and conservation of glycerol, and expression of aquaporins and glyceroporins, during cold acclimation in Cope's gray tree frog, *Hyla chrysoscelis*. *Am J Physiol Regul Integr Comp Physiol* 292:R544–R555

Chapter 3

Correlation between aquaporin and water permeability in response to vasotocin, hydrin, and β-adrenergic effectors in the ventral pelvic skin of the tree frog, *Hyla japonica*

Abstract

The ventral pelvic skin of the tree frog, *Hyla japonica* expresses two kinds of arginine vasotocin (AVT)-stimulated aquaporins (AQP-h2 and AQP-h3), which affect the capacity of the frog's skin to absorb water. As such, it can be used as a model system for analyzing molecular mechanisms of water permeability. We investigated AQP dynamics and water permeability in the pelvic skin of *H. japonica* following challenge with AVT, hydrins (intermediate peptides of pro-AVT) and β-adrenergic effectors. In the *in vivo* experiment, both AQP-h2 and AQP-h3 proteins were translocated to the apical plasma membrane in the principal cells of the first reacting cell (FRC) layer in the pelvic skin following challenge with AVT, hydrin 1 and hydrin 2, thereby increasing the water permeability on the pelvic skin. The β-adrenergic receptor agonist isoproterenol (IP) and its antagonist propranolol (PP) in combination with AVT or hydrins were used as challenge in the *in vitro* experiment. IP increased water permeability whereas PP inhibited it, and both events were well correlated with the translocation of the AQPs to the apical membrane. In the PP + AVT-treated skins, labels for AQP-h2 and AQP-h3 were differentially visible among the principal cells; the apical plasma membrane of some cells was labeled while others were not, indicating that the response of PP or AVT is different from cell to cell. These results provide morphological evidence that the principal cells of the FRC layers may have two kinds of receptors; a V2 receptor and β-adrenergic receptor.

Introduction

Anuran amphibians are adapted to living in the diverse range of water environments. A general classification of anurans according to habitat distinguishes four groups, *i.e.*, aquatic, semi-aquatic, terrestrial, and arboreal species (Hillman et al., 2009). Anurans have developed a number of unique physiological systems for maintaining water balance in these diverse habitats (Bentley & Main, 1972; Bentley & Yorio, 1979). For example, most adult anuran amphibians do not drink water through their mouth. This is particularly true for many terrestrial and arboreal species, such as *Hyla* (arboreal) and *Bufo* (terrestrial), utilize a region in the posterior or pelvic region of the ventral skin that is specialized for rapid rehydration from shallow water sources or moist substrates. In addition, periods of terrestrial activity can be prolonged by the reabsorption of dilute urine from bladder. The degree to which these adaptations have been developed varies among the different anurans. For example, the terrestrial environment-adapted species have high water permeability in their ventral pelvic skin and a high capacity for urine storage in their urinary bladder, whereas the pelvic skin of an aquatic species, such as *Xenopus laevis*, has a low water permeability (Bentley & Main, 1972). In addition, the stimulation of water permeability of the pelvic skin by arginine vasotocin (AVT) is higher in arboreal and terrestrial species than in aquatic species (Yorio and Bentley 1978).

Brown et al. (1983) measured a correlation between the aggregation of intramembrane particles (termed aggrephore) and water flow in toads skin in response to the mammalian antidiuretic hormone arginine vasopressin. These particles were subsequently shown to be a class of integral membranes [termed aquaporins (AQPs)], that form selective water channels in the plasma membranes in various cells of various organisms (Preston *et al.*, 1992).

In mammals, 13 isoforms of AQPs (AQP0 – AQP12) have been identified to date and have been characterized by cloning and sequencing of their cDNA (Ishibashi *et al.*, 2000; Takata *et al.*, 2004). A subfamily of AQPs (termed aquaglyceroporins) that form membrane pores, which are permeated by glycerol and urea has also been reported (Ishibashi *et al.*, 2000; Agre, 2006). Our group recently discovered three forms of AVT-stimulated AQP in the tree frog, *Hyla japonica*: AQP-h2 in the ventral pelvic skin and urinary bladder (Hasegawa *et al.*, 2003), AQP-h3 in the pelvic skin (Tanii *et al.*, 2002) and AQP-h2K in the kidney (Ogushi *et al.*, 2007). The expression of AQP-h2 and AQP-h3 in the pelvic skins of tree frogs raises the interesting question whether other factors that stimulate water permeability and absorption by anurans involve a similar insertion of AQPs in the apical membrane.

Hydrin is an intermediate peptide derived from a pro-vasotocin-neurophysin precursor. It plays a pivotal role in the water absorption/reabsorption process in the skin and bladder but is devoid of antidiuretic activity in the kidney (Michel *et al.*, 1993; Rouille *et al.*, 1989). Hydrin 2 (vasotocinyl-Gly) is present in an amount equal to that of AVT in the neurohypophysis of Ranidae and Bufonidae. By contrast, the aquatic frog *Xenopus laevis* secretes hydrin 1 (vasotocinyl-Gly-Lys-Arg) as well as AVT. Both peptides are generated from a downregulation in the processing, *i.e.*, hydrin 1 by a decrease in carboxypeptidase E activity and hydrin 2 by a reduction in the activity of the β-amidating enzymatic system. These hydrins are found in anuran amphibians, but not in other vertebrates, raising the question of whether hydrin has a stimulatory potency in the translocation of frog AQPs to the apical membrane.

Water permeability in the pelvic skin of frogs is considered to be regulated by at least two systems: the first is *via* the AVT V2 receptor and the other is *via* the β-adrenergic receptor (Brown *et al.*, 1980; De Sousa and Grosso, 1982). Our group has shown that both AQP-h2 and AQP-h3 proteins are translocated in response to AVT to

the apical plasma membrane of principal cells in the outermost granular layer [*i.e.*, the first-reacting cell (FRC) layer] of the pelvic skin in tree frogs (Hasegawa *et al.*, 2003).

In the study reported here, we examined the effect of AVT, hydrin, and effectors of the β-adrenergic receptor on the water permeability and translocation of both AQP-h2 and AQP-h3 in the FRC layer of two pelvic skins of the tree frog.

Materials and Methods

Animals

Adult male tree frogs (*Hyla japonica* Günter) were captured in a field near our university (Shizuoka University, Shizuoka, Japan) and kept under laboratory conditions where they were fed crickets. On average, the frogs used in this study had a body length of approximately 2.9 cm and weighed approximately 2.6 g. The ventral pelvic skins were removed under anesthesia (MS 222; Nacalai tesque, Kyoto, Japan) and then processed for experiments involving hormone or reagent treatments. All animal experiments were carried out in compliance with the Guide for Care and Use of Laboratory Animals of Shizuoka University.

Experimental Protocol for Treatment with Chemical Reagents

For the *in vivo* experiments, the frogs were bathed to above two-third of their ventral skin in distilled water for 30 min and then injected with 10 μl 0.65% (w/v) NaCl saline containing 10^{-6} M [Arg^8]-vasotocin (Peptide Institute, Inc., Osaka, Japan), -hydrin 1 or -hydrin 2 (Bachem, Bubendorf, Switzerlan) per 1g of body mass. Following the injection, the body weight of the frogs was measured chronologically on an analytical balance (Sartorius, Tokyo, Japan).

For the *in vitro* experiments, the frogs were rinsed in water for 30 min before being killed as described above and the pelvic skins removed. The apparatus for

measuring water flow consists of two chambers with a 1-cm-diameter hole at the center of the wall separating the two chambers, which was a modification of the device by Kohno *et al.* (Kohno *et al.*, 2004). The isolated skin was washed with Ringer solution and then mounted over the hole. The chamber on the serosal side of the skin was filled with a Ringer solution: 11.301 mM NaCl, 1.877 mM KCl, 1.081 mM $CaCl_2$, 0.064 mM NaH_2PO_4 and 1.429 mM $NaHC0_3$ having an osmolarity of 220 mOsmol, while that on the mucosal side of the skin was filled with water. Water movement from the mucosal side to the serosal side of the skin was measured directly using a 0.1-ml pipette horizontally attached the serosal chamber of the apparatus. The isolated pelvic skins were preincubated for 30 min in the Ringer solution as described above or in a Ringer solution containing 10^{-8} M AVT, hydrin 1 or hydrin 2. Following the addition of each of the solutions to the serosal side of the chamber, water movement was measured using the pipette. Applying the same procedure, we added Ringer solution containing 10^{-8} M of the β-adrenergic receptor agonist isoproterenol (IP; Sigma-Aldrich, Tokyo, Japan) and its antagonist propranolol (PP; Sigma-Aldrich), respectively, to the serosal side of the chamber to examine the effects of these substances on the actions of AVT, hydrin 1 and hydrin 2. After incubation, the skin specimens were examined by immunofluorescence microscopy.

Immunofluorescence

The pelvic skins used in the *in vivo* and *in vitro* experiments were quickly fixed overnight in periodate-lysine-paraformaldehyde (PLP) fixative, dehydrated and embedded in Paraplast. Four-μm sections were cut and mounted on gelatin-coated slides. The deparaffinized sections were rinsed with phosphate-buffered saline (PBS). Double-immunofluorescence labeling was carried out according to Hasegawa *et al.* (Hasegawa *et al.*, 2003). In brief, for the double-immunofluorescence labeling of AQP-h2 and

AQP-h3, sections were incubated with a mixture of guinea pig anti-AQP-h2 (ST-140; 1:5,000, Hasegawa *et al.*, 2003) and rabbit anti-AQP-h3 (ST-141; 1:10,000, Tanii *et al.*, 2002), and then reacted with a mixture of indocarbocyanine (Cy3)-labeled donkey anti-guinea pig IgG (1:400; Jackson Immunoresearch, West Grove, PA, USA), Alexa 488-labeled donkey anti-rabbit IgG (1:200; Molecular probes, Eugene, OR, USA) and DAPI. Rabbit anti-*Hyla* AQP-h3BL serum (ST-184) was also used for labeling the basolateral membrane of the principal cells (Akabane et al. 2007). Specimens were examined with an Olympus BX61 microscope equipped with a BX-epifluorescence attachment (Olympus Optical Co., Tokyo, Japan).

Statistical analysis

Statistical analysis was performed by Duncan's multiple range test.

Results

In vivo experiment

The body mass of the frogs increased significantly with time following the injection of AVT reaching a body mass approximately 1.15-fold greater than that of the control frogs after 60 min ($p<0.01$) (Fig. 3-1). Hydrin 1 and hydrin 2 were equally as effective as AVT in stimulating the increase in body mass (Fig. 3-1). By contrast, the control frogs injected with 0.65% NaCl solution did not show any change in body mass within the experimental interval. In the control group, the labels for AQP-h2 and AQP-h3 were observed in the basolateral membrane of the principal cells in the FRC layer (Fig. 3-2 A-C). In comparison, when sections from the AVT-injected frogs were labeled with anti-AQP-h2 or anti-AQP-h3, these labels were visible in the apical membrane of the principal cells in the FRC layer and throughout the entire plasma membrane of the principal cells underlying the FRC layer (Fig. 3-2 D-F). Similar labeling patterns for

AQP-h2 and AQP-h3 were observed on sections from the hydrin 1- and hydrin 2-injected frogs (Fig. 3-2 G-L).

In vitro experiment

The effect of AVT was to gradually stimulate the water permeability of the isolated pelvic skins with increasing incubation time; by contrast, the water permeability of the control pelvic skins did not increase (Fig. 3-3). Hydrin 1 and hydrin 2 also were effective in increasing the water permeability of the isolated pelvic skins, but at slightly lower levels than those observed for the AVT-treated skins (Fig. 3-3). At the end of the experimental period (30 min), the water permeability of the AVT-, hydrin 1-, and hydrin 2-treated skins had increased significantly compared to the control group ($p<0.01$) (Fig. 3-4). However, there was no significant difference among the AVT-, hydrin 1- and hydrin 2-treated groups. In each of the histological sections from the control group, labels for AQP-h2 and AQP-h3 were observed near or in the basolateral membrane in the FRC layer whereas the label for AQP-h3BL, which is expressed constitutively in the basolateral plasma membrane (Akabane *et al.*, 2007), was visible at the same sites (Fig. 3-5 A-C). In the AVT-, hydrin 1- and hydrin 2-treated groups, however, labels for AQP-h2 and AQP-h3 were intensely visible in the apical plasma membrane of the principal cells in the FRC layer (Fig. 3-5 D,E,G,H,J,K). In the AVT-treated group, many spot-like AQP-h3-posive reactions were found in the cytoplasm of the principal cells, and the same intense positive reaction as described above was also visible throughout the entire plasma membrane of the principal cells underlying the FRC layer (Fig. 3-5 D-F).

Water permeability in the IP-treated pelvic skin specimen increased in a similar manner to that observed for the hydrin-treated skin. At the 30-min incubation point, water permeability of the IP-treated pelvic skin was significantly lower than that of the

IP + AVT-treated skin ($p<0.01$) (Fig. 3-4). In turn, when the pelvic skins were challenged with IP+PP, water permeability was not as low as that of the PP-treated and contral skin (Fig. 3-4). In turn, when the pelvic skins were challenged with IP + PP, water permeability was not as high as that of the PP-treated and control skins (Fig. 3-4). The water permeability of the IP-treated pelvic skins was lower than that of the AVT-treated skins ($p<0.01$) but there was no significant difference in the water permeability between the AVT- and the IP + AVT-treated skins in terms of water permeability (Fig. 3-4). The treatment with PP + AVT induced a mean increase in water permeability *via* the isolated pelvic skins but the levels were higher than those observed in the control group (Fig. 3-4).

Similar stimulatory and inhibitory experiments with IP or PP using hydrin 1 and hydrin 2 produced the same results as those using AVT (data not shown).

Intense labels were observed in the apical membrane of the principal cells in the FRC layers when sections of the IP-treated pelvic skins were labeled with anti-AQP-h2 or anti-AQP-h3. Similar labeling was only found in the AVT-treated skins (Fig. 3-5 D-F, Fig. 3-6 A-C).

Increased water permeability was not observed in the PP-treated and control skins, which is consistent with the distribution of AQP-h2 and AQP-h3 labels, which were visible in the basolateral plasma membrane (Fig. 3-6 D-F). In the PP-treated group, labels for AQP-h2 and AQP-h3 were visible in the basolateral plasma membrane of the principal cells in the FRC layer (Fig. 3-6 D-F).

When the sections of the IP + AVT-treated skins were labeled for AQP-h2, more intense labels were found in the apical membrane of the principal cells. Similar results were obtained in the IP+AVT+PP-treated pelvic skins (data not shown).

When the sections of the PP + AVT-treated group were labeled for AQP-h2 and AQP-h3, positive labels were found in the apical plasma membrane of several principal

cells but not all cells in the FRC layer (Fig. 3-5 D-F, 3-6 M-O). When all of the reagents were used, labels for AQP-h3BL were visible in the basolateral plasma membrane in the principal cells (Fig. 3-5 C,F,I,L and Fig. 3-6 C,F,I,L,O).

Discussion

The present study demonstrated that hydrins as well as AVT stimulate water permeability across the ventral pelvic skin, *in vivo* and *in vitro*, by translocation of AQP-h2 and AQP-h3 from the cytoplasmic pool to the apical plasma membrane of principal cells in the FRC later. This process of water permeability is induced by two AQPs - AQP-h2 and AQP-h3 - which translocate from the cytoplasmic pool to the apical plasma membrane of the principal cells in the FRC layer (Tanii *et al.*, 2002; Hasegawa *et al.*, 2003). AVT binds to V2 receptors and stimulates the formation of cyclic AMP and protein kinase A, thereby moving from the cytoplasmic pool to the apical plasma membrane through the phosphorylation of AQP-h2 and/or AQP-h3 protein (Hasegawa *et al.*, 2005). Concerning hydrin, Acher *et al.* (Acher *et al.*, 1997) propose that the primary effect of AVT at its physiological concentration is antidiuresis whereas hydrins have a higher affinity for V2 receptors in the skin and bladder in order to stimulate rehydration and the utilization of bladder water. Our results provide experimental evidence supporting part of this hypothesis by showing that hydrins have a stimulatory effect on water permeability across the pelvic skin. This is the first report of a study showing a good correlation between hydrin and AQP protein in the ventral pelvic skin of the tree frog. However, further investigation is necessary to elucidate whether hydrins affect the translocation of AVT-stimulated AQP, AQP-h2K in the kidney (Ogushi *et al.*, 2007). We also found that IP, a β-receptor agonist, and AVT have equal effects on water permeability, *in vitro*. This finding is consistent with *in vivo* studies on the hydrated toads, *Bufo cognatus*, dehydrated toads, *Bufo bufo*, and hydrated

spadefoot toad, *Scaphiopus couchi* (Hillyard, 1979; Yokota and Hillman, 1984; Viborg and Rosenkilde, 2004).

IP stimulates the increase in the synthesis of cyclic AMP *via* β-receptor (De Sousa and Grosso, 1982). This process is identical to the action of AVT in terms of stimulation of the formation of cyclic AMP. We were able to show here that IP induces the translocation of AQP-h2 and AQP-h3 proteins from the cytoplasmic pool to the apical plasma membrane, thereby increasing water permeability. This observation confirms earlier findings using freeze fracture techniques that showed IP stimulating the movement of the intramembrane particle aggregates (Brown *et al.*, 1983). However, our experiments provide new insight to this field in terms of elucidating the molecular mechanisms underlying the water flow across the pelvic skin of the tree frog by identifying the AQP molecules as AQP-h2 and AQP-h3. The combined application of IP + AVT increased water permeability to levels not significantly different from AVT alone. Hillyard (Hillyard, 1979) did find an additive effect of IP and AVT as did De Sousa and Grosso (De Sousa and Grosso, 1982) with isolated skin. It is possible that there is a maximum level of water permeability given that the production of cyclic AMP is considered to reach a plateau. In comparison, water permeability did not increase in the PP (β-receptor antagonist)-treated pelvic skins or in the control skin to nearly the same degree, which is consistent with there being no evidence of translocation of AQP-h2 and AQP-h3 proteins to the apical plasma membrane. This finding suggests that AQP protein plays an important role in facilitating the permeation of water across the ventral pelvic skin by mediation *via* the β-receptor. We observed that the effect of AVT was inhibited when the pelvic skins were treated with PP + AVT combined. This inhibition may be dependent upon the physiological status of the principal cells in the FRC layer as our immunoflurorescence studies indicated the presence of two cell types: the apical plasma membrane of some cells in the FRC layer is labeled while others are

not, suggesting two cellular compartments that could be activated independently. In this context, De Sousa and Grosso demonstrated that the β-adrenergic response appears to be independent of AVT (De Sousa and Grosso, 1982). It is important to note that one of several β-adrenergic actions is the induction of not only translocation of AQP in the apical membrane of the principal cells but also vascular perfusion in the connective tissue underlying the epidermis (Viborg and Hillyard, 2005; Willumsen *et al.*, 2007). Both actions stimulate the absorption of water from the pelvic skin.

In conclusion, our data demonstrate that AVT, hydrins and β-adrenergic agents stimulate water permeability *via* a common mechanism of AQP insertion into the apical membrane of the principal cells in the FRC layers. The issue of whether V2 receptor and β-adrenergic receptor may act independently or in different principal cells in the FRC layers remains an important question.

Acknowledgment

This work was supported in part by a grant-in-aid for scientific research from the Ministry of Education, Science, Sports, and Culture of Japan to S.T.

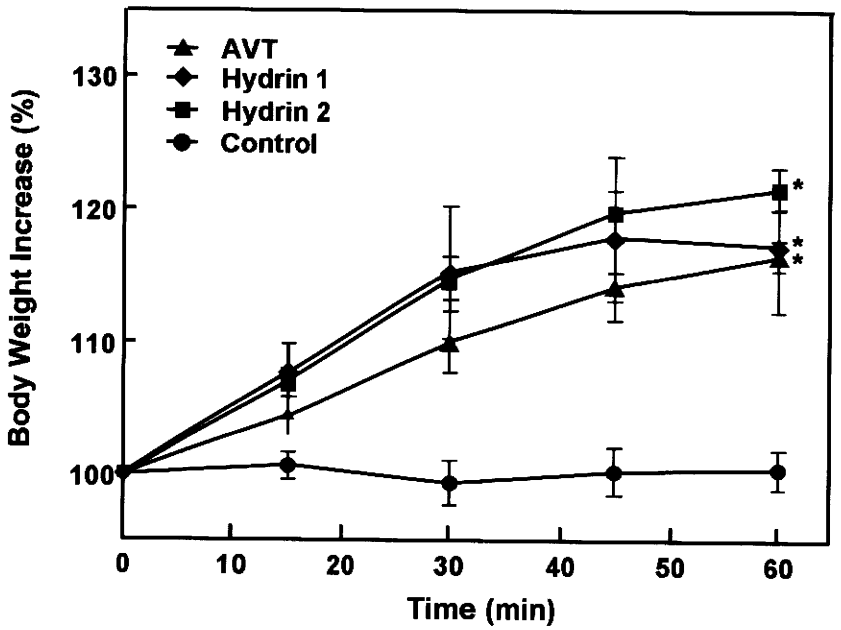

Fig. 3-1. Time course of water permeability across the ventral pelvic skin *in vivo* following challenge with arginine vasotocin (AVT), hydrin 1 and hydrin 2. The body mass of these frogs challenged with each the hormone increases significantly with the time. At sixty minutes there are significant difference between control group and hormone-treated groups ($p<0.01$) but not among the hormone-treated groups.

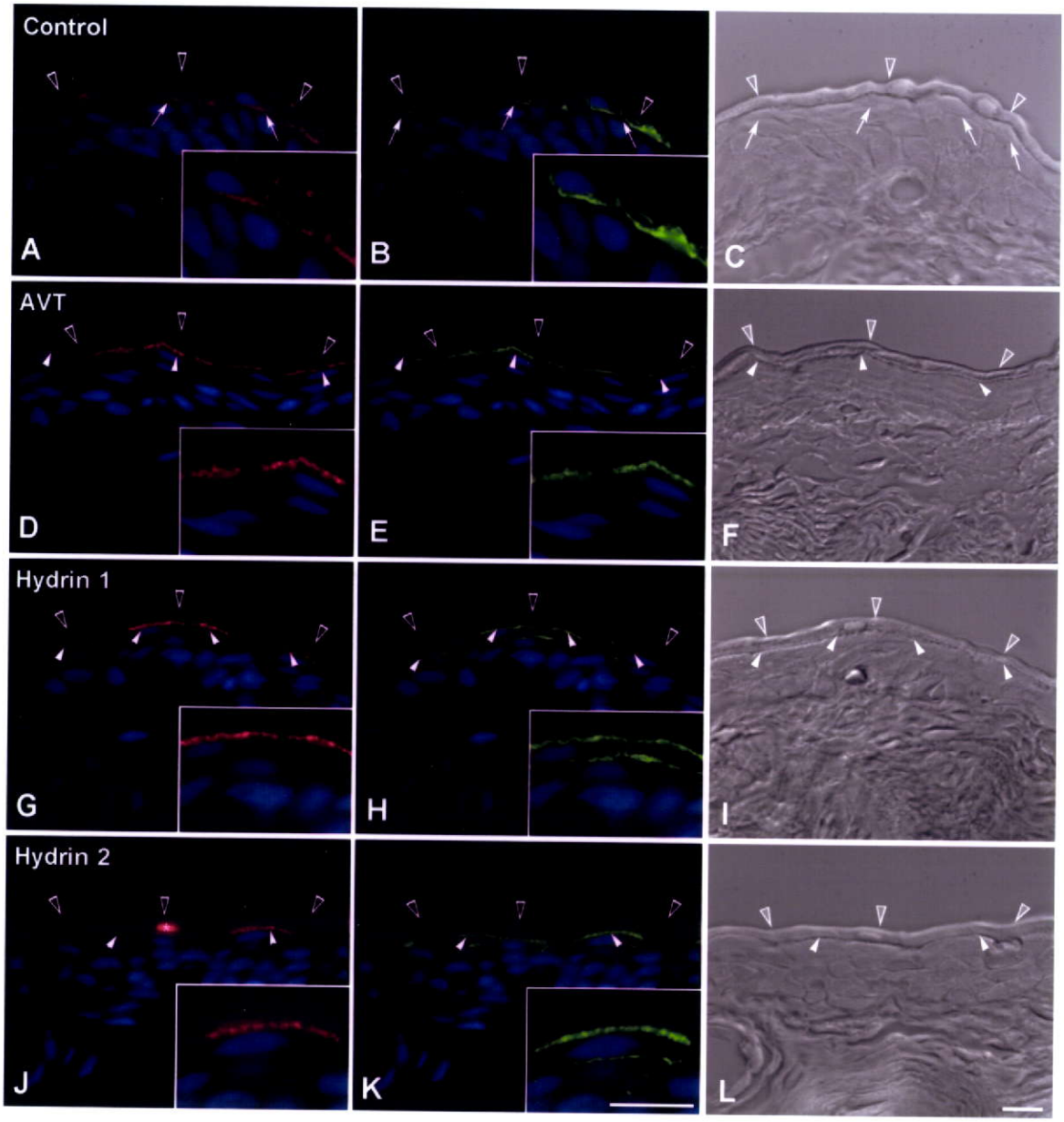

Fig. 3-2. Fluorescence images of the pelvic skin *in vivo* experiment. The labels for AQP-h2 (red) and AQP-h3 (green) are observed in the basolateral plasma membrane in the principal cells in the control group (A-C). In the arginine vasotocin (AVT) (D-F)-, hydrin 1 (G-I)-, and hydrin 2 (J-L)-treated groups, labels for AQP-h2 (red) and AQP-h3 (green) are visible in the apical plasma membrane in the principle cells in the first reacting cell layers of the pelvic skin. C, F, I and L are the corresponding Nomarski differential interference images. Arrows and white arrowheads indicate basolateral and apical plasma membrane, respectively. Asterisk: non-specific label. Open arrowheads: cornified layer. Nucleus: blue color. Scale bar, 10 μm.

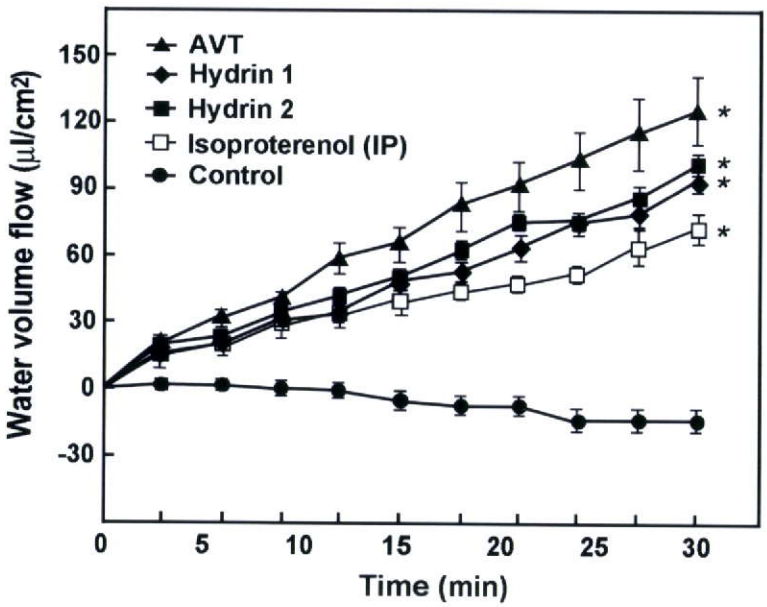

Fig. 3-3. Time course of water permeability across the isolated ventral pelvic skin in vitro after challenged with arginine vasotocin (AVT), hydrin 1, hydrin 2 and isoprpterenol (IP). The amount of water in the chamber on the serosal side increased significantly with time following the addition of the hormones. *$p<0.01$ vs control.

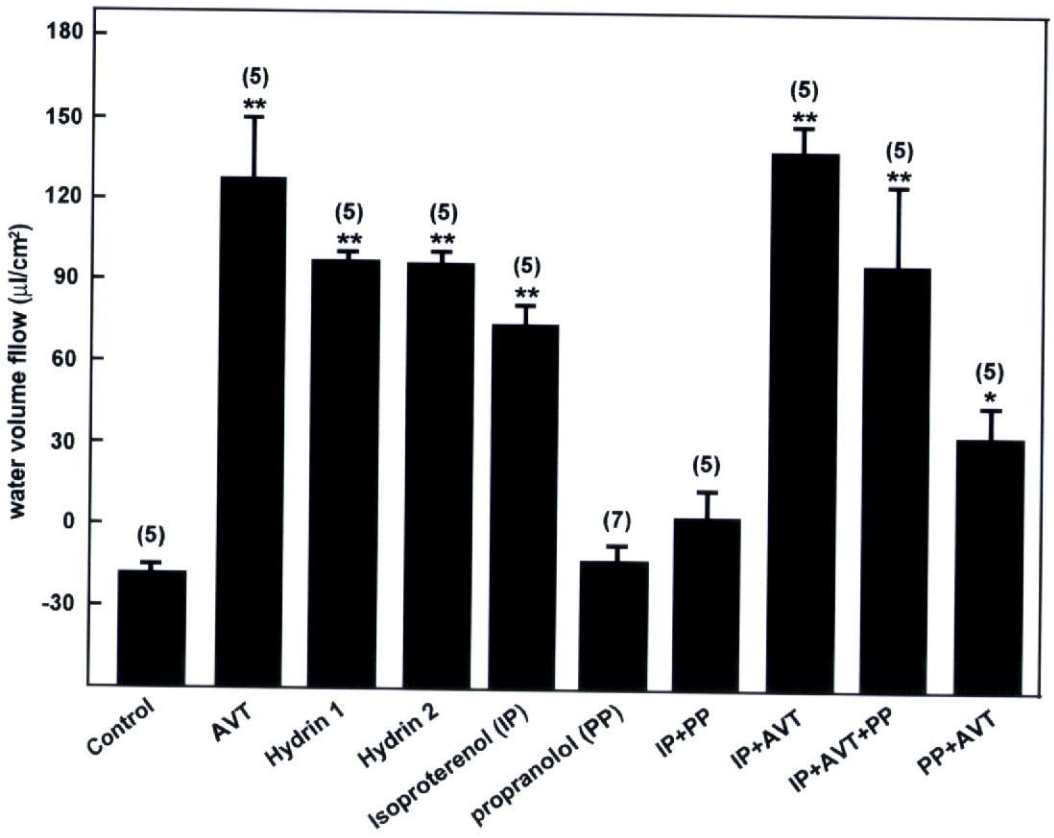

Fig. 3-4. Comparison of water permeability *in vitro* experiment at the final incubation time (thirty minutes) among the arginine vasotocin (AVT)-, hydrin 1-, hydrin 2-, isoproternol (IP)-, propranolol (PP)-, IP+PP-, IP+AVT-, IP+AVT+PP- and PP+AVT-groups. AVT, hydrin 1, hydrin 2 and IP significantly increased water permeability when compared with the control ($p<0.01$). By contrast, there is no significant difference among the PP-, IP+PP-treated skins and the control skins. The IP+AVT and the IP+AVT+PP treatments resulted in a strong increase of water permeability, similar to AVT-treatment. However, the PP+AVT treatment significantly decreasesed significantly water permeability when compared with the AVT group but water permeability was high than that of the control skins. The number of individuals used in each group is indicated in parentheses. *$p<0.01$ ver. control.

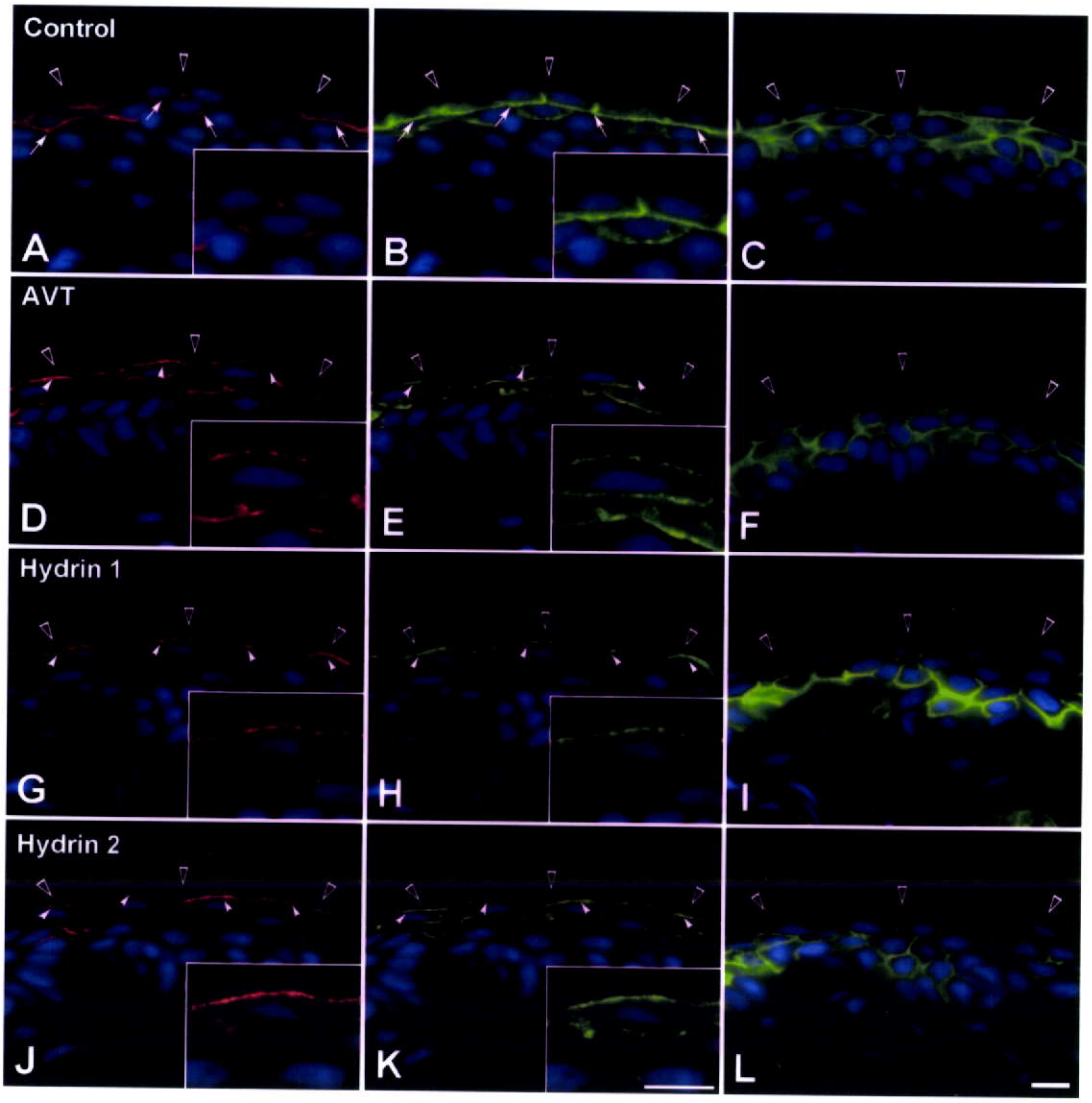

Fig. 3-5. Fluorescence images of the pelvic skin in the *in vitro* experiment. In the control skins, the labels for AQP-h2 (red) (A) and AQP-h3 (green) (B) are obserbed in the basolateral plasma membrane in the principal cells. In the arginine vasotocin (AVT)-, hydrin 1-, and hydrin2-treated skins, labels for AQP-h2 (D, G and J) and AQP-h3 (E, H and K) are visible in the apical plasma membrane (white arrows) in the principal cells in the first-reacting cell (FRC) layers of the pelvic skin. AQP-h3BL is constitutively expressed in the basolateral membrane in all the groups (C, F, I and L). Insets in A, B, D, E, G, H, J and K show higher magnificantion of each of the figure. Open arrow-heads: cornified layer. Nucleus: blue color. Scale bars, 10μm.

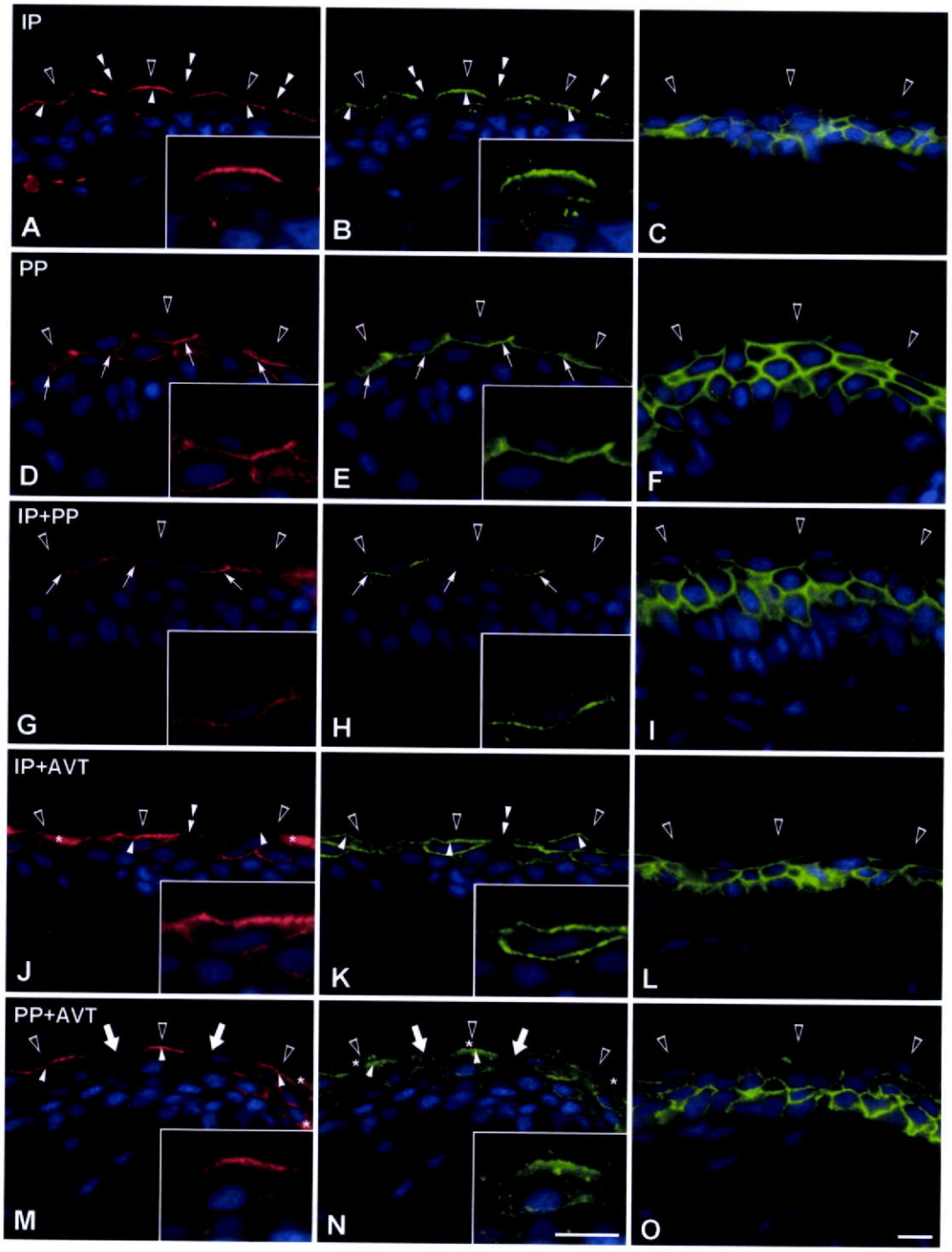

Fig. 3-6. Fluorescence images of the pelvic skin *in vitro* experiment. In the isoproterenol (IP)-treated skins, labels for AQP-h2 (red) (A) and AQP-h3 (green) (B) are visible in the apical plasma membrane. In the propranolol (PP)- and IP+PP treated skins, the labels for AQP-h2 (D and G) and AQP-h3 (E and H) are observed in the basolateral plasma membrane in the principal cells. In the IP+arginine vasotocin (AVT)-treated skins, labels for AQP-h2 (J) and AQP-h3 (K) are visible in the apical plasma membrane in the principal cells in the first-reacting cell (FRC) layers of the pelvic skin. In the PP+AVT-treated skins, labels for AQP-h2 (M) and AQP-h3 (N) are obserbed differentially among the principal cells; one label is in the apical plasma membrane in all of the groups (C, F, I, L and Q). Arrows and white arrowheads indicate the basolateral and apical plasma membrane, respectively. Insets in A, B, D, E, G, H, J, K, M and N shows higher magnification of each of the figures. Open arrowheads: cornified layer. Nucleus: blue color. Scale bars, 10μm.

References

Acher R, Chauvet J, Rouille Y. (1997) Adaptive evolution of water homeostasis regulation in amphibians: vasotocin and hydrins. *Bio Cell* 89: 283-291

Agre P. (2006) The aquaporin water channels. *Proc Am Thorac Soc* 3: 5-13

Akabane G, Ogushi Y, Hasegawa T, Suzuki M, Tanaka S. (2007) Gene cloning and expression of an aquaporin (AQP-h3BL) in the basolateral membrane of water-permeable epithelial cells in osmoregulatory organs of the tree frog. *Am J Physiol Regul Integr Comp Physio.* 292: R2340-R2351

Bentley PJ, Main AR. (1972) Zonal differences in permeability of the skin of some anuran Amphibia. *Am J Physiol* 223: 361-363

Bentley PJ, Yorio T. (1979) Do frogs drink? *J Exp Biol* 79: 41-46

Brown D, Grosso A, de Sousa RC. (1980) Isoproterenol-induced intramembrane particle aggregation and water flux in toad epidermis. *Biochim Biophys Acta* 596: 158-164

Brown D, Grosso A, DeSousa RC. (1983) Correlation between water flow and intramembrane particle aggregates in toad epidermis. *Am J Physiol* 245: C334-342

De Sousa RC, Grosso A. (1982) Osmotic water flow across the abdominal skin of the toad bufo marinus: effect of vasopressin and isoprenaline. *J Physiol* (Lond) 329: 281-296

Hillyard SD. (1979) The effect of isoproterenol on the anuran water balance response. *Comp Biochem Physiol C* 62C: 93-95

Ishibashi K, Kuwahara M, Sasaki S. (2000) Molecular biology of aquaporins. *Rev Physiol Biochem Pharmacol* 141: 1-32

Hasegawa T, Tanii H, Suzuki M, Tanaka S. (2003) Regulation of water absorption in the frog skins by 2 vasotocin-dependent water-channel aquaporins, AQP-h2 and AQP-h3. *Endocrinology* 144: 4087-4096

Hasegawa T, Suzuki M, Tanaka S. (2005) Immunocytochemical studies on translocation of phosphorylated AQP-h2 protein in granular cells of the frog urinary bladder before and after stimulation with vasotocin. *Cell Tissue Res* 322: 407-415

Hillman SS, Withers PC, Drewes RC, Hillyard SD. (2009) In *Ecological and Environmental Physiology of Amphibians pp.* 1-68. New York,: Oxford University Press.

Michel G, Ouedraogo Y, Chauvet J, Katz U, Acher R. (1993) Differential processing of provasotocin: relative increase of hydrin 2 (vasotocinyl-Gly) in amphibians able to adapt to an arid environment. *Neuropeptides* 25: 139-143

Ogushi Y, Mochida H, Nakakura T, Suzuki M, Tanaka S. (2007) Immunocytochemical and phylogenetic analyses of an arginine vasotocin-dependent aquaporin, AQP-h2K, specifically expressed in the kidney of the tree frog, *Hyla japonica*. *Endocrinology* 148: 5891-5901

Rouille Y, Michel G, Chauvet MT, Chauvet J. (1989) Hydrins, hydroosmotic neurohypophysial peptides: osmoregulatory adaptation in amphibians through vasotocin precursor processing. *Proc Natl Acad Sci USA* 86: 5272-5275

Takata K, Matsuzaki T, Tajika Y. (2004) Aquaporins: water channel proteins of the cell membrane. *Prog Histochem Cytochem* 39: 1-83

Tanii H, Hasegawa T, Hirakawa N, Suzuki M, Tanaka S. (2002) Molecular and cellular characterization of a water channel protein, AQP-h3, specifically expressed in the frog ventral skin. *J Membr Biol* 188: 43-53

Viborg AL, Rosenkilde P. (2004) Water potential receptors in the skin regulate blood perfusion in the ventral pelvic patch of toads. *Physiol Biochem Zool* 77: 39-49

Viborg AL, Hillyard SD. (2005) Cutaneous blood flow and water absorption by dehydrated toads. *Physiol Biochem Zool* 78: 394-404

Yokota SD, Hillman SS. (1984) Adrenergic control of the anuran cutaneous hydroosmotic response. *Gen Comp Endocrinol* 53: 309-314

Yorio T, Bentley PJ. (1978) The permeability of the skin of the aquatic anuran *Xenopus laevis* (Pipidae). *J Exp Biol* 72: 285-289

Willumsen NJ, Viborg AL, Hillyard SD. (2007) Vascular aspects of water uptake mechanisms in the toad skin: perfusion, diffusion, confusion. *Comp Biochem Physiol A Mol Integr Physiol* 148: 55-63

Chaptor 4

Water Adaptation Strategy in Anuran Amphibians: Molecular Diversity of Aquaporin

Abstract

Most adult anuran amphibians except for the aquatic species absorb water across the ventral pelvic skin and reabsorb it from urine in the urinary bladder. Many terrestrial and arboreal species use a region in the posterior or pelvic region of the ventral skin that is specialized for rapid rehydration from shallow water sources or moist substrates. Periods of terrestrial activity can be prolonged by reabsorption of dilute urine from the urinary bladder. Aquaporin (AQP), a water channel protein, plays a fundamental role in these water absorption/reabsorption processes, which are regulated by antidiuretic hormone. Characterization of AQPs from various anurans revealed that the unique water homeostasis is basically mediated by two types of anuran-specific AQPs, *i.e.* ventral pelvic skin and urinary bladder type, respectively. The bladder-type AQP is further expressed in the pelvic skin of terrestrial and arboreal species, together with the pelvic skin-type AQP. In contrast, the pelvic skin-type AQP (AQP-x3) of the aquatic *Xenopus* has lost the ability of efficient protein production. The extra C-terminal tail in AQP-x3 consisting of 33 nucleotides within the coding region appears to participate in the posttranscriptional regulation of AQP-x3 gene expression by attenuating protein expression. The positive transcriptional regulation of bladder-type AQP in the pelvic skin and negative posttranscriptional regulation of pelvic skin-type AQP provide flexibility in the water regulation mechanisms, which might have contributed to the evolutionary adaptation of anurans to a wide variety of water environments.

Introduction

Anuran amphibians are widely distributed throughout the world and have successfully adapted to a wide range of habitats (Hillman *et al.*, 2009; Pough, 2007). These include totally aquatic species such as *Xenopus laevis*, semiaquatic species such as *Rana catesbeiana*, *R. nigromaculata*, and *R. japonica* that are generally found near permanent water sources, and more terrestrial species such as *Bufo japonicus* and *Hyla japonica* that have expanded their habitats to varying degree to include drier land. Both semiaquatic and terrestrial species are subjected to evaporative water loss across their thin skin when foraging away from the water (Lyllywhite, 2006) and have developed osmoregulatory systems for maintaining water balance. One of these is that most adult anurans do not drink water through their mouth; rather, they absorb water across their skin, primarily on the ventral pelvic surface because the dorsal skin is relatively impermeable to water (Bentley *et al.*, 1972; Bentley *et al.*, 1979). The osmotic permeability of the pelvic skin can be greatly stimulated by the amphibian antidiuretic hormone arginine vasotocin (AVT; the nonmammalian vertebrate counterpart of vasopressin) (Bentley *et al.*, 1972; Bentley *et al.*, 1979; Bentley, 2002) and allows for rehydration from shallow puddles or moist substrates. As with absorption across the skin, reabsorption from the bladder and renal tubules is stimulated by AVT. These responses have collectively been termed the water balance response or antidiuretic response (Bentley *et al.*, 2002; Heller *et al.*, 1979). More recently, water permeability of cell membranes has been shown to be mediated by aquaporins (AQPs) (Preston *et al.*, 1992). AQPs are a class of integral membrane proteins that form selective water channels (pores) in the plasma membrane of various cells of organisms (Zardoya, 2005). In mammals, the AQP family consists of 13 different members (AQP0–AQP12) (Ishibashi *et al.*, 2000; Takata *et al.*, 2004).Wehave recently identified three distinct

types of AVT-stimulated AQPs in the tree frog, *H. japonica*; AQP-h2 in both the urinary bladder and ventral pelvic skin, AQP-h3 in the pelvic skin, and AQP-h2K in the kidney (Hasegawa *et al.*, 2003; Tanii *et al*, 2003; Ogushi *et al.*, 2007). Transepithelial water transport in the tree frog seems to be regulated through the actions of these apically expressed AQPs in concert with a fourth AQP, AQP-h3BL, which is expressed in the basolateral plasma membrane of the epithelial cells (Akabane *et al.*, 2007). Phylogenetic analyses of AQP proteins from anurans and mammals have defined 12 clusters of anuran AQP: 10 conventional types corresponding to mammalian AQP0–AQP5 and AQP7– AQP10 and two anuran-specific types designated as a1 and a2 (the letter a represents anuran) (Ogushi *et al.*, 2007; Suzuki *et al.*, 2009). The cluster of type a2 includes AQP-h2 and AQP-h3 from *H. japonica* (Hasegawa *et al.*, 2003; Tanii *et al.*, 2002) and AQP-t2 (AF02622) and AQP-t3 (AF020622) from *B. marinus*. In contrast, AQP-h2K and AQP HC-2, which have been isolated from the kidney of *H. japonica* and *H. chrysoscelis*, and mammalian AQP2 belong to the type 2 cluster, suggesting that both AQP-h2K and AQP HC-2 are anuran orthologs of vasopressin-stimulated mammalian AQP2 (Ogushi *et al.*, 2007; Zimmerman *et al.*, 2007). Weconducted this study to elucidate whether and, if so, how AQPs have contributed to anuran adaptation to various water environments.

Materials and Methods

Animals

Sexually mature *H. japonica, B. japonicus, R. catesbeiana, R. nigromaculata, R. japonica*, and *X. laevis* of both sexes were purchased from a commercial dealer (Ouchi, Saitama, Japan). The ventral pelvic skins were removed under anesthesia (MS222; Nacalai tesque, Kyoto, Japan) and then processed for cDNA cloning of the pelvic skin-type AQP. We designated the AQPs as AQP-rj3, AQP-rn3, AQP-rc3, AQP-bj3,

and AQP-x3, respectively. Similarly, various tissues (the ventral pelvic skin, dorsal skin, urinary bladder, kidney, stomach, small and large intestines, lung, heart, skeletal muscle, and brain) were removed for analysis by RT-PCR. All animal experiments were carried out in compliance with the Guide for Care and Use of Laboratory Animals of Shizuoka University.

Construction of the ventral pelvic skin cDNA library

Total RNA was prepared from 0.5 g of the pelvic skin from *R. japonica* and *X. laevis*, with Trizol RNA extraction reagent (Invitrogen, Tokyo, Japan), and poly(A)$^+$ RNA was isolated from the total RNA using oligo-deoxythymidine (dT)-coated latex beads (Oligotex-dT30 Super; Takara, Kyoto, Japan) according to the manufacturer's instructions. λZAP DNAlibraries were constructed as previously described by Tanii *et al.* (Tanii *et al.*, 2002).

Oligonucleotide primers for the PCR analysis

Degenerate primers for the original amplification of anuran AQP fragments were designed based on the amino acid sequences around the two conserved NPA (asparagine-prolinealanine) boxes of the major intrinsic protein (MIP) family AQPs (Agre *et al.*, 1995). All primers were commercially synthesized (Operon Biotechnologies, Tokyo, Japan) as shown in supplemental Table S1 (published as supplemental data on The Endocrine Society's Journals Online web site at http://endo.endojournals.org).

RT-PCR amplification and sequence analysis

The skin poly(A)$^+$ RNA (0.5 μg) was reverse transcribed using Moloney murine leukemia virus (M-MLV) reverse transcriptase (Invitrogen) according to the

manufacturer's instructions, and partial sequences of each anuran cDNA were amplified by PCR with the primers (supplemental Table S1), as described by Tanii *et al.* (Tanii *et al.*, 2002). Amplified fragments were subcloned into pGEM-3Z vectors (Promega, Madison, WI) and sequenced using an Aloka DNA sequencing system [model Lic-4200L(S); Aloka, Japan].

Screening of the anuran skin cDNA library

A DNA probe, obtained from the first PCR product, was synthesized using a digoxigenin High Prime kit (Roche Molecular Biochemicals, Meylan, France) and used to screen the pelvic skin cDNA library, as previously described (Tanii *et al.*, 2002).

Oligonucleotide design for rapid amplification of cDNA ends (RACE) technique

The sense primer and antisense primer used for cloning AQP-rn3, AQP-rc3, and AQP-bj3 are given in supplemental Table S1.

Cloning of the partial-length cDNA

The ventral pelvic skins were used for totalRNApreparation. PCR was performed using primers 1 and 4 (supplemental Table S1), as described previously (Ogushi *et al.*, 2007). The PCR products were purified after gel electrophoresis and sequenced using the Aloka DNA sequencer.

3'- and 5'-RACE

The RACE technique was used to obtain the full-length AQPrn3, AQP-rc3, and AQP-bj3 sequences. For 3'-RACE, isolated poly(A)$^+$ RNA was primed with oligo-dT 19 adaptor primer (supplemental Table S1) and reverse transcribed using M-MLV reverse transcriptase (Invitrogen).A1-μl aliquot of the RT product was then PCR

amplified with primer 2 and the adaptor primer (supplemental Table S1); subsequent amplification was performed using primer 3 and the adaptor primer (supplemental Table S1). After denaturation at 95 C for 5 min, PCR amplification program consisted of five cycles of 60 sec at 94 C, 60 sec at 60 C, and 90 sec at 72 C; five cycles of 60 sec at 94 C, 60 sec at 58 C, and 90 sec at 72 C; five cycles of 60 sec at 94 C, 60 sec at 56 C, and 90 sec at 72 C; and 15 cycles of 60 sec at 94 C, 60 sec at 55 C, and 90 sec at 72 C. The obtained clone was sequenced as described in the text. For 5'-RACE, poly(A)$^+$ RNAwas primed with primer 4 (supplemental Table S1) and reverse transcribed using the M-MLVreverse transcriptase (Invitrogen). This first strand of cDNA was purified with the QIA Quick PCR purification kit (QIAGEN, Hilden, Germany), and a poly(A) tail was synthesized at the 3' terminus of thecDNAwith 1mMdATP and 0.8 U/20μl terminal deoxynucleotidyl transferase (Toyobo, Osaka, Japan). After the resultant cDNA was purified once again using the same kit, the second cDNA was synthesized with Ex *Taq* polymerase (1.25 U/50 μl) and oligo-dT (19) adaptor primer (supplemental Table S1) sequentially for 5 min at 93 C, 90 sec at 42 C, and 3 min at 72 C. A 1-μl aliquot of second-strand cDNA was then amplified by PCR with primer 5 and the adaptor primer (supplemental Table S1). This product was then amplified by PCR with the primer 6 and the adaptor primer (supplemental Table S1). These PCR amplifications were carried out under conditions identical to those described for the 3'-RACE-PCR. The obtained sequences are described in the text.

RT-PCR of anuran tissues

The tissue expression of ventral-type AQP mRNA in each anuran was analyzed by RT-PCR. Trizol reagent was used to prepare total RNA from various tissues of anuran species. Total RNA (20 μg) was first treated with deoxyribonuclease I (4 U; Takara), after which a 10-μg aliquot of the total RNA product was reverse transcribed

with M-MLV reverse transcriptase (Invitrogen) at 37 C for 1 h and then at 70 C for 30 min. The RT-PCR analysis was performed basically by the same method described above, using the homologous primers P3 (sense) and P4 (antisense) (supplemental Table S1, *underlined*). The RTPCR products were analyzed on a 2% agarose gel containing ethidium bromide (0.5 μg/ml).

Antibodies

An oligopeptide corresponding to the amino acids 241-255 (ST-186:NYDPEYEGEREEHRK)of the *Xenopus* AQP-x3 protein, with an amino-terminal cysteine, was synthesized as described previously (Ogushi *et al.*, 2007). The antibody was raised in a rabbit with the ST-186 peptide coupled to keyhole limpet hemocyanin. Similarly, the C-terminal (CT) regions of AQP-rc3 (ST-188, amino acids 260-273: LNSLNNYSKNMEKA) and AQP-rj3 (ST-157, amino acids 260-273: LNSLNNYSKNMDKA) were synthesized as antigen peptides. The rabbit anti-*Hyla* AQP-h2 serum (ST-140) had been generated and characterized previously (Hsegawa *et al.*, 2003). To detect AQP-bj3 protein, we were able to use rabbit anti-*Hyla* AQP-h3 (ST-141; Tanii *et al.*, 2002) because 13 in 17 amino acid residues in the CT sequence of *Hyla* AQP-h3 protein used as the antigen are identical to that of *B. japonicus*. For a similar reason, we used rabbit-anti-AQP-rc3 to detect AQP-rn3 protein.

Mutant

To obtain mutated *Xenopus* AQP-x3, we constructed two kinds of reverse primers containing mutated sites (supplemental Table S1) and a forward primer bearing *Sac*I (Takara) and Kozak sequences. We then performed the PCR analysis performed using the AQP-x3 cDNA as the template, described above. The amplified AQP-x3 fragments were digested with *Sac*I, purified further from the agarose gel using the Ultra Clean

DNA purification kit(MOBIO Laboratories, Solana Beach, CA), and inserted into a pGEM-5Z vector with 3'-terminus of AQP-x3, which was produced by digesting the pGEM-5Z vector (Promega) bearing the full-length AQP-x3 cDNA with *Sac*I and *Hin*dIII. In the chimeric construct encoding AQP-h2K-AQP-x3CT, the AQP-x3 CT tail sequence was added to the C terminus of AQP-h2K. To generate this chimera, we digested AQP-x3 cDNA/pGEM-5Z with *Xba*I and *Spe*I, purified the pGEM-5Z vector bearing the C terminus of AQP-x3 with the gel, and stored the latter at -23 C until use. To obtain the insert DNA (AQP-h2K), we performed a PCR analysis using a forward primer with a Kozak sequence and *Spe*I recognition sequence in the start codon and a reverse primer with the stop codon of AQP-h2K replaced with *Xba*I recognition sequence (supplemental Table S1). The PCR product was digested with *Xba*I and *Spe*I by the same method described above and ligated to the pGEM-5Z vector bearing the C terminus of AQP-x3 with a Mighty Mix ligation kit (Takara).

Osmotic water permeability of oocytes

The full length of each ventral pelvic skin-type AQP was produced by RT-PCR using a pelvic skin-type AQP-specific primer with the Kozak sequence (supplemental Table S1) and the pelvic skin-type AQP-specific primer with poly(A)25 (supplemental Table S1). The product of the PCR amplification was cloned into the pGEM-5Z vector. cRNAs were prepared from linearized pGEM-5Z vectors containing the entire open reading frame of the pelvic-type AQP by transcription and capping with SP6RNA polymerase (mCAP RNA capping kit; Stratagene, La Jolla, CA). Stage V and VI *Xenopus* oocytes were defolliculated by collagenase (1 mg/ml; Roche Molecular Biochemicals), microinjected with either cRNAs (50 ng) or water, and incubated for 3 d in Barth's buffer at 18 C, after which they were transferred from 200 to 70mOsmBarth's buffer. The osmotically elicited increase in volume was monitored at

24 C under an Olympus BX50 microscope with a x4 magnifying objective lens and a CCD camera connected to a computer. The coefficient of osmotic water permeability (*Pf*) was calculated from the initial slope of oocyte swelling according to accepted methodology (Fushimi et al., 1993; Zhang et al., 1990). In some experiments, AQP cRNA-injected oocytes were incubated with 50 mM forskolin (FSK) (Sigma-Aldrich, Tokyo, Japana) or 0.3 mM $HgCl_2$ for 10 min. To confirm whether the pelvic skin-type AQP protein was expressed in *Xenopus* oocytes after the injection of the cRNA, we evaluated AQP cRNA-injected or water injected oocytes by Western blot analysis and immunohistochemistry as described below.

Western blot analysis

The pelvic skin including the thighs and urinary bladder from *H. japonica*, *B. japonicus*, *R. japonica*, *R. nigromaculata*, *R. catesbeina*, and *X. laevis* were homogenized in cell lysis buffer [50 mM Tris-HCl (pH 8.0), 0.15 M NaCl, 1% Triton X-100, 0.1 mg/ml phenylmethylsulfonyl fluoride, and 1 μg/ml aprotinin] and centrifuged at 16,000xg in a microcentrifuge for 10 min to remove insoluble materials. In *R. nigromaculata*, we treated the extract from the cRNA-injected oocytes at 37 C with peptide-*N*-glycosidase F (Daiichi Pure Chemicals, Tokyo, Japan) before SDS-PAGE and Western blot to remove the sugar chain. The protein (10μg) was denatured at 70C for 10 min in denaturation buffer comprising 3% sodium dodecyl sulfate, 70 mM Tris (pH 6.8), 11.2% glycerol, 5% 2-mercaptoethanol, and 0.01% bromophenol blue, subjected to electrophoresis on a 12% polyacrylamide gel, and then transferred to an Immobilon-P membrane (Millipore, Tokyo, Japan). The proteins on the membrane were reacted sequentially with rabbit anti-AQP-h2 (ST-140), rabbit anti-AQP-h3 (ST-141), rabbit anti-AQP-rc3 (ST-188), rabbit anti-AQP-rj3 (ST-157), or rabbit anti-AQP-x3 (ST-186) serum, biotinylated goat anti rabbit IgG (Jackson

ImmunoResearch, West Grove, PA), and streptavidin-conjugated horseradish peroxidase (Dako Japan, Co., Ltd., Kyoto, Japan). The reaction products on the membrane were visualized using an ECL Western blot detection kit (Amersham Pharmacia Biotech, Buckinghamshire, UK). To check the specificity of the immunoreaction, we performed an absorption test by preincubating anti-AQP antibody with the antigen peptide (10 μg/ml). Similarly, the anuran cRNA-injected or AQP-x3 and its mutant cRNA-injected oocytes were analyzed by the same method described above.

Immunofluorescence staining

The oocytes were fixed overnight at 4 C in periodate-lysine paraformaldehyde fixative, dehydrated, and embedded in Paraplast. Thin (4 μm) sections were cut and mounted on gelatincoated slides, deparaffinized, and rinsed with distilled water and PBS. For single labeling of the respective pelvic skin-type AQP proteins, immunofluorescence staining was performed essentially as described previously (Ogushi *et al.*, 2007). The sections were sequentially incubated with 1% BSA-PBS, primary antiserum [rabbit anti-AQP-h3serum, rabbit anti-AQP-rj3 (1:2000), rabbit anti-AQP-rc3 (1:3000), or rabbit anti-AQP-x3 serum (1:2000)], and Cy3-labeled affinity-purified donkey antirabbit IgG (1:400; Jackson Immunoresearch). For nuclear counterstaining, 4', 6-diamidino-2-phenylindole was included in the secondary antibody solution. The sections were finally washed with PBS and then mounted in PermaFluor (Immunon, Pittsburgh, PA). The specificity of the immunostaining was checked using an absorption test by preincubating the anti-AQP-x3 or anti-AQP-rc3 antiserum with the corresponding antigen peptide (10μg/ml). Specimens were examined with an Olympus BX61 microscope equipped with a BX-epifluorescence attachment (Olympus Optical, Tokyo, Japan).

Statistical analysis

Statistical analyses for the *Pf* values were performed by using Ekuseru-Toukei 2008 software (Social Survey Research Information Co., Tokyo, Japan). The data were compared by the Steel test after the Kruskal-Wallis test.

Results and Discussion

In a set of molecular cloning experiments, we successfully identified primary structure of AQP-h3 homologs in the ventral pelvic skin of all the species examined: AQP-bj3 from *B. japonicus*, AQP-rc3 from *R. catesbeiana*, AQP-rn3 from *R. nigromaculata*, AQP-rj3 from *R. japonica*, and AQP-x3 from *X. laevis* (Fig. 4-1 A and supplemental Figs. S1–S5). The putative precursors of the AQP-h3 homologs were identified as 29.1- to 29.4-kDa proteins composed of 271 or 273 amino acids, except for AQP-x3 of *X. laevis* (30.8 kDa with 283 residues). The common features of the AVT-stimulated AQPs appeared to be conserved in all of these AQP-h3 homologs in that all had 1) a single protein kinase A phosphorylation site at Ser-255 or -257, 2) six transmembrane regions with both the N and C terminus located in the cytoplasm, consistent with other members of the major intrinsic protein (MIP) family, 3) one or two *N*-glycosylation sites, and 4) two conserved NPA motifs as well as 5) a mercurysensitive cysteine residue just upstream of the second NPA motif. In addition, RT-PCR revealed that AQP-h3 homologous mRNA was predominantly expressed in the ventral pelvic skin in all of the anuran species examined (Fig. 4-1B). Based on these results, we designated the AQP-h3homolog as the pelvic skin-type AQP. In the Western blot analyses using extracts of native ventral pelvic skin from *H. japonica*, *B. japonicus*, *R. catesbeiana*, *R. nigromaculata*, and *R. japonica*, we detected a major band at approximately 29 kDa, which corresponds to the molecular masses estimated

from the predicted amino acid sequences of the pelvic skin-type AQPs. In the Western blot analysis using anti-AQP-x3 antibody; however, no bands were detected in the extract of native ventral pelvic skin in *X. laevis* (Fig. 4-2). Using Western blot analysis with anti-*Hyla* AQP-h2 antibody (ST-140), we next determined whether the AQP-h2 homolog is expressed in anuran species occupying different habitats. An examination of the immunostaining of extracts of the urinary bladder of *H. japonica*, *B. japonicus*, *R. catesbeiana*, *R. nigromaculate*, and *X. laevis* revealed signals on a band at approximately 30 kDa and on smeary bands between 35 and 90 kDa in each species (Fig. 3-3 A, lane 1). The AQP-h2-immunoreactive 30-kDa protein was also detected in the pelvic skin of the terrestrial *B. japonicus* and arboreal *H. japonica* but not in the semiaquatic *Rana* or the aquatic *X. laevis* (Fig. 3-3 A, lane 2). No positive band was detectable in the dorsal skin of any of the species analyzed (Fig. 3-3 A, lane 3). All of the immunoreactive signals except for the nonspecific ones disappeared when the anti-AQP-h2 was preincubated with the corresponding antigen peptide (Fig. 4-3 B, lane 1). The smeary bands with a higher molecular weight appeared to correspond to the glycosylated form of these AQPs, the presence of which has been reported in several tissues of *H. japonica* (Hasegawa *et al.*, 2003; Tanii *et al.*, 2002; Ogushi *et al.*, 2007; Akabane *et al.*, 2007). No positive band was detectable in the protein extract of the urinary bladder of *R. japonica* with anti-AQP-h2 (Fig. 4-3 A, lane 1). This may be attributed to a difference in amino acid sequence of the CT portion of the urinary bladder-type AQP between *R. japonica* and *H. japonica*, because anti-AQP-h2 antibody was raised against the 14 CT amino acids of AQP-h2 (Hasegawa *et al.*, 2003). Based on these results, we postulated that the AQP-h2 homolog is the urinary bladder-type AQP, which is also expressed in the pelvic skin of terrestrial and arboreal anurans but not in that of aquatic and semiaquatic ones. The acquisition of a gene regulatory system that directs the expression of both bladder-type AQP and pelvic skin-type AQP in the

ventral pelvic skin is likely to provide terrestrial anurans with the molecular mechanism for efficient water absorption, leading to rapid rehydration from limited water sources and allows greater exploitation of terrestrial habitats. In contrast, the skin of the aquatic clawed frog, *X. laevis*, has a much lower water permeability that reduces excessive entry of water into the body and is not stimulated by AVT (Bentley et al., 1972; Bentley, 1966). How can aquatic anurans reduce the water permeability of their ventral skin while expressing the ventral skin-type AQP-x3? This was investigated with functional expression analysis of the pelvic skin-type AQP proteins by injecting their cRNAs into *Xenopus* oocytes. The membrane permeability (*Pf*), *i.e.* volume increase rate, of the AQP-bj3-, AQP-rc3-, AQP-rn3-, and AQP-rj3-injected oocytes was approximately 2.7-, 3.6-, 3.2-, and 3.9-fold higher than that of the water-injected oocytes, respectively (supplemental Figs. S6–S9, C and D). This artificially stimulated water permeability was significantly inhibited by 0.3mM $HgCl_2$ ($P<0.01$ or $P<0.001$). These results show that the pelvic skin-type AQPs in the terrestrial and semiaquatic species were functionally expressed in the oocytes and also indicate the respective potency of these AQPs in stimulating water permeation. Furthermore, Western blot analysis detected a single major 29-kDa band and smeary bands larger than 31 kDa in the oocytes injected with the different cRNAs (supplemental Figs. S6–S9, A). This finding was confirmed by immunofluorescence studies, in which an intense immunopositive reaction was observed in the plasma membrane of the oocytes (supplemental Figs. S6–S9, B). On the other hand, native AQP-x3 cRNA, when injected into *Xenopus* oocytes, failed to induce either detectable AQP-x3 protein expression (Fig. 4-4 A) or a change in the *Pf* (Fig. 4-4 C). Immunofluorescence staining corroborated that no immunopositive substances are visible in the AQP-x3 cRNA-injected oocytes, because there are no differences in the staining when the sections were compared with those labeled with the preabsorbed antiserum (Fig. 4-4 B).

Because AQP-x3 has the unusual CT tail but likely a full set of functional features common to the AVT-stimulated AQP family as mentioned above, we next examined the effects of manipulating the CT tail of AQP-x3 in the oocyte system. The cRNA of an AQP-x3 deletion mutant that lacks the CT tail (C273Stop) was injected into the *Xenopus* oocytes. Surprisingly, the deletion of the CT tail resulted in AQP-x3 protein being expressed in the respective cRNA-injected oocyte as two intense bands of approximately 31 kDa and weak smeary bands of 37–97 kDa when examined by immunostaining with anti-*Xenopus* AQP-x3 (ST-186) (Fig. 4-4 A a). Immunofluorescence staining of the cRNA-injected oocytes showed AQP-x3 C273Stop mutant. These signals were completely abolished by preabsorption of the antiserum with the immunogen peptide (Fig. 4-4 A b). Immunofluorescence staining of the cRNA-injected oocytes showed that immunopositive AQP-x3 C273Stop substances are visible predominately in the cytoplasm near the plasma membrane. The corresponding Nomarski differential interference image and the immunofluorescence images of oocytes after the addition of FSK showed the presence of immunopositive substances in the plasma membrane. The immunolabelings were also intensified in the cytoplasm near the plasma membrane. In the absorption test with the antigen, the immunopositive substances nearly disappeared to background levels in the oocytes injected with AQP-x3 C273Stop mutant cRNA. Without FSK stimulation, there was no change in water permeation (*Pf*) in the oocytes injected with wild-type and AQP-x3 C273Stop cRNA (Fig. 4-4 B). However, water permeation did increase after the addition of FSK in those oocytes injected with AQP-x3 C273Stop cRNA but not in the case with the wild-type AQP-x3 cRNA (Fig. 4-4 C). These results are consistent with those obtained by the Western blot and immunofluorescence analyses (Fig. 4-4, A and B). The FSK-stimulated osmotic water permeability of AQP-x3 mutant-injected oocytes was reduced with 0.3 mM $HgCl_2$ (Fig. 4-4 C). These results indicate that the mutant

AQP-x3 protein without its CT tail was functionally expressed and translocated to the plasma membrane in response to FSK/intracellular cAMP in the *Xenopus* oocyte. The effect of adding the CT tail of AQP-x3 to the AQP-h2K protein was also examined in the oocyte expression system. Native AQP-h2K is fully functional as an AVT-responsive AQP *in vivo* and *in vitro* (Ogushi *et al.*, 2007). Nevertheless, as shown in Fig. 4-5, the cRNA for chimeric AQP-h2K with the CT tail failed to induce either the expression of detectable AQP protein or an increase in the membrane permeability, thereby demonstrating that the CT tail of AQP-x3 is necessary and sufficient for posttranscriptional attenuation of AQP gene expression. A substitution mutant of AQP-x3 with the serine residue replacing cysteine-273 (C273S) was fully functional as an AVT/FSK-responsive AQP when expressed in the oocyte (Fig. 4-4), suggesting the singular importance of this Cys-273 residue and/or the Cys-273-coding region of AQP-x3 mRNA in the unique negative regulation of AQP-x3 protein production. Thus, in aquatic *Xenopus*, the extra CT sequence of pelvic skin type AQP and/or its coding region in AQP mRNA negatively regulate protein expression, which may contribute to the impermeability of the skin and to the prevention from excessive water entry in the low osmotic freshwater environments. The more detailed molecular mechanisms for attenuating AQP-x3 protein expression remain an unsolved mystery. There are several posttranslational steps known to regulate the amounts of specific proteins, which include the translational initiation step regulated partly by RNA-binding proteins that keep specific mRNA away from the ribosomal machinery (Keene, 2007), translational elongation step that can be attenuated by some unique structure of mRNA or nascent polypeptide (Berisio *et al.*, 2003), and posttranslational steps, i.e. sorting and turnover of nascent protein (Bonifacino *et al.*, 2003). Additional experiments are required to discern which steps are responsible for regulation of AQP-x3 gene. Loss of functional pelvic skin-type AQP protein appears reasonable for aquatic life of *X. laevis*. The data

presented here show that AQP-x3 mRNA is considerably expressed in the ventral pelvic skin (Fig. 4-1B) and that AQP-x3 protein without the CT tail fully functioned as a hormone-sensitive pelvic skin-type AQP (Fig. 4-4) imply physiological importance of this gene in *X. laevis*. *X. laevis* is not a completely aquatic anuran but is able to adapt to diverse natural conditions in its tropical habitat (25–27). Thus, it is possible that in the dry season, this species may absorb water from the wet soil through the skin, in which AQP-x3 protein, liberating from the negative posttranscriptional regulation through a yet to be described mechanism, could be produced in the pelvic skin. Further studies are necessary to find conditions that may result in the expression of mature AQP-x3 protein. In conclusion, we have described two unique types of anuran-specific AQPs, the bladder and pelvic skin type, respectively, in terms of their molecular diversity and possible importance in osmoregulation. During evolutionary adaptation to various water environments, anurans may have acquired molecular adaptive mechanisms that regulate the positive transcription of bladder-type AQP in the ventral pelvic skin and negative posttranscription of pelvic skin-type AQP. Our results provide evidence for potential molecular mechanisms that may underlie the diversified physiological processes of anuran-specific water economy, which has been studied since the discovery of Robert Townson in the 1790s (Jorgensen, 1997; Macknight *et al.*, 1980).

Acknowledgment

We thank Dr. Hidetsugu Sakai (Department of Biology, NihonUniversity School of Dentistry) for assistance with the statistical analysis.

This work was supported in part by a grant-in-aid for scientific research from the Ministry of Education, Science, Sports, and Culture of Japan to S.T. and M.S.

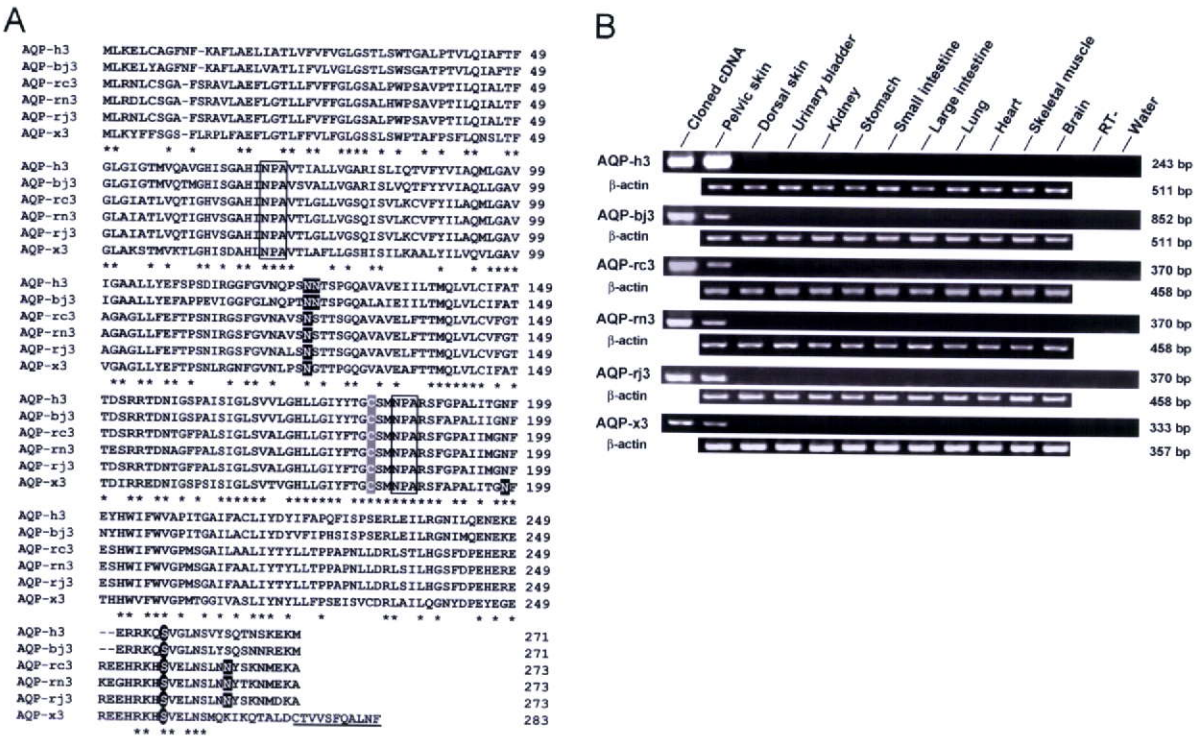

FIG. 4-1. A, Comparison of the predicted sequence of anuran ventral pelvic skin-type AQPs. Gaps indicated by the *dashed lines* have been introduced to obtain maximum homology. NPA (asparagines-proline-alanine) motifs are outlined. C in the *gray box*, S in the *solid circle*, and N in the *solid square* indicate mercury-sensitive cysteine residues, phosphorylation sites for protein kinase A, and *N*-glycosylation sites, respectively. The *underline* indicates the additional 11 amino acids seen only in the C terminus of AQP-x3 protein. The amino acid residues that match those of the AQP-h3 homologs are indicated by *asterisks*. B, Tissue expression of AQP-h3, AQP-bj3, AQP-rc3, AQP-rn3, AQP-rj3, and AQP-x3 mRNA by RT-PCR. RT-PCR products obtained using the primers (supplemental Table S1) were separated on a 2% agarose gel. RT and water represent the negative control using the ventral pelvic skin sample without a RT reaction and with water instead of cDNA, respectively. β-actin was used as positive control.

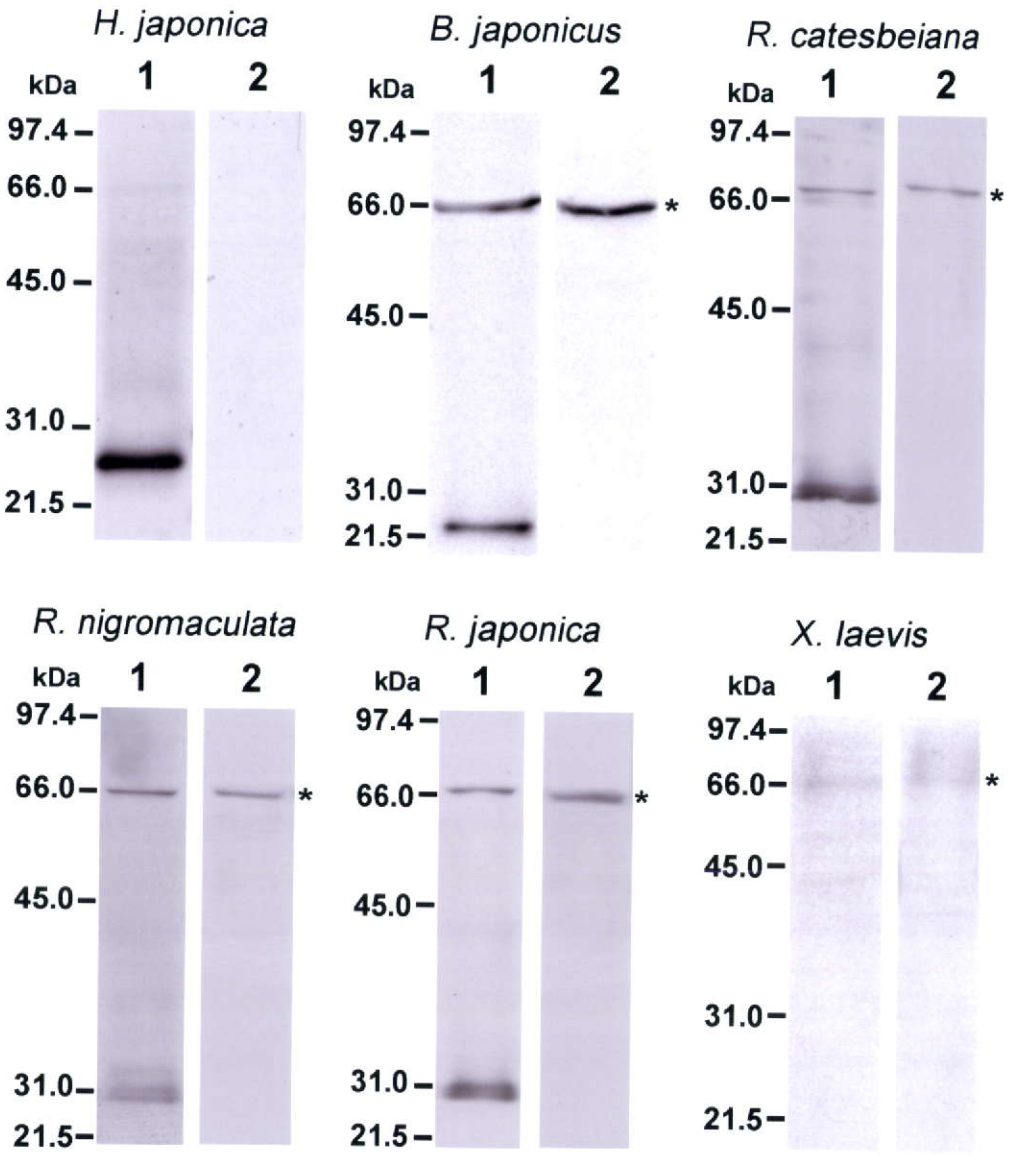

FIG. 2. Western blot analysis of extracts from the native ventral pelvic skin of several anuran species. In the extract of *H. japonica*. *B. japonicus*, *R. nigromaculata*, *R. catesbeina* and *R. japonica*, immunoreactive bands are detected in major bands at approximately 29 kDa (lane 1). The positive bands disappear at background levels when the membranes are incubated with the preabsorbed antibody with the respective antigen (lane 2). However, no band is visible in the extract of *X. laevis*. *Asterisks* indicate nonspecific bands. The antisera used in the Western blot are described in *Materials and Methods*.

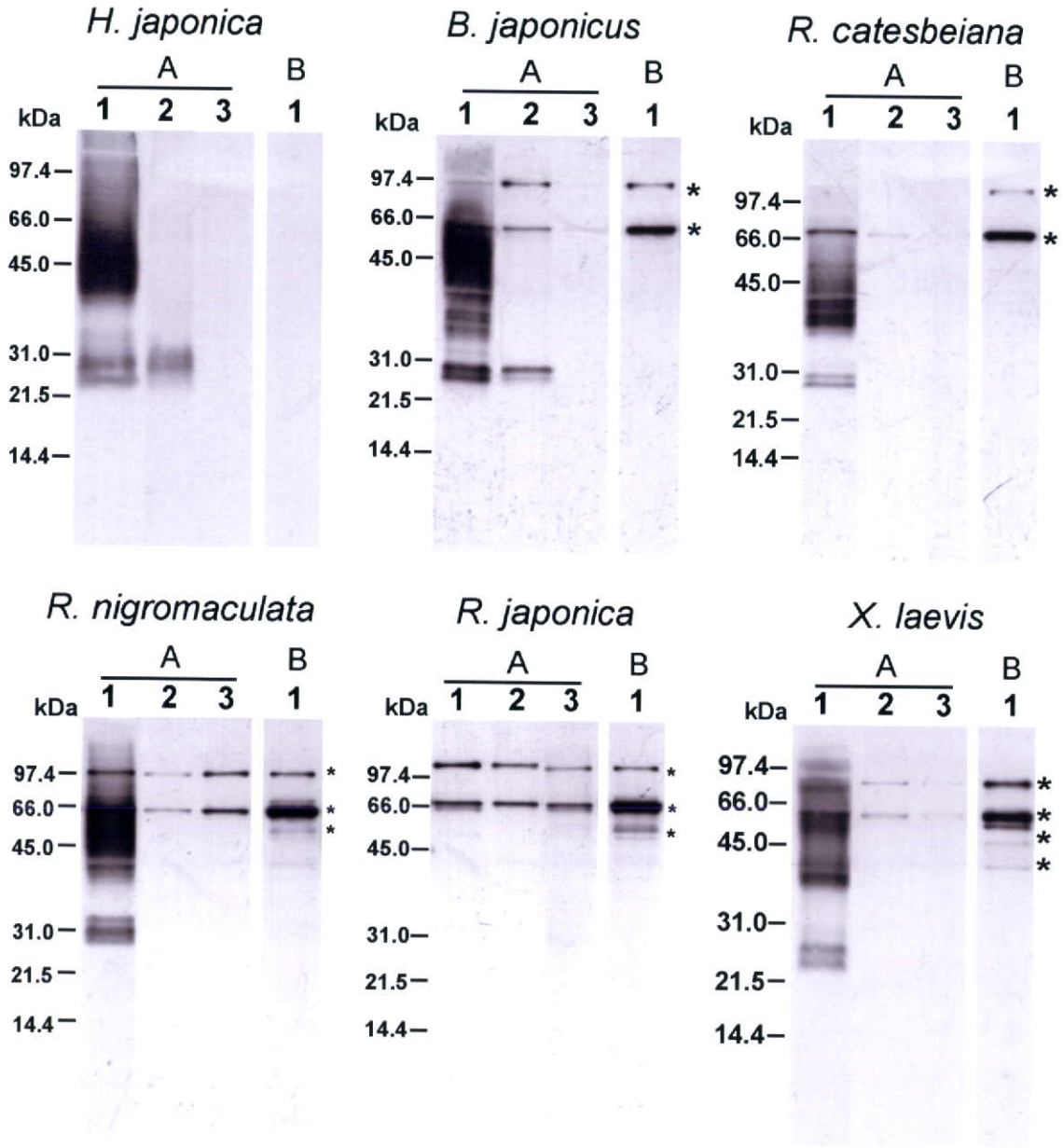

FIG. 3. Western blot analysis of extracts from the urinary bladder, ventral pelvic skin, and dorsal skin using rabbit anti-*Hyla* AQP-h2. A, Lane 1, urinary bladder, with positive bands seen at 29 or 31 kDa and smeary bands at 35–90 kDa in all species examined except for *R. japonica*; lane 2, pelvic skin, with the AQP-h2-positive band detected in the pelvic skin of *B. japonicus* and *H. japonica* but not in that of the other species; lane 3, dorsal skin, with no positive bands visible in the dorsal skin of all the species examined. B, Lane 1, in absorption test, the immunopositive bands visible in the urinary bladder are nearly abolished at background levels. *Asterisks* indicate nonspecific bands.

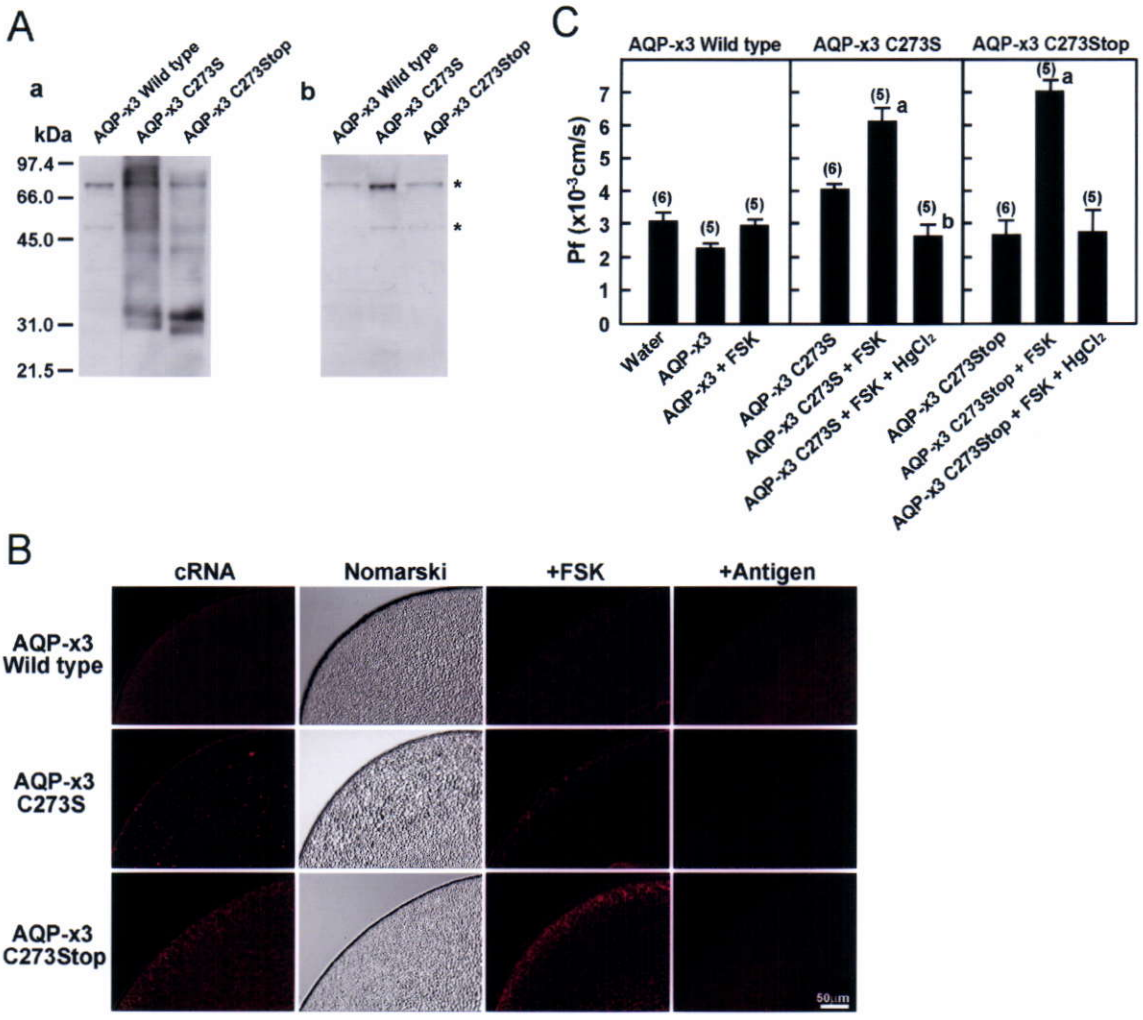

FIG. 4. Functional expression analysis using *Xenopus* oocytes injected with cRNA of AQP-x3 (wild-type) and its mutants. A, Western blot analysis of AQP-x3 (wild-type)-injected oocytes prepared after complete swelling. No immunoreactive bands are seen in the membrane. Immunoreactive bands are seen at approximately 31 and 37–97 kDa in the extract of AQP-x3 C273S- and AQP-x3 C273Stop-injected oocytes (a). In the absorption test, these positive bands disappeared at the background levels. *Asterisks* indicate nonspecific bands (b). B, Immunofluorescence images of the oocytes after the injection of the cRNA of AQP-x3 and its mutants. No immunopositive substances are visible in the AQP-x3 cRNA-injected oocytes. For the AQP-x3 C273S and AQP-x3 C273Stop mutants, immunopositive AQP-x3 substances are visible predominately in the cytoplasm near the plasma membrane. The corresponding Nomarski differential interference image and the immunofluorescence images of oocytes after the addition of FSK show the presence of immunopositive substances in the plasma membrane in the AQP-x3 C273S and AQP-x3 C273Stop images. In the absorption test (Antigen), the immunopositive substances have nearly disappeared in the oocytes. C, Swelling assay with *Xenopus* oocytes. Although there was no change in water permeation (*Pf*) in the oocytes injected with wild-type, AQP-x3 C273S, and AQP-x3 C273 Stop cRNA, water permeation did increase after the addition of FSK, but only in those oocytes injected with AQP-x3 C273S and AQP-x3 C273Stop cRNA. The FSK-stimulated osmotic water permeability of AQP-x3 mutant-injected oocytes was reduced with 0.3 mM $HgCl_2$. The representative data shown are given as the mean SE of measurements for five to six oocytes in each experimental group. AQP-3x C273S: a, P 0.05 *vs.* AQP-x3 C273S; b, P 0.05 *vs.* AQP-x3 C273S FSK; AQP-x3 C273Stop: a, P 0.05 *vs.* AQP-x3 C273Stop; b, P 0.05 *vs.* AQP-x3 C273Stop FSK.

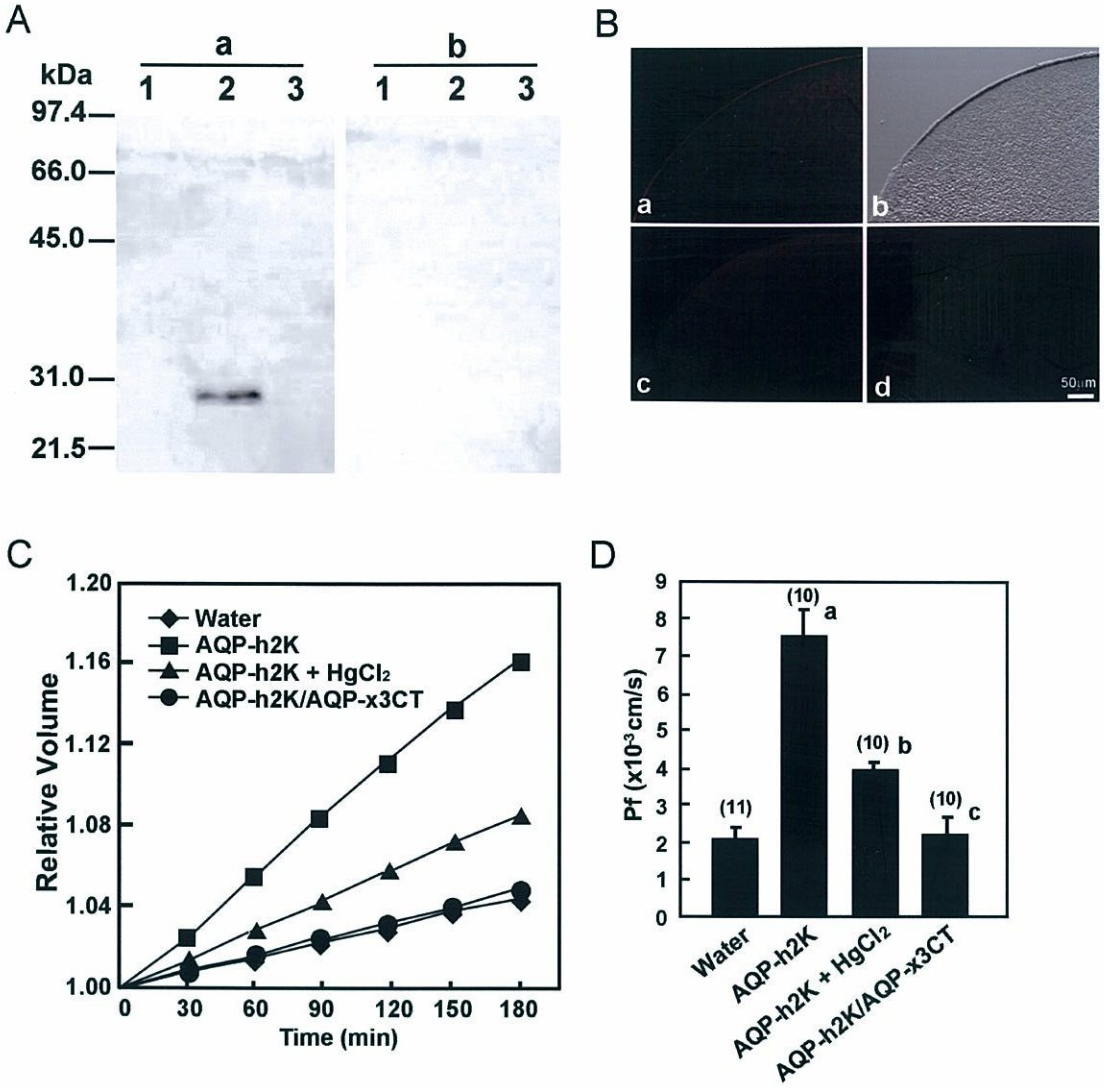

FIG. 5. Functional expression analysis using *Xenopus* oocytes injected with cRNA forchimeric AQP-h2K containing the C terminus of AQP-x3 (AQP-x3CT). A, Western blot analysis of the oocytes injected with the chimera cRNA using anti-*Hyla* AQP-h2K (a) and the antibody preabsorbed with the immunogen (b). Lane 1, Extract of waterinjected oocytes; lane 2, extract of AQP-h2K cRNA-injected oocytes; lane 3, extract of AQP-h2K/AQP-x3CT cRNA-injected oocytes. A positive band is visible at 29 kDa only in the AQP-h2K cRNA-injected oocytes, but it disappears with the addition of the preabsorbed antiserum. B, Immunofluorescence images of the AQP-h2K cRNA- or AQP-h2K/AQP-x3CT cRNA-injected oocytes: a, after complete swelling of the oocytes injected with AQP-h2K cRNA, immunoreactive substances are visible predominately in the plasma membrane; b, corresponding Nomarski differential interference image; c, absorption test showing that the immunoreactive substances obtained with anti-AQPh2K nearly disappear to background levels in the AQP-h2K-injected oocytes. d, only background levels are observed in the AQP-h2K/AQP-x3CT-injected oocytes. C, Time course of the osmotic swelling. Oocytes were microinjected with water or cRNAs encoding AQP-h2K or AQP-h2K/AQP-x3CT, respectively. Some of the AQP-h2Kinjected oocytes were incubated with 0.3 mM HgCl2. D, The *Pf* was calculated from the initial rate of oocyte swelling. Water permeability increased significantly in the AQP-h2K-injected oocytes but deceased significantly after the addition of $HgCl_2$ to the oocytes. In contrast, no increase in water permeation was induced in the AQP-h2K/ AQP-x3CT-injected oocytes. The representative data are given as the mean SE of measurements for 10–11 oocytes in each experimental group. a, P 0.001 *vs.* water; b, P 0.01 *vs.* AQP-h2K; c, P 0.01 *vs.* AQP-h2K/AQP-x3CT.

Table S1 Primers used for cloning and PCR analysis of anuran AQP sequences

Name	Primer sequence (5'-3')	bp
Oligo-dT(19) adaptor	$(T)_{19}$ GACTCGAGTCGACATCGAT	
RACE Adaptor	GACTCGAGTCGACATCGAT	
AQP master primer		
Master (M) primer 1	AGCGGGG (CG) (CT) CAC (AC) T (CT) AACCC	
M primer 2	A (AG) (AG) GA (CG) C (GT) (GT) GC (AT) GG (AG) TTCA	
M primer 3	GG (AT) CC (AG) A (CT) CCA (AG) AAGA (T) CCA	
AQP-h3 specific primer		
h3-primer 1	TCGTGGCAACATTTTGCAAG	763-782
h3-primer 2	TGGTCTGATGTATGGATGAG	988-1007
AQP-bj3 specific primer		
bj3-primer 1	CTTTTATTGACTGTCATCATGC	65 - 86
bj3-primer 2	CTTTTTAGCTGAGCTGGTAGC	121 - 141
bj3-primer 3	TAGGACTGTCAGTGGTACTG	576 - 594
bj3-primer 4	AGAATACAGAATAGGATTTCAC	895 - 916
bj3-primer 5	ACGAGAAGTGCTACACTTACAG	294 - 315
bj3-primer 6	TACCACTGACAGTCCTATGG	573 - 592
Kozak-bj3-primer	GCCACCATGCTTAAGGAGCTATATGC	
bj3-A_{25}tail-primer	$(T)_{25}$ ACAGAATAGGATTTCAC	
AQP-rc3 specific primer		
rc3-primer 1	TGCATTACCTTGGCCCTCAGC	161 - 181
rc3-primer 2	AACATTGGGCTTACTGGTGG	284 - 305
rc3-primer 3	CCATCCAATATACGAGGTAGC	396 - 416
rc3-primer 4	CTTCTGCTGTCTGTTGTTCCG	508 - 529
rc3-primer 5	GCTACCTCGTATATTGGATGC	396 - 406
rc3-primer 6	ACTTCAGGACTGAGATCTGTG	307 - 327
Kozak-rc3-primer	TAGCCACCATGCTTAGAAACCTGTGC	
rc3-A_{25}tail-primer	$(T)_{25}$ CATCACATAATCATATTTATTTTC	
AQP-rn3 specific primer		
rn3-primer 1	AACATTGGGCTTACTGGTGG	284 - 305
rn3-primer 2	ATCTCAGTCCTGAAGTGTGTC	312 - 332
rn3-primer 3	AAAAGAGGGACACCGTAAGC	815 - 834
rn3-primer 4	CTACCTTAAGCTTTCTCCATG	875 - 895
rn3-primer 5	CTCCTGCTGTCTGTTGTTCCG	508 - 529
rn3-primer 6	CACAGATCTCAGTCCTGAAGT	307 - 327
Kozak-rn3-primer	TAGCCACCATGCTTAGAAACCTGTGC	
rn3-A_{25}tail-primer	$(T)_{25}$ AAGGAACAAAAGGTTCTTATTG	
AQP-rj3 specific primer		
rj3-primer 1	AACATTGGGCTTACTGGTGG	141 - 161
rj3-primer 2	ACTTCAGGACTGAGATCTGTG	488 - 509
AQP-x3 specific primer		
x3 primer 1	GTGACACTAGCATTCCTCTT	224 - 244
x3 primer 2	GCAGCCAGTGAAGTAAATCC	537 - 557
rc β-actin primer		
rc β-primer1	TACCTCATGAAGATCCTGACC	4 - 24
rc β-primer2	TGATCCACATCTGCTGGAAGG	462 - 481
rc β-primer3	TGATCCACATCTGCTGGAAGG	494 - 514
x β-actin primer		
x β-primer 1	ACTGTGACCTGACAGACTACC	579 - 598
x β-primer 2	CAGTATTGGCATAGAGGTCC	906 - 598
X3 mutant		
Sac1-Kozak-x3 primer	GGAGCTCGCCACCATGCTGAAATA	
C273Stop	GCTTGAAAAGATACTACAGTTCAATC	
C273S	GCTTGAAAAGATACTACAGTAGAATC	

The underlined primers are those used for the RT-PCR analyses

A

```
-82                                                    ATCATCCTGTAAACAGTAGCAC   -61
-60  AAGGAAGAACACCAGCGGGGATTTTGTTTTTAGTCTCCTTGGCTTTTATAGACTGTCATC             -1
  1  ATGCTTAAGGAGCTATATGCGGGATTTAATTTTAAGGCCTTTTTAGCTGAGCTAGTGGCA              60
  1   M  L  K  E  L  Y  A  G  F  N  F  K  A  F  L  A  E  L  V  A              20

 61  ACCCTCATATTTGTTCTTGTTGGCCTGGGTTCAACGCTATCATGGTCAGGAGCTACGCCA             120
 21   T  L  I  F  V  L  V  G  L  G  S  T  L  S  W  S  G  A  T  P              40

121  ACTGTCTTACAAATAGCCTTCACTTTTGGCTTGGGAATAGGTACAATGGTACAAACTATG             180
 41   T  V  L  Q  I  A  F  T  F  G  L  G  I  G  T  M  V  Q  T  M              60

181  GGCCACATCAGCGGGGCCCACATTAACCCTGCTGTAAGTGTAGCACTTCTCGTTGGGGCC             240
 61   G  H  I  S  G  A  H  I  N  P  A  V  S  V  A  L  L  V  G  A              80

241  CGAATATCTCTGGTCCAGACCTTTTACTATGTGATCGCTCAGCTACTGGGAGCTGTCATA             300
 81   R  I  S  L  V  Q  T  F  Y  Y  V  I  A  Q  L  L  G  A  V  I             100

301  GGGGCTGCTTTACTGTATGAGTTTGCACCACCTGAAGTCATTGGAGGATTTGGACTGAAT             360
101   G  A  A  L  L  Y  E  F  A  P  P  E  V  I  G  G  F  G  L  N             120

361  CAGCCAACTAACAATACATCACCCGGACAAGCACTGGCTATAGAAATCATTCTTACAATG             420
121   Q  P  T  N  N  T  S  P  G  Q  A  L  A  I  E  I  I  L  T  M             140
                ▲  ▲
421  CAGCTGGTCCTCTGCATCTTTGCTACAACGGACAGCCGGAGGACGGACAACATTGGTTCT             480
141   Q  L  V  L  C  I  F  A  T  T  D  S  R  R  T  D  N  I  G  S             160

481  CCAGCCATTTCCATAGGACTGTCAGTGGTACTGGGACACTTACTTGGGATTTATTACACT             540
161   P  A  I  S  I  G  L  S  V  V  L  G  H  L  L  G  I  Y  Y  T             180

541  GGATGTTCCATGAATCCAGCACGGTCCTTTGCTCCAGCTTTGATTATAGGAAACTTCAAT             600
181   G  C  S  M  N  P  A  R  S  F  A  P  A  L  I  I  G  N  F  N             200
         △
601  TACCATTGGATTTTCTGGGTGGGACCGATAACAGGAGCAATCTTGGCATGCTTGATTTAT             660
201   Y  H  W  I  F  W  V  G  P  I  T  G  A  I  L  A  C  L  I  Y             220

661  GACTATGTCTTCATCCCTCACTCAATAAGCCCCAGTGAAAGACTGGAAATCCTACGTGGC             720
221   D  Y  V  F  I  P  H  S  I  S  P  S  E  R  L  E  I  L  R  G             240

721  AACATTATGCAGGAAAATGAAAAAGAAGAAAGACGGAAACAATCTGTAGGCCTCAATTCT             780
241   N  I  M  Q  E  N  E  K  E  E  R  R  K  Q  S  V  G  L  N  S             260
                                                  ■
781  CTTTACAGCCAATCAAATAACAGGGAAAAAATGTGAAATCCTATTCTGTATTTTTTTTGT             841
261   L  Y  S  Q  S  N  N  R  E  K  M  *                                     271

841  CATTTTTTTGCAGTGAATATATTGTATTGTACAGAATATGTTGAGATATTAACAATGGTT             901
901  ATATAGTTTGGTTACAGATCATATGGCTACACTGCTACATGTCAGACCATGCAAGGTGGC             961
961  CCGTAGGAAAAAAAAAAGGCTATCCCTAGCTACAAAATGTTATACTTTATGAGATGAAAAA            1021
1021 TCAACACATTTACACATCATTGTGTTAGAGCATGTCCGATGTACTAACTATACATCTTTA            1081
1081 TAAAGTTTGAATATAAGATAAAAAAAAAAAAAAAAAAAAAAA                              1123
```

B

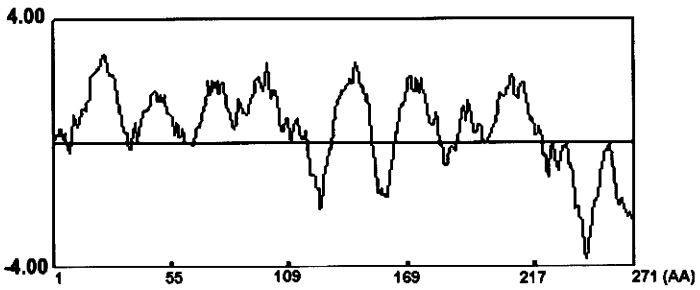

Supplemental Figure 1- A: Nucleotide and deduced amino acid sequence of aquaporin (*B. japonicus* AQP-bj3) cDNA. The predicted amino acid is shown below the nucleotide sequence (DDBJ/EBBL/GenBank accession no. AB500708). The asterisk indicates the stop codon. NPA motifs are outlined. The solid triangle indicates putative N-glycosylation sites. The square and open triangle indicate a phosphorylation site for protein kinase A and the mercurial-inhibition site, respectively. B: Kyte-Doolittle hydropathy profile (window 11) of the deduced AQP-bj3 amino acid sequence.

A

```
-68                                                          GGTCATTG   -61
-60  CAATGACATATAGCATAGAGTATACGAGAGCACGGCTTTAGAAAGACTTTGGTAGAAACC     -1
  1  ATGCTTAGAAACCTGTGCTCAGGTGCCTTTTCTCGGGCAGTTCTAGCTGAATTTTTAGGC     60
  1   M  L  R  N  L  C  S  G  A  F  S  R  A  V  L  A  E  F  L  G     20

 61  ACATTGTTATTTGTATTCTTTGGTCTTGGCAGTGCATTACCTTGGCCCTCAGCAGTGCCC    120
 21   T  L  L  F  V  F  F  G  L  G  S  A  L  P  W  P  S  A  V  P     40

121  ACTATCCTGCAGATCGCACTAACATTTGGTCTAGGTATAGCAACATTGGTCCAGACAATA    180
 41   T  I  L  Q  I  A  L  T  F  G  L  G  I  A  T  L  V  Q  T  I     60

181  GGACATGTCAGTGGTGCTCACATCAATCCTGCAGTAACATTGGGCCTACTGGTGGGATCA    240
 61   G  H  V  S  G  A  H  I  [N  P  A] V  T  L  G  L  L  V  G  S     80

241  CAGATCTCAGTCCTGAAGTGTGTCTTCTACATCCTGGCTCAGATGCTGGGAGCTGTGGCT    300
 81   Q  I  S  V  L  K  C  V  F  Y  I  L  A  Q  M  L  G  A  V  A    100

301  GGAGCTGGCTTACTCTTTGAGTTCACCCCATCCAATATACGAGGTAGCTTCGGAGTCAAT    360
101   G  A  G  L  L  F  E  F  T  P  S  N  I  R  G  S  F  G  V  N    120

361  GCGGTTAGCAATAGCACCACTTCTGGACAGGCTGTAGCTGTGGAGCTCTTCACTACTATG    420
121   A  V  S  N  S  T  T  S  G  Q  A  V  A  V  E  L  F  T  T  M    140
            ▲
421  CAGCTTGTGTTGTGTGTTTTCGGAACAACAGACAGCAGAAGAACAGACAATACAGGATTT    480
141   Q  L  V  L  C  V  F  G  T  T  D  S  R  R  T  D  N  T  G  F    160

481  CCAGCCTTATCCATTGGTTTATCAGTTGCTTTAGGACATTTACTTGGGATCTACTTCACT    540
161   P  A  L  S  I  G  L  S  V  A  L  G  H  L  L  G  I  Y  F  T    180

541  GGCTGTTCCATGAACCCTGCGAGGTCTTTTGGCCCTGCTATAATTATGGGAAATTTTGAA    600
181   G  C  S  M [N  P  A] R  S  F  G  P  A  I  I  M  G  N  F  E    200
         △
601  TCACATTGGATCTTCTGGGTAGGCCCCATGTCCGGTGCGATCCTTGCGGCCTTAATCTAT    660
201   S  H  W  I  F  W  V  G  P  M  S  G  A  I  L  A  A  L  I  Y    220

661  ACTTATCTTCTTACACCACCTGCACCAAATCTCCTAGATAGACTATCCACCTTGCATGGT    720
221   T  Y  L  L  T  P  P  A  P  N  L  L  D  R  L  S  T  L  H  G    240

721  AGCTTCGATCCAGAGCATGAACGTGAAAGAGAGGAACACCGTAAGCACTCAGTGGAACTC    780
241   S  F  D  P  E  H  E  R  E  R  E  E  H  R  K  H  S  V  E  L    260
                                                        ■
781  AATTCTCTTAACAACTATTCAAAGAACATGGAGAAAGCTTAAGGTGCTTTCAGGTTTCTG    840
261   N  S  L  N  N  Y  S  K  N  M  E  K  A  *                     273
            ▲
841  GCCTAGGCCCAATAATATCATAAACTCCCAGAAGTCTCCATTTTTTTTATTTCATCTGGA    900
901  GGAGGGAGTGAGAGGTTTTTTTCAGCCAAGTACACCCTCCTGCCTGCATGCCTGAGGCTAA    960
961  AGGCAAATCGTTTCCAGGAAGAAAATGTTACATGAATCCATCTGCCTATACTCAAGATGA   1020
1021 CTGTGGCTAGAAATGCTAGGGGGTGTTTTTTCAAAGTGATTTCTCAACAAAATAAAGTATG   1080
1081 GGCACATGGGTGGATGGGTGAATTTGCTATGAATATTAAAAATTTATAAAATTGTGTTTT   1140
1141 CGGTTCATAATGTTCCGATACAGTTACATTCTACTTTTACTGTTCCCTATTGTATGTTGA   1200
1201 TTGCCACATTACAGAACTCACCAACATATTTAGAAAATAAATATGATTATGTGATGAAAA   1260
1261 AAAAAAAAAAAAAAA                                               1275
```

B

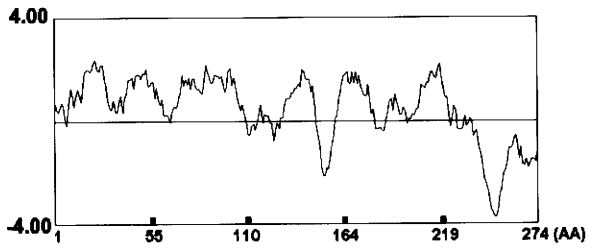

Supplemental Figure 2 - A: Nucleotide and deduced amino acid sequence of Aquaporin (*R. nigromaculata* AQP-rn3) cDNA. The predicted amino acid is shown below the nucleotide sequence (DDBJ/EBBL/GenBank accession no. AB500707). The asterisk indicates the terminal codon. NPA motifs are outlined. The solid triangle indicates a putative N-glycosylation site. The square and open triangle indicate phosphorylation sites for protein kinase A and the mercurial-inhibition site, respectively. B: Kyte-Doolittle hydropathy profile (window 11) of the deduced AQP-rn3 amino acid sequence.

A

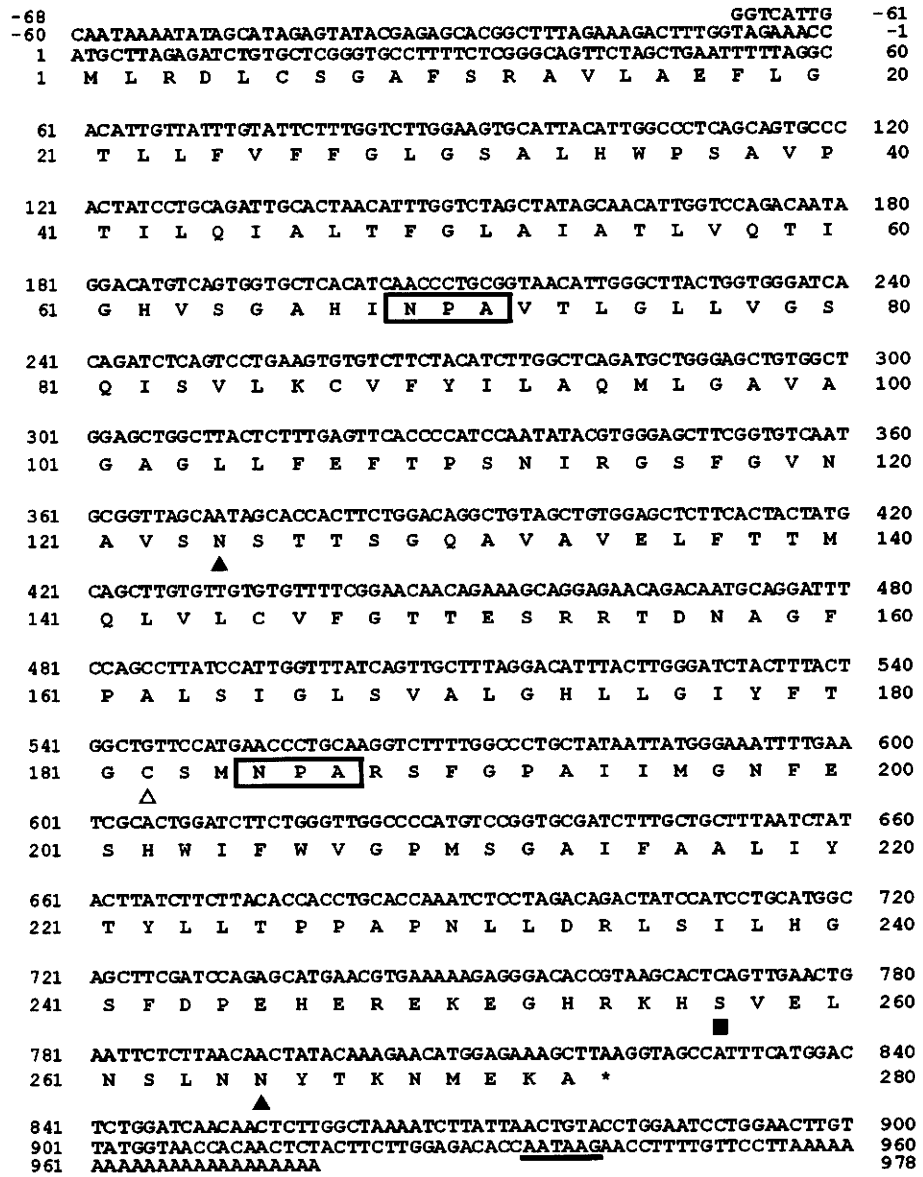

B

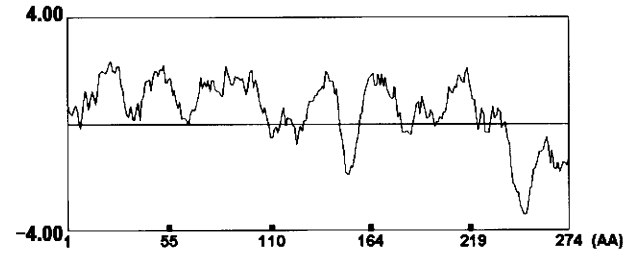

Supplemental Figure 3 - A: Nucleotide and deduced amino acid sequence of Aquaporin (*R. catesbeian* AQP-rn3) cDNA. The predicted amino acid is shown below the nucleotide sequence (DDBJ/EBBL/GenBank accession no. AB500705). The asterisk indicates the terminal codon. NPA motifs are outlined. The solid triangle indicates a putative N-glycosylation site. The square and open triangle indicate phosphorylation sites for protein kinase A and the mercurial-inhibition site, respectively. B: Kyte-Doolittle hydropathy profile (window 11) of the deduced AQP-rc3 amino acid sequence.

A

```
-47                AATTCGGCACGAGGAGAGCACGGCTTTAGAAAGACTTGGGAAGAAACC   -1
  1  ATGCTTAGAAATCTGTGCTCGGGTGCCTTTTCTCGGGCAGTTCTAGCTGAATTTTTAGGT    60
  1    M  L  R  N  L  C  S  G  A  F  S  R  A  V  L  A  E  F  L  G    20

 61  ACATTGTTATTTGTATTCTTTGGTCTTGGCAGTGCATTACCTTGGCCCTCAGCAGTGCCC   120
 21    T  L  L  F  V  F  F  G  L  G  S  A  L  P  W  P  S  A  V  P    40

121  ACTATCCTGCAGATCGCACTAACATTTGGTTTAGCTATAGCAACACTGGTCCAGACAATA   180
 41    T  I  L  Q  I  A  L  T  F  G  L  A  I  A  T  L  V  Q  T  I    60

181  GGACATGTCAGTGGTGCTCACATCAATCCTGCAGTAACATTGGGCTTACTGGTGGGATCA   240
 61    G  H  V  S  G  A  H  I  [N  P  A]  V  T  L  G  L  L  V  G  S    80

241  CAGATCTCAGTCCTGAAGTGTGTCTTCTACATCCTGGCTCAGATGCTGGGAGCTGTGGCT   300
 81    Q  I  S  V  L  K  C  V  F  Y  I  L  A  Q  M  L  G  A  V  A   100

301  GGAGCTGGCTTACTCTTTGAGTTCACCCCATCCAATATACGAGGGAGCTTTGGAGTCAAT   360
101    G  A  G  L  L  F  E  F  T  P  S  N  I  R  G  S  F  G  V  N   120

361  GCGCTTAGCAATAGCACTACTTCTGGACAGGCTGTAGCTGTGGAGCTCTTCACTACTATG   420
121    A  L  S  N  S  T  T  S  G  Q  A  V  A  V  E  L  F  T  T  M   140
                ▲
421  CAGCTTGTGTTGTGTGTTTTCGGAACAACAGACAGCAGAAGAACAGACAATACAGGATTT   480
141    Q  L  V  L  C  V  F  G  T  T  D  S  R  R  T  D  N  T  G  F   160

481  CCAGCCTTATCCATTGGTTTATCAGTTGCTTTAGGACATTTACTTGGGATCTACTTCACT   540
161    P  A  L  S  I  G  L  S  V  A  L  G  H  L  L  G  I  Y  F  T   180

541  GGCTGTTCCATGAACCCTGCAAGGTCTTTTGGCCCTGCTATAATTATGGGAAATTTTGAA   600
181    G  C  S  M  [N  P  A]  R  S  F  G  P  A  I  I  M  G  N  F  E   200
          △
601  TCACATTGGATCTTCTGGGTAGGCCCCATGTCCGGTGCAATCTTTGCTGCCTTAATCTAT   660
201    S  H  W  I  F  W  V  G  P  M  S  G  A  I  F  A  A  L  I  Y   220

661  ACTTATCTTCTGACACCACCTGCACCAAATCTCCTAGATAGACTATCCATCTTGCATGGT   720
221    T  Y  L  L  T  P  P  A  P  N  L  L  D  R  L  S  I  L  H  G   240

721  AGTTTTGATCCAGAACATGAACGTGAAAGAGAGGAACACCGTAAACACTCAGTGGAACTG   780
241    S  F  D  P  E  H  E  R  E  R  E  E  H  R  K  H  S  V  E  L   260
                                                  ■
781  AATTCTCTTAACAACTATTCAAAGAACATGGATAAAGCTTAAGTTTTTTCCTGGATGCCA   840
261    N  S  L  N  N  Y  S  K  N  M  D  K  A  *                    273
             ▲
841  CAAACAATGGAAAAGAGGGTTCATCTGAGAAAATGACTTTACCAGTCGTCCAATCCTTGT   900
901  ACCTTTTTGCAGAATATCAGTCTGTCTCTGATGTTTTTCCTGAAGAGAAGTGGCTTCTTT   960
961  GCTGCCCTTCTTGACATCAGGCCATCCTCCAAAAGTTTTCTCCTCACTGTGCATGCACAC  1020
1021 TTTTTCTCCTTTTTGCCACACCTTCCTGCTGCCATTCCTGAGCAAGCTCTGCACTGGCGA  1080
1081 TGCCCCTATCCTGTAGCTGAACGAACTGTAGAAGACGGTCCTGGAACTTGCTGGACTTTC  1140
1141 TTGGGCACCCTGAAGCCTTCTTCACAAATACAGTGGAAATATTATTTATGGAATTAAGTT  1200
1201 TATAAAAAAATATTTTTATAATAAAATATTTCCCTCTGCTTCCCTGGGCCTTTGCTGAAC  1260
1261 CAATGAGGCATGAGGCTGGTGGCTGTCCCCAAAAATACCTAAAAGGTCCCCTCTCTGCAC  1320
1321 CTAGGCCTCATGCTGAAATGATGGGGCCCAGAAGCATAAAGTGGACTATTTAAAGTGGAG  1380
1381 CGTTAACCTCCCTTACTTACTTTCCATAATTTCACTACTGCCCCCTTTCTCTCTAACAAG  1440
1441 GTGTTTTAAAAAATGAAGACACTACGGTAATGTTACATATTACAGAATATGTCTGTTTTC  1500
1501 AGATTTAATTGATTAAATGTATAGACTATTTAATTTGGTTTGTATAAACATGTAAATGAA  1560
1561 ATCAGCTCGATGTAAATAAACTATAATATTAGTGCAAAAAAAAAAAAAAAAA          1612
```

B

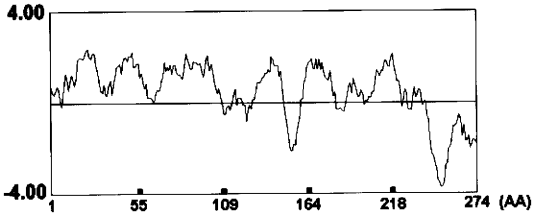

Supplemental Figure 4 A: Nucleotide and deduced amino acid sequence of Aquaporin (*R. japonica* AQP-rn3) cDNA. The predicted amino acid is shown below the nucleotide sequence (DDBJ/EBBL/GenBank accession no. AB500706). The asterisk indicates the terminal codon. NPA motifs are outlined. The solid triangle indicates a putative N-glycosylation site. The square and open triangle indicate phosphorylation sites for protein kinase A and the mercurial-inhibition site, respectively. B: Kyte-Doolittle hydropathy profile (window 11) of the deduced AQP-rj3 amino acid sequence.

A

```
                                                                  TATACTAGCC   -1
-10
  1  ATGCTGAAATATTTTTTCTCTGGGTCCTTTTTAAGACCCCTATTTGCTGAATTCTTAGGC   60
  1   M  L  K  Y  F  F  S  G  S  F  L  R  P  L  F  A  E  F  L  G    20

 61  ACTCTTTTCTTTGTGCTCTTTGGCCTTGGGAGTTCTCTCTCCTGGCCCACAGCGTTTCCC  120
 21   T  L  F  F  V  L  F  G  L  G  S  S  L  S  W  P  T  A  F  P    40

121  AGTTTCCTGCAGAACTCCCTAACATTTGGCCTGGCGAAAAGTACTATGGTAAAGACACTG  180
 41   S  F  L  Q  N  S  L  T  F  G  L  A  K  S  T  M  V  K  T  L    60

181  GGACATATTAGTGATGCTCACCTAAACCCTGCAGTGACACTAGCATTCCTCTTGGGATCC  240
 61   G  H  I  S  D  A  H  L  N  P  A  V  T  L  A  F  L  L  G  S    80

241  CATATCTCTATCTTGAAAGCTGCTTTGTACATATTAGTTCAGGTGCTGGGAGCTGTGGTT  300
 81   H  I  S  I  L  K  A  A  L  Y  I  L  V  Q  V  L  G  A  V  V   100

301  GGAGCCGGGTTGCTCTACGAATTTACTCCATCAAACCTGCGTGGAAACTTTGGTGTCAAC  360
101   G  A  G  L  L  Y  E  F  T  P  S  N  L  R  G  N  F  G  V  N   120

361  TTGCCAAGCAATGGAACTACCCCCGGACAAGGTGTTGCAGTAGAAGCCTTCACCACAATG  420
121   L  P  S  N  G  T  T  P  G  Q  G  V  A  V  E  A  F  T  T  M   140
           ▲
421  CAGCTGGTTCTTTGTATATTTGCCACAACTGACATTCGTCGAGAGGACAATATTGGGTCT  480
141   Q  L  V  L  C  I  F  A  T  T  D  I  R  R  E  D  N  I  G  S   160

481  CCATCTATTTCCATTGGTCTTTCAGTTACAGTGGGTCACCTCCTGGGGATTTACTTCACT  540
161   P  S  I  S  I  G  L  S  V  T  V  G  H  L  L  G  I  Y  F  T   180

541  GGCTGCTCTATGAATCCTGCCAGGTCTTTTGCTCCAGCATTGATCACAGGAAATTTCACC  600
181   G  C  S  M  N  P  A  R  S  F  A  P  A  L  I  T  G  N  F  T   200
           △
601  CATCACTGGGTCTTCTGGGTTGGTCCCATGACTGGTGGAATCGTTGCTTCTCTGATCTAC  660
201   H  H  W  V  F  W  V  G  P  M  T  G  G  I  V  A  S  L  I  Y   220

661  AACTACCTACTTTTCCCTTCAGAAATTAGTGTTTGTGACAGACTGGCTATTCTGCAGGGT  720
221   N  Y  L  L  F  P  S  E  I  S  V  C  D  R  L  A  I  L  Q  G   240

721  AACTATGACCCAGAGTACGAGGGGGAGAGAGAGGAGCACCGCAAGCACTCCGTTGAACTC  780
241   N  Y  D  P  E  Y  E  G  E  R  E  E  H  R  K  H  S  V  E  L   260
                                                    ■
781  AACTCTATGCAAAAAATCAAGCAGACAGCTCTAGATTGTACTGTAGTATCTTTTCAAGCT  840
261   N  S  M  Q  K  I  K  Q  T  A  L  D  C  T  V  V  S  F  Q  A   280

841  TTGAATTTTTGAACTTGAGGTTCTCACACTTTTTAATAAAACCTGATTCAAACCAAAAAA  901
281   L  N  F  *                                                    283

901  AAAAAAAAAAAAAA                                                914
```

B

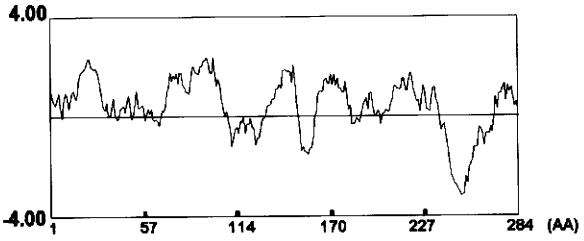

Supplemental Figure 5 A: Nucleotide and deduced amino acid sequence of Aquaporin (*Xenopus leavis* AQP-x3) cDNA. The predicted amino acid is shown below the nucleotide sequence (DDBJ/EBBL/GenBank accession no. AB500709). The asterisk indicates the terminal codon. NPA motifs are outlined. The solid triangle indicates a putative N-glycosylation site. The square and open triangle indicate phosphorylation sites for protein kinase C and protein kinase A and the mercurial-inhibition site, respectively. B: Kyte-Doolittle hydropathy profile (window 11) of the deduced AQP-x3 amino acid sequence.

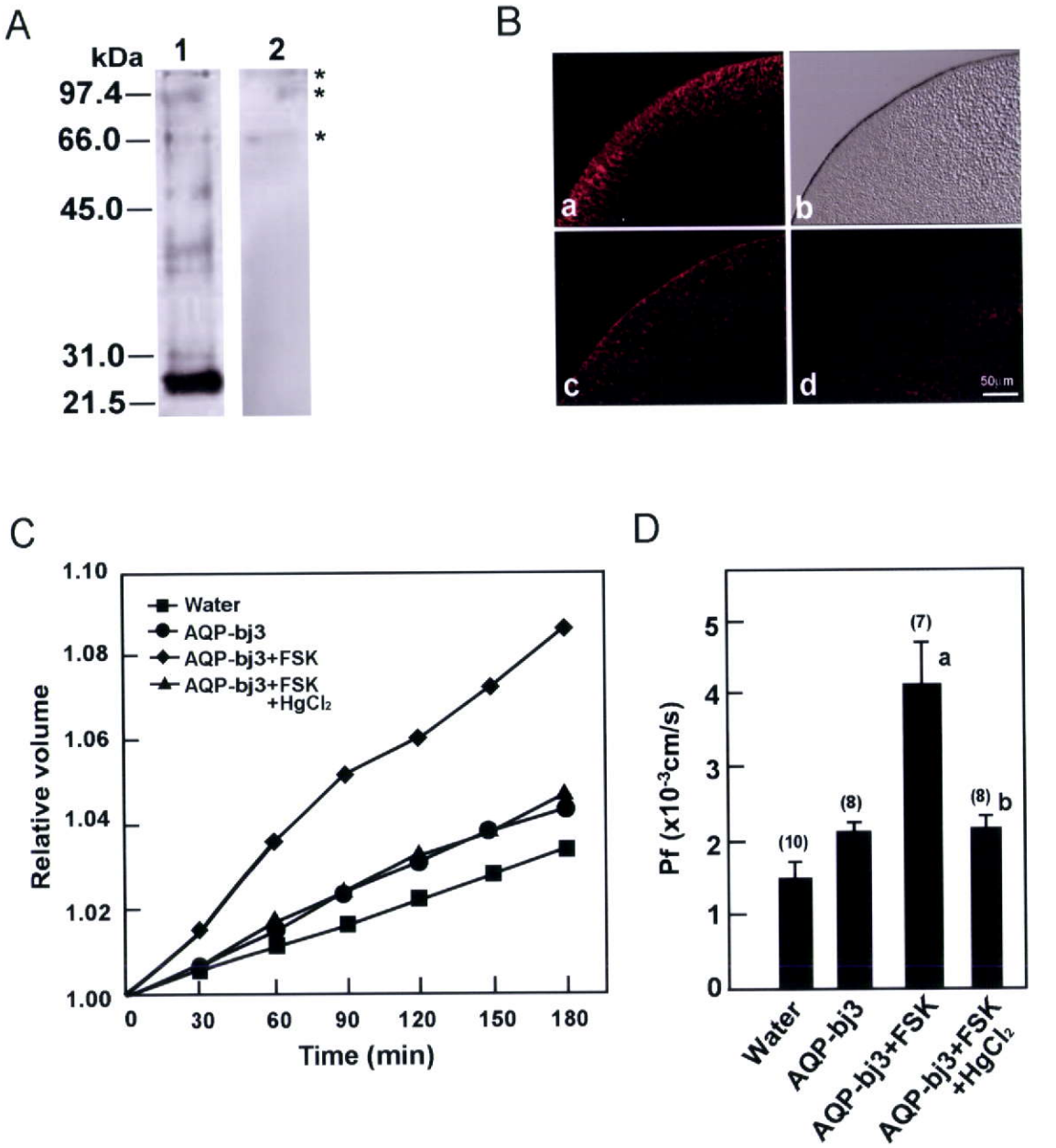

Supplemental Figure 6 - Functional evaluation of AQP-bj3 in *Xenopus* ooctes. (A) Western blot analysis of the extract from AQP-bj3-injected oocytes using anti-AQP-h3 (ST-141). Positive bands are detected a major band at 29 kDa and a smear band between 38.9 and 102.6 (lane 1). No bands are visible except none-specific bands (asterisk) (lane 2). (B) Immunofluorescence images of the AQP-bj3 protein in AQP-bj3-injected oocytes: after complete swelling of the oocytes, (a) immunoreactive AQP-bj3 substance are visible, slightly in the cytoplasm; (b) the corresponding Nomarski differential interference image; (c) in the oocytes injected with AQP-bj3 cRNA after stimulation of forskolin, positive reaction is visible in the plasma membrane, and (d) in the absorption test, immunopositive substances obtained with anti-AQP-h3 are nearly abolished at back-ground levels in the AQP-bj3-injected oocyte after addition of forskolin. (C) Time course of the osmotic swelling. Ooytes were microinjected with water or cRNA encoding AQP-bj3. Some of the AQP-bj3-injected oocytes were incubated with 0.3 mM $HgCl_2$. (D) Pf was calculated from the initial rate of oocyte swelling. The representative data shown are given as the mean ± SE of measurements from from 7 to 10 oocytes in each experimental group. a, $P<0.01$ vs. Water; b, $P<0.01$ vs. AQP-bj3+FSK.

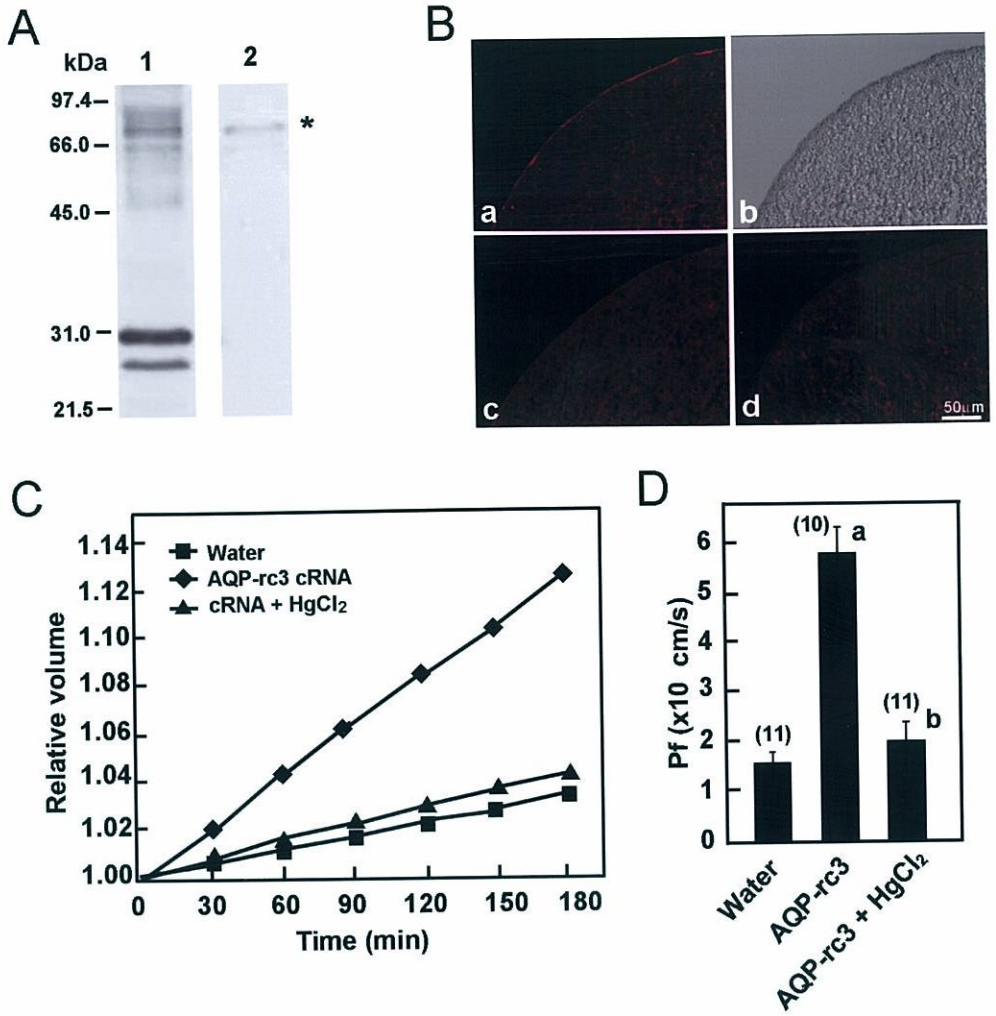

Supplemental Figure 7 - Functional evaluation of AQP-rn3 in *Xenopus* oocytes. (A) Western blot analysis of the extract from AQP-rn3 cRNA-injected oocytes using anti-AQP-rc3 (ST-188). Positive bands are detected a major band at 25.7 kDa (lane 1), but smeary bands are not visible, because the sample was treated with peptide-N-glycosidase F by removing the hind of the antigen. No bands are visible except none-specific bands (asterisk) (lane 2). (B) Immunofluorescence images of the AQP-rn3 protein in AQP-rn3-injected oocytes: after complete swelling of the oocytes, immunoreactive AQP-rn substance are visible, (a) predominately in the cytoplasm (AQP-rn3); (b) the corresponding Nomarski differential interference image; (c) in the absorption test, immunopositive substances obtained with anti-AQP-rc3 are nearly abolished at back-ground levels in the AQP-rn3-injected oocyte, and (d) only background levels are observed in the water-injected oocyte with anti-AQP-rc3. (C) Time course of the osmotic swelling. Ooytes were microinjected with water or cRNA encoding AQP-rn3. Some of the AQP-rn3-injected oocytes were incubated with 0.3 mM $HgCl_2$. (D) Pf was calculated from the initial rate of oocyte swelling. The representative data shown are given as the mean ± SE of measurements from from 9 to 10 oocytes in each experimental group. a, $P<0.001$ vs. Water; b, $P<0.01$ vs. AQP-rn3.

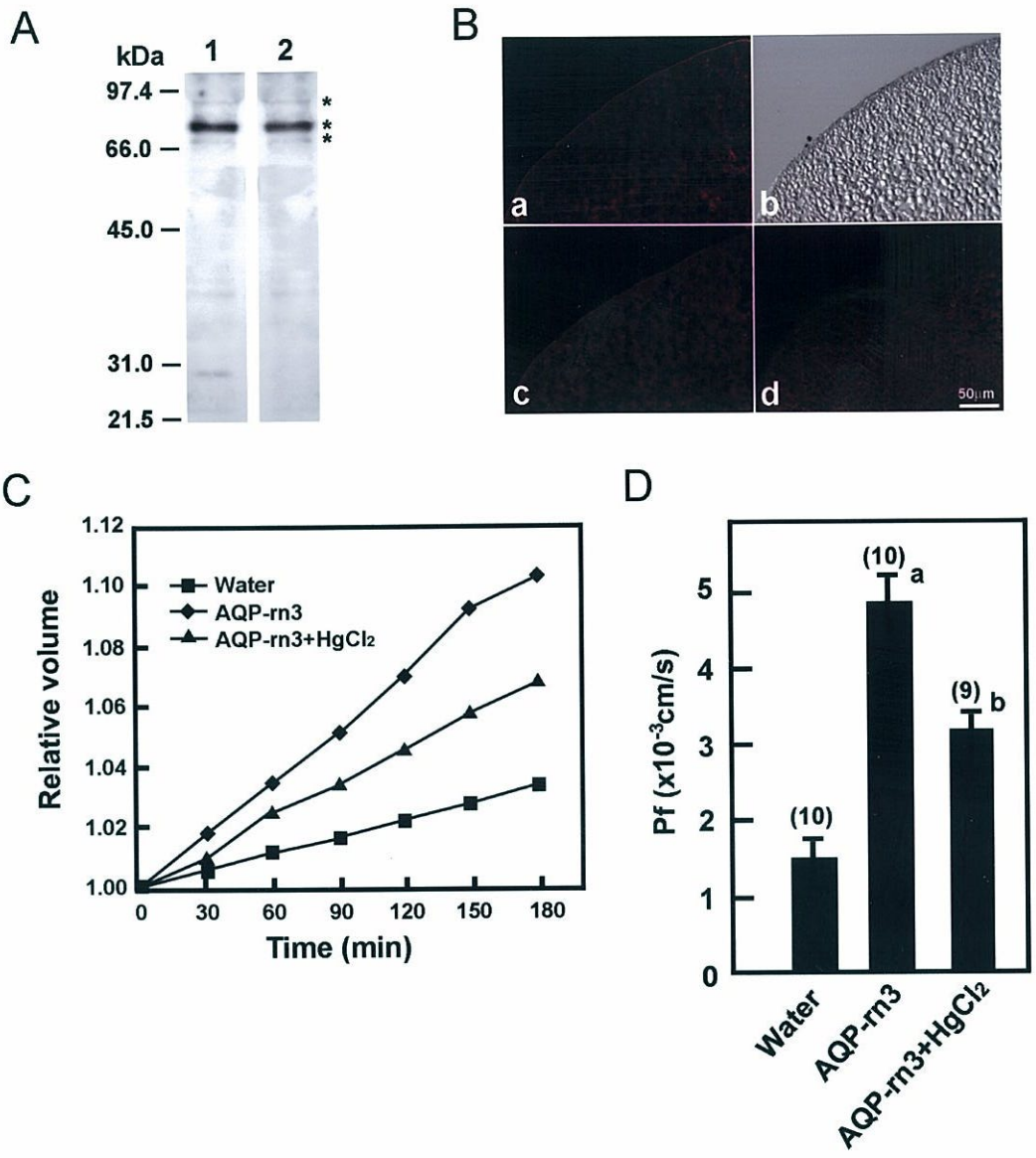

Supplemental Figure 8 - Functional evaluation of AQP-rc3 in *Xenopus* oocytes. (A) Western blot analysis of the extract from AQP-rc3-injected oocytes using anti-AQP-rc3 (ST-188). Positive bands are detected two major bands at 29 and 31 kDa and a smear band between 44.6 and 91.0 kDa (lane 1). No bands are visible except none-specific bands (asterisk) (lane 2). (B) Immunofluorescence images of the AQP-rc3 protein in AQP-rc3-injected oocytes: after complete swelling of the oocytes, (a) immunoreactive AQP-rc3 substance are visible, predominately in the plasma membrane; (b) the corresponding Nomarski differential interference image; (c) in the absorption test, immunopositive substances obtained with anti-AQP-rc3 are nearly abolished at back-ground levels in the AQP-rc3-injected oocyte, and (d) only background levels are observed in the water-injected oocyte with the preabsorbed anti-AQP-rc3 with the antigen. (C) Time course of the osmotic swelling. Ooytes were microinjected with water or cRNA encoding AQP-rc3. Some of the AQP-rc3-injected oocytes were incubated with 0.3 mM $HgCl_2$. (D) Pf was calculated from the initial rate of oocyte swelling. The representative data shown are given as the mean ± SE of measurements from 10 to 11 oocytes in each experimental group. a, $P<0.001$ vs. Water; b, $P<<0.01$ vs. AQP-rc3.

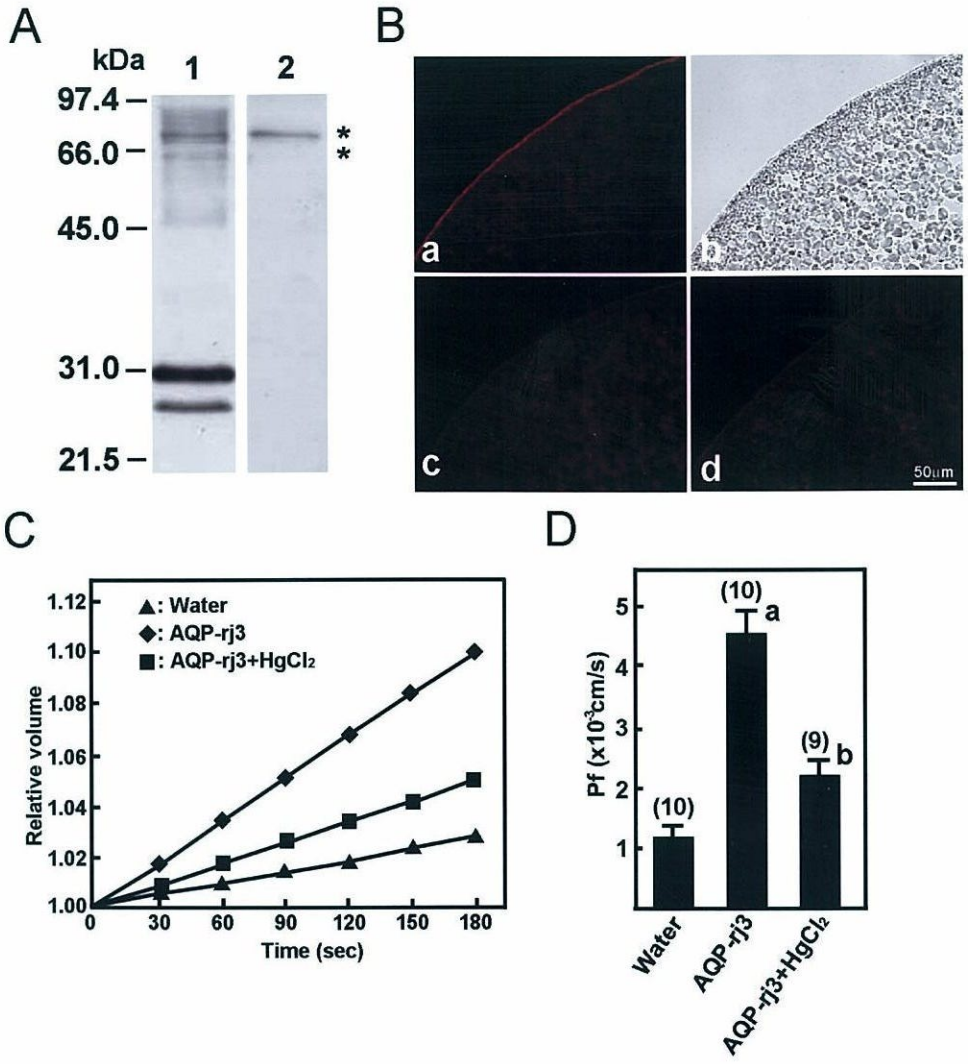

Supplemental Figure 9-Functional evaluation of AQP-rj3 in *Xenopus* oocytes. (A) Western blot analysis of the extract from AQP-rj3-injected oocytes using anti-AQP-rj3 (ST-157). Positive bands are detected two major bands at 29 and 31 kDa and a smear band between 44.8 and 91.3 (lane 1). No bands are visible except none-specific bands (asterisk) (lane 2). (B) Immunofluorescence images of the AQP-rj3 protein in AQP-rj3-injected oocytes: after complete swelling of the oocytes, (a) immunoreactive AQP-rj3 substance are visible, predominately in the plasma membrane; (b) the corresponding Nomarski differential interference image; (c) in the absorption test, immunopositive substances obtained with anti-AQP-rj3 are nearly abolished at back-ground levels in the AQP-rj3-injected oocyte, and (d) only background levels are observed in the water-injected oocytes with the preabsorbed anti-AQP-rj3 with antigen. (C) Time course of the osmotic swelling. Ooytes were microinjected with water or cRNA encoding AQP-rj3. Some of the AQP-rj3-injected oocytes were incubated with 0.3 mM $HgCl_2$. (D) Pf was calculated from the initial rate of oocyte swelling. The representative data shown are given as the mean ± SE of measurements from 9 to 10 oocytes in each experimental group. a, $P<0.001$ vs. Water; b, $P<0.01$ vs. AQP-rj3.

References

Agre P, Brown D, Nielsen S. (1995) Aquaporin water channels: unanswered questions and unresolved controversies. *Curr Opin Cell Biol* 7:472–483

Akabane G, Ogushi Y, Hasegawa T, SuzukiM,Tanaka S. (2007) Gene cloning and expression of an aquaporin (AQP-h3BL) in the basolateral membrane of water-permeable epithelial cells in osmoregulatory organs of the tree frog. *Am J Physiol Regul Integr Comp Physiol* 292:R2340–R2351

Alexander SS, BellerbyCW. (1938) Experimental studies on the sexual cycle of the South African clawed toad (*Xenopus laevis*). *I. J Exp Biol* 15:74–81

Bentley PJ. (1966) Adaptations of amphibia to arid environments. *Science* 152:619–623

Bentley PJ. (1969) Neurohypophyseal hormones in amphibia: a comparison of their actions and storage. *Gen Comp Endocrinol* 13: 39–44

Bentley PJ, Main AR. (1972) Zonal differences in permeability of the skin of some anuran Amphibia. *Am J Physiol* 223:361–363

Bentley PJ, Yorio T. (1979) Do frogs drink? *J Exp Biol* 79:41–46

Bentley PJ. (2002) The amphibia. In: Bradshw SD, Burggren W, Heller HC, Ishi S, Langer H, Neuweiler G, Randall DJ, eds. Endocrines and osmoregulation: a comparative account in vertebrates. Berlin: Springer-Verlag; 155–186

Berisio R, Schluenzen F, Harms J, Bashan A, Auerbach T, Baram D, Yonath A. (2003) Structural insight into the role of the ribosomal tunnel in cellular regulation. *Nat Struct Biol* 10:366–370

Bonifacino JS, Traub LM. (2003) Signals for sorting of transmembrane proteins to endosomes and lysosomes. *Annu Rev Biochem* 72:395–447

Deuchar EM. (1975) *Xenopus*: the South African clawed frog. London: Wiley

Fushimi K, Uchida S, Hara Y, Hirata Y, Marumo F, Sasaki S. (1993) Cloning and expression of apical membrane water channel of rat kidney collecting tubule. *Nature* 361:549–552

Hasegawa T, Tanii H, Suzuki M, Tanaka S. (2003) Regulation of water absorption in the frog skins by two vasotocin-dependent water- channel aquaporins, AQP-h2 and AQP-h3. *Endocrinology* 144: 4087–4096

Heller H. (1979) The pituitary gland and its neuroendocrine control. Part 1. In: Handbook of physiology. Endocrinology. Vol IV. Washington, DC: *Am Physiol Soc*; 103–117

Hillman SS, Withers PC, Drewes RC, Hillyard SD. (2009) Ecological and environmental physiology of amphibians. New York: *Oxford University Press*; 1–68

Ishibashi K, KuwaharaM,Sasaki S. (2000) Molecular biology of aquaporins. *Rev Physiol Biochem Pharmacol* 141:1–32

Jørgensen CB. (1997) 200 years of amphibian water economy: from Robert Townson to the present. *Biol Rev Camb Philos Soc* 72:153– 237

Keene JD. (2007) RNA regulations: coordination of post-transcriptional events. *Nat Rev Genet* 8:533–543

Lillywhite HB. (2006) Water relations of tetrapod integument. *J Exp Biol* 209:202–226

Macknight AD, DiBona DR, Leaf A. (1980) Sodium transport across toad urinary bladder: a model "tight" epithelium. *Physiol Rev* 60: 615–715

Ogushi Y, Mochida H, Nakakura T, Suzuki M, Tanaka S. (2007) Immunocytochemical and phylogenetic analyses of an arginine vasotocin-dependent aquaporin, AQP-h2K, specifically expressed in the kidney of the tree frog, *Hyla japonica.* Endocrinology 148:5891–5901

Pough FH. (2007) Amphibian biology and husbandry. *ILAR J* 48: 203–213

Preston GM. Carroll TP, Guggino WB, Agre P. (1992) Appearance of water channels in *Xenopus* oocytes expressing red cell CHIP28 protein. *Science* 256:385–387

Suzuki M, Tanaka S. (2009) Molecular and cellular regulation of water homeostasis in anuran amphibians by aquaporins. *Comp Biochem Physiol A Mol Integr Physiol* 153:231–241

Takata K, Matsuzaki T, Tajika Y. (2004) Aquaporins: water channel proteins of the

cell membrane. *Prog Histochem Cytochem* 39:1–83

Tanii H, Hasegawa T, Hirakawa N, Suzuki M, Tanaka S. (2002) Molecular and cellular characterization of a water channel protein, AQP-h3, specifically expressed in the frog ventral skin. *JMembrBiol* 188:43–53

Zardoya R. (2005) Phylogeny and evolution of the major intrinsic protein family. *Biol Cell* 97:397–414

Zhang RB, Logee KA, Verkman AS. (1990) Expression of mRNA coding for kidney and red cell water channels in *Xenopus* oocytes. *J Biol Chem* 265:15375–15378

Zimmerman SL, Frisbie J, Goldstein DL, West J, Rivera K, Krane CM. (2006) Excretion and conservation of glycerol, and expression of aquaporins and glyceroporins, during cold acclimation in Cope's gray treefrog, *Hyla chrysoscelis. Am J Physiol Regul Integr Comp Physiol* 292: R544–R555

Chapter 5

General discussion

In this thesis, I first identified and characterized the anuran orthologue of AQP2, AQP-h2K of the tree frog, *Hyla japonica*. Chapter 2 describes the detailed structure and function of AQP-h2K. AQP-h2K consists of 280 amino acid residues, and its predicted structure is shown in Figure 5-1. AQP-h2K contains a pair of asparagine-proline -alanine (NPA) motifs, which are considered to be located in the centre of the pore and to form a specific passage for water molecules (Yasui, 2004; de Groot and Grubmuller, 2005). The amino acid residues, shown to form the selectivity filter in mammalian AQP1, *i.e.* Phe-55, His-177, Cys-186, and Arg-192 (de Groot and Grubmuller, 2005; Fu and Lu, 2007), are also conserved in AQP-h2K (Fig. 5-1). In addition, two possible *N*-linked glycosylation sites at Asn-120 and Asn-128, one protein kinase C phosphorylation site at Ser-236, and one protein kinase A phosphorylation site at Ser-262 are predicted (Fig. 5-1). The physiological properties of AQP-h2K were assessed by expressing it in *Xenopus* oocytes, and the coefficient of osmotic water permeability, *Pf*, of AQP-h2K was approximately four times greater than the control (Ogushi *et al.*, 2007). The AQP-h2K mRNA was strongly expressed in the kidney, and immunohistological staining localized AQP-h2K protein to the collecting duct. AQP-h2K was observed abundantly in the cytoplasm and slightly in the apical plasma membrane of the principal cells under hydrated conditions (Ogushi *et al.*, 2007). After stimulation with arginine vasotocin (AVT), a large population of AQP-h2K appeared to be translocated from the cytoplasmic pool to the apical membrane, suggesting that this AQP is a key player for AVT-dependent water reabsorption in the anuran kidney. It seems likely that AQP-h2K controls the water transport from the tubular fluid into the

principal cells of collecting duct through AVT-dependent translocation, like AQP2 in the mammalian kidney (Sasaki and Noda, 2007).

Although the tissue distribution of anuran AQP2 orthologues has not been studied in species other than *Hyla* (Zimmerman *et al.*, 2006; Ogushi *et al.*, 2007), AQP-h2K and HC-2 AQP appear to be a kidney-type AQP because of their expression in the kidney and their position in the molecular phylogenetic trees (Ogushi *et al.*, 2007). It seems that, in anurans, the three AVT-dependent osmoregulatory organs, the pelvic skin, urinary bladder, and kidney, utilize the same AQP, namely AQP3, at the exit of the transepithelial water transport, whereas at the entry they basically adopt different AQPs as translocatable water channels: AQP-h2-like AQPa2 in the urinary bladder, AQP-h3-like AQPa2 in the pelvic skin, and AQP2 in the kidney (Fig. 5-2). In all these osmoregulatory organs, however, intracellular localization of the relevant AQPs has not been fully determined. Immunoelectron microscopic study would be needed to address this issue and to define the precise role of each AQP in the AVT-dependent transepithelial water transport.

In adult anurans, AVT exerts antidiuretic effects on the kidney, as well as the urinary bladder, to aid water economy (Bentley, 2002). The renal effect of AVT is considered to be weak in the aquatic species, such as *X. laevis* (Kloas and Hanke, 1992), while the kidney of most adult anurans shows significant antidiuretic responses to AVT in two modes: a decreased glomerular filtration rate and an increased water reabsorption across the renal tubule (Pang, 1983; Bentley, 2002). The anuran renal tubule does not have an extended U-shaped medullary portion like the Henle's loop in the avian and mammalian kidneys, so that hyperosmotic urine cannot be produced in the kidney (Bentley, 1998). I also discovered new finding in the phylogenetic relationship of anuran AQPs. The full sequences of 17 AQP cDNAs have been elucidated in anurans, but only expressed sequence tags (ESTs) are registered in urodels.

A phylogenetic analysis suggested that anuran AQPs can be assigned to six clusters: types 1, 2, 3, and 5, and two anuran-specific types, designated as a1 and a2 (The letter "a" represents *a*nuran). The cluster of type-a1 AQPs is composed of AQPxlo from *Xenopus laevis* oocytes (Virkki *et al.*, 2002). The cluster of type-a2 AQPs contains AQP-h2 (Hasegawa *et al.*, 2003) and AQP-h3 from a frog, *H. japonica* (Tanii *et al.*, 2002), and AQP-t2 (AF020621) and AQP-t3 (AF020622) from a toad, *B. marinus*. AQP-h2K belongs to the type 2, together with mammalian AQP2, suggesting that AQP-h2K is an anuran ortholog of the neurohypophyseal hormone-regulated mammalian AQP2 and that AQP2 molecule is already present in anuran mesonephros.

In Chapter 3, it is described that antidiuretic hormone, AVT and β-adrenergic neuron are involved in the water permeability across the pelvic skin of the tree frog. The water absorption/reabsorption in the ventral pelvic skin and urinary bladder is stimulated by AVT, and the regulatory mechanisms for water permeability of the tight-junctioned epithelium by neurohypophyseal hormone seem to be basically common between the anuran osmoregulatory organs and mammalian kidney. Therefore, numerous studies have been conducted using anuran ventral skin and urinary bladder as model systems, to elucidate the general mechanisms for ion-coupled water movement across the tight epithelium (Jorgensen, 1997; Macknight *et al.*, 1980). The ventral pelvic skin of the tree frog, *H. japonica* expresses two kinds of AVT-stimulated aquaporin, AQP-h2 and AQP-h3, and thereby stimulates the capacity to absorb water. I investigated AQP dynamics and water permeability in the pelvic skin of *H. japonica* with AVT, hydrins (intermediate peptides of pro-AVT), and β-adrenergic effectors. In the *in vivo* experiment, both AQP-h2 and AQP-h3 proteins were translocated to the apical plasma membrane in the principal cells of the first reacting cell (FRC) layer in the pelvic skin following challenge with hydrin 1, hydrin 2, and AVT, thereby increasing the water permeability on the pelvic skin. The β-adrenergic receptor agonist

isoproterenol (IP) and its anatagonist propranolol (PP) in combination with AVT, or hydrins were used as challenge in the *in vitro* experiment. IP increased water permeability, while PP inhibited it, and both events were well correlated with the translocation of the AQPs to the apical membrane. In the PP + AVT-treated skins, labels for AQP-h2 and AQP-h3 were differentially visible among the principal cells; the apical plasma membrane of some cells was labeled while others were not, indicating that the response of PP or AVT is different from the cell to the cell. These results provide morphological evidence that the principal cells of the FRC layers may have two kinds of receptors; a V2 receptor and β-adrenergic receptor.

Finally, in the last chapter, I reported that the role of the ventral pelvic skin-type AQP in the water balance in the body of various frogs; terrestrial, arboreal, semi-aquatic, and aquatic species. Most adult anuran amphibians except for the aquatic species absorb water across the ventral pelvic skin and reabsorb it from urine in the urinary bladder. Many terrestrial and arboreal species utilize a region in the posterior or pelvic region of the ventral skin that is specialized for rapid rehydration from shallow water sources or moist substrates. Periods of terrestrial activity can be prolonged by reabsorption of dilute urine from the urinary bladder. AQP plays a fundamental role in these water absorption/reabsorption processes, which are regulated by antidiuretic hormone. Characterization of AQPs from various anurans revealed that the unique water homeostasis is basically mediated by two types of AQP-a2, *i.e.* ventral pelvic skin- and urinary bladder-type, respectively. The bladder-type AQPa2 is further expressed in the pelvic skin of terrestrial and arboreal species, together with the pelvic skin-type AQPa2. In contrast, the pelvic skin-type AQP (AQP-x3) of the aquatic *Xenopus* has lost the ability of efficient protein production. The extra C terminal tail in AQP-x3 and/or the 33 nucleotides encoding this tail appear to participate in the post-transcriptional regulation of AQP-x3 gene expression by attenuating protein

expression. The positive transcriptional regulation of bladder-type AQP in the pelvic skin and negative post-transcriptional regulation of pelvic skin-type AQP provide flexibility in the water regulation mechanisms, which might have contributed to the evolutionary adaptation of anurans to a wide variety of water environments. Furthermore, I expect that the molecular mechanism of AQP-x3 expression will be solved in the near future.

Acknowledgment

I am grateful to Professor Shigeyasu Tanaka and Associate Professor Masakazu Suzuki for helpful advice, discussion and encouragements during my doctoral coursework.

This work was supported in part by a Grant-in-Aid for Research Fellow of the Japan Society for the Promotion of Science (21-3448) from the Ministry of Education, Culture, Sports, Science and Technology of Japan to Y. Ogushi.

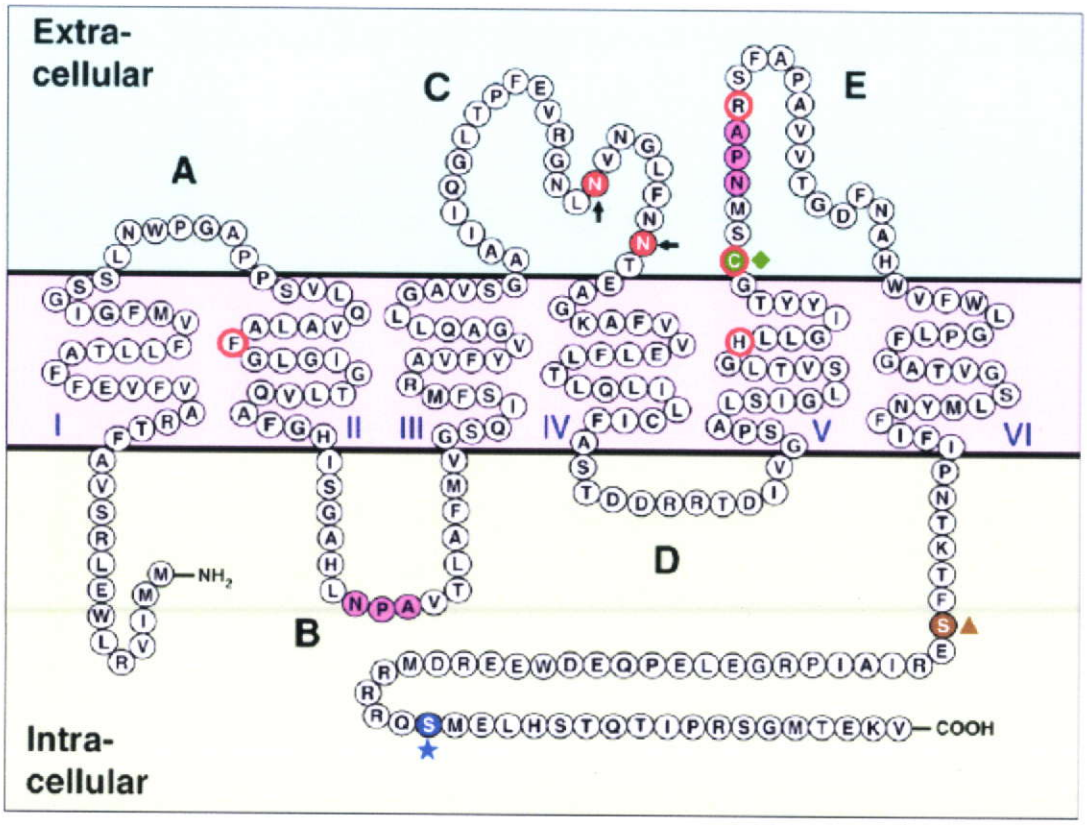

Fig. 5-1. Deduced amino acid sequence and putative topology of AQP-h2K with six membrane-spanning α-helices (I–VI) connected by intra- and extracellular loops (A–E). The pink overlay highlights NPA motifs. The phenylalanine, histidine, cysteine, and arginine residues in thick red circles are putative amino acids important for aromatic/arginine constriction in the water-specific channels. The arrow, diamond, star, and triangle indicate N-glycosylation sites, a mercurial inhibition site, and phosphorylation sites for protein kinase A and protein kinase C, respectively.

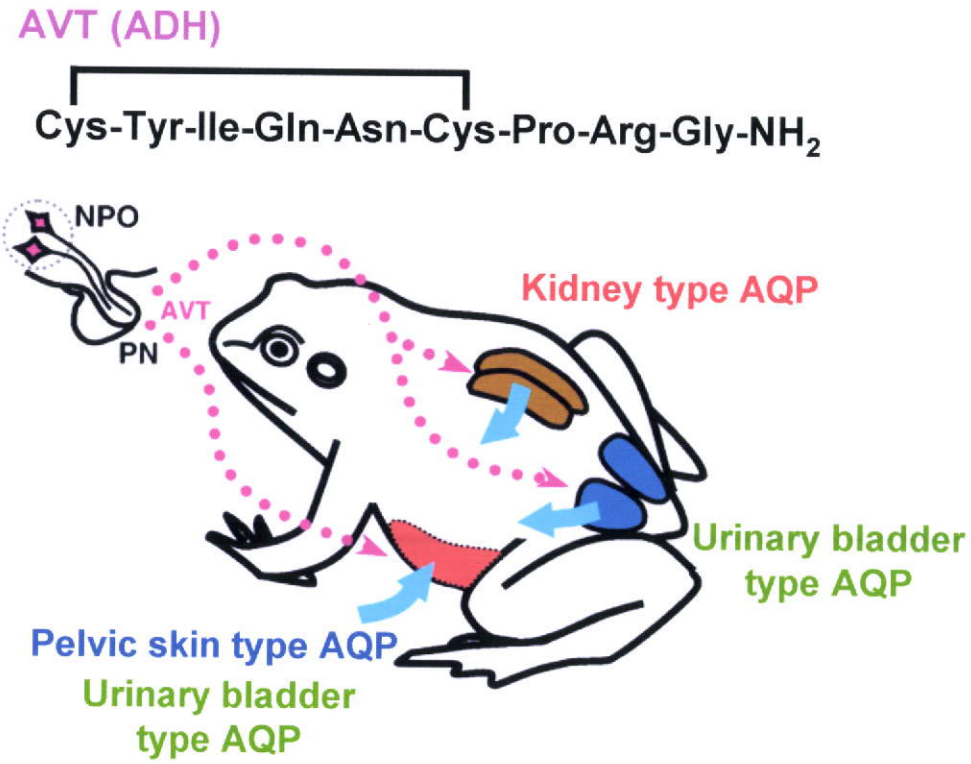

Fig. 5-2. Arginine vasotocin (AVT) and AQPs in the major osmoregulatory organs of anurans. AVT functions as an antidiuretic hormone (ADH) in anurans. AVT is synthesized in the magnocellular neurosecretory neurons whose cell bodies reside in the preoptic nucleus (NPO) of the hypothalamus. During dehydration, AVT is secreted from their axon terminals within the pars nervosa (PN) of the pituitary gland. The secreted AVT induces not only water absorption through the ventral pelvic skin, but also water reabsorption through the urinary bladder and in the kidney. Specific AQPs seem to regulate AVT-dependent water transport in these osmoregulatory organs, i.e. kidney type AQP for the kidney, urinary bladder type for the urinary bladder, and pelvic skin type AQP for the pelvic skin, by translocation from intracellular vesicles to the apical plasma membrane in the principal cells of the tight epithelium. In the terrestrial and arboreal species, such as *Bufo japonicus* and *Hyla japonica*, urinary bladder-type AQP is likely to function in the pelvic skin, as well as in the urinary bladder. Light blue arrows indicate the water flow.

References

Bentley PJ. (1998) Hormones and osmoregulation, In: Bentley, P.J. (Ed.), Comparative Vertebrate Endocrinology, 3rd ed. *Cambridge Univ., Cambridge, pp.* 337–378

Bentley PJ. (2002) Endocrines and osmoregulation: a comparative account in vertebrates. *Springer, Berlin, pp.* 155–186

de Groot BL, Grubmuller H. (2005) The dynamics and energetics of water permeation and proton exclusion in aquaporins. *Curr Opin Struct* Biol 5: 176–183

Fu D, Lu M. (2007) The structural basis of water permeation and proton exclusion in aquaporins. *Mol Membr Biol* 24: 366–374

Hasegawa T, Tanii H, Suzuki M, Tanaka S. (2003) Regulation of water absorption in the frog skins by 2 vasotocin-dependent water-channel aquaporins, AQP-h2 and AQP-h3. *Endocrinology* 144:4087–4096

Jorgensen CV. (1997) 200 years of amphibian water economy: from Robert Towson to the present. *Biol Rev Camb Philos Soc 72, pp.* 153–237

Kloas W, HankeW. (1992) Localization and quantification of nonapeptide binding sitesin the kidney of *Xenopus laevis*: evidence for the existence of two different nonapeptide receptors. *Gen Comp Endocrinol* 85: 71–78

Macknight AD, DiBona DR, Leaf A. (1980) Sodium transport across toad urinary

bladder: a model "tight" epithelium. *Physiol Rev* 60:615–715

Ogushi Y, Mochida H, Nakakura T, Suzuki M, Tanaka S. (2007) Immunocytochemical and phylogenetic analyses of an arginine vasotocin-dependent aquaporin, AQP-h2K, specifically expressed in the kidney of the tree frog, *Hyla japonica. Endocrinology* 148: 5891–5901

Pang PKT. (1983) Evolution of control of epithelial transport in vertebrates. *J Exp Biol* 106: 283–299

Sasaki S, Noda Y. (2007) Aquaporin-2 protein dynamics within the cell. Curr *Opin Nephrol Hypertens* 16: 348–352

Tanii H, Hasegawa T, Hirakawa N, Suzuki M, Tanaka S. (2002) Molecular and cellular characterization of a water channel protein, AQP-h3, specifically expressed in the frog ventral skin. *J Membrane Biol* 188:43–53

Virkki LV, Franke C, Somieski P, Boron WF. (2002) Cloning and functional characterization of a novel aquaporin from Xenopus laevis oocytes. *J Biol Chem* 277 40610–40616

Yasui M. (2004) Molecular mechanisms and drug development in aquaporin water channel diseases: structure and function of aquaporins. *J Pharmacol Sci* 96: 260–263

Zimmerman SL, Frisbie J, Goldstein DL, West J, Rivera K, Krane CM. (2006) Excretion and conservation of glycerol, and expression of aquaporins and glyceroporins,

during cold acclimation in Cope's gray tree frog *Hyla chrysoscelis*. *Am J Physiol* 292: R544–R555